

## Electrochemical Energy Storage for Green Grid

Zhenguang Yang,\* Jianlu Zhang, Michael C. W. Kintner-Meyer, Xiaochuan Lu, Daiwon Choi, John P. Lemmon, and Jun Liu

Pacific Northwest National Laboratory, Richland, Washington 99352, United States

### CONTENTS

1. Introduction	3577	6. Lead–Carbon Batteries	3601
1.1. Energy Reality and Increasing Renewable Penetration	3577	6.1. Lead–Acid Batteries: Chemistries, Design, and Application Challenges	3601
1.2. The Need for Electrical Energy Storage in the Future Grid	3578	6.2. Lead–Carbon Electrochemical Storage Devices or Batteries	3602
2. Potential EES Technologies	3580	6.2.1. Effects of Carbon Additives	3603
2.1. Technical and Economic Considerations of EES	3580	6.2.2. Lead–Carbon (PbC) Asymmetric Electrochemical Capacitors	3603
2.2. Potential Technologies	3581	6.2.3. Lead–Carbon (PbC) Ultrabatteries	3603
3. Redox Flow Batteries	3583	6.3. Electrochemical Performance and Challenges for Grid Applications	3604
3.1. All Vanadium Redox Flow Batteries	3584	7. Perspectives	3605
3.1.1. Electrolytes	3584	Author Information	3606
3.1.2. Electrodes/Bipolar Plates	3586	Biographies	3606
3.1.3. Membranes and Separators	3587	Acknowledgments	3608
3.2. Other RFB Chemistries	3589	Acronym List	3608
3.3. Challenges and Future R&D Needs for RFBs	3591	References	3609
4. Sodium–Beta Alumina Membrane Batteries	3591		
4.1. Cell Structure and Electrochemistry	3591		
4.1.1. Sodium–Sulfur Batteries	3591		
4.1.2. Sodium–Metal Halide Batteries	3591		
4.2. Beta-Alumina Solid Electrolyte (BASE)—Structure, Chemistry, Processing, and Properties	3592		
4.3. Negative Electrodes or Sodium–Anodes (for both Sodium–Sulfur and Sodium–Metal Halide Batteries)	3594		
4.4. Positive Electrodes or Cathodes	3595		
4.4.1. Sulfur Cathodes in Sodium–Sulfur Batteries	3595		
4.4.2. Metal–Halide Cathodes in Sodium–Metal Halide Batteries	3595		
4.5. Challenges and Future Trends in the Development of the Na–Batteries	3596		
5. Li–Ion Batteries	3596		
5.1. Concept of Li–Ion Batteries and Traditional Chemistries	3596		
5.2. Challenges of Traditional Li–Ion Chemistries for Stationary Applications	3599		
5.3. Long Life, Low Cost, Safe Li–Ion Batteries for Stationary Applications	3600		
5.4. Li–Ion Battery Design for Stationary Applications	3601		

### 1. INTRODUCTION

#### 1.1. Energy Reality and Increasing Renewable Penetration

The current worldwide electric generation capacity is estimated to be about 20 terawatt hours (TW,  $\times 10^{12}$  watts).<sup>1</sup> Approximately 68% of today's electrical energy is supplied from fossil fuels: coal (42%), natural gas (21%), oil (5%), nuclear (14%), hydro (15%), and the remaining 3% from renewable energy technologies. Even with aggressive conservation and development of new, efficient technologies, the worldwide electricity demand is predicted to double by the middle of the century and triple by the end of the century. Electricity is the dominant form of energy used (e.g., 40% of all energy consumption in the United States by 2002), and the demand for electricity is increasing at a faster pace than overall energy consumption. At the same time, oil and natural gas production is predicted to peak over the next few decades. Coal has been the dominant source of electricity generation in the world;<sup>2</sup> abundant coal reserves may maintain current consumption levels longer than oil and gas. However, every kWh of electricity generated by burning coal coproduces an average 1000 g lifecycle CO<sub>2</sub> emission, a greenhouse gas that is widely considered as the primary contributor to global warming.<sup>3,4</sup> In the United States alone, coal power plants emit 1.5 billion tons of CO<sub>2</sub> per year, and emissions from developing countries are accelerating. To reduce greenhouse gas emissions, many countries are adopting emission regulations

**Received:** September 1, 2010

**Published:** March 04, 2011

(i.e., cap-and-trade or variants) and carbon “trading,” which benefits industries with a small “carbon footprint” and requires those producing higher emissions to purchase carbon “allowances.”

The environmental concerns over the use of fossil fuels and their resource constraints, combined with energy security concerns, have spurred great interest in generating electric energy from renewable sources. Solar and wind energy are among the most abundant and potentially readily available.<sup>3,5,6</sup> The solar radiation energy the Earth receives in 1 h is enough to meet worldwide energy requirements for a year. Capturing a small percentage of potential wind energy could also contribute significantly to meeting the world’s electrical energy requirements. While advances in technology are still needed to harvest renewable energy economically, solar and wind power technologies have grown quickly. Globally, the total electricity from installed wind power reached 74.3 gigawatts (GW) in 2006 and 94 GW in 2007.<sup>7</sup> The World Energy Council estimates that new wind capacity worldwide will total up to 474 GW by 2020. The output from photovoltaic (PV) module installations is currently growing at 40% per year worldwide.<sup>5</sup> The United States targets 100 GW solar power by 2020.

However, solar and wind are not constant and reliable sources of power. The variable nature of these renewable sources causes significant challenges for the electric grid operators because other power plants (usually fossil fueled power plants) need to compensate for the variability. For example, as shown in Figure 1a, wind power profiles in Tehachapi, California, vary over minutes, hours, and days while peaking at night when demand is low. During the day, wind power can be a few GW at some moments and only a few megawatts (MW) and even zero at others. Similarly, in Figure 1b, solar power is generated only during the daytime and varies when clouds pass by. A further concern is the fact that the renewable resources are localized and are often away from load centers. In the United States, wind sources are concentrated in the midwest regions, and solar sources in southwest regions. To smooth out the intermittency of renewable energy production, low-cost electrical energy storage (EES) will become necessary. EES has been considered as a key enabler of the smart grid or future grid, which is expected to integrate a significant amount of renewable energy resources while providing fuel (i.e., electricity) to hybrid and electrical vehicles,<sup>8</sup> although the cost of implementing EES is of great concern.<sup>9</sup>

## 1.2. The Need for Electrical Energy Storage in the Future Grid

Indeed, EES is an established, valuable approach for improving the reliability and overall use of the entire power system (generation, transmission, and distribution [T&D]). Sited at various T&D stages (Figure 2), EES can be employed for providing many grid services, including a set of ancillary services such as (1) frequency regulation and load following (aggregated term often used is balancing services), (2) cold start services, (3) contingency reserves, and (4) energy services that shift generation from peak to off-peak periods. In addition, it can provide services to solve more localized power quality issues and reactive power support.

Balancing services are used to balance generation and demand in tightly limited situations to maintain the alternating current (AC) system frequency of 60 Hz. EES is perfectly suited to provide this service by absorbing electric energy (charging cycle) whenever there is too much generation for a given demand and by injecting electric energy into the power grid (discharging cycle) when there

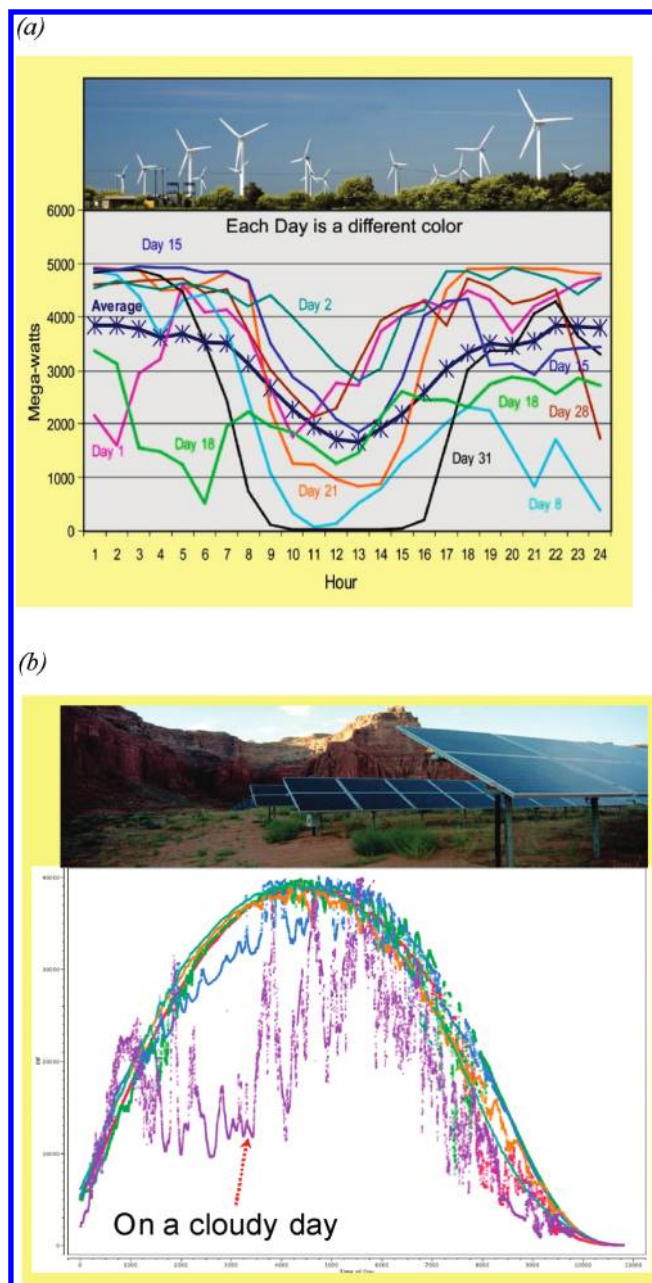


**Figure 1.** (a) Daily profiles of wind power projected by  $7\times$  output in April 2005 for the year 2011 in Tehachapi, California (Courtesy of ISO California). (b) 5 MW PV power over a span of 6 days in Spain (Courtesy of AES).

is too little generation. Traditionally, these services have been performed by conventional gas or steam turbine technologies. But rather than varying the torque of large rotary turbo-machinery on a second-by-second basis, electrochemical EES is much better suited to quickly respond to the grid needs. To operate the electric grid reliably requires contingency reserves that are used in cases of a grid contingency such as an unplanned outage of a power plant or transmission line. Various kinds of contingency reserves are necessary to step in when the contingency occurs. Reserves are classified by how quickly they can be brought online and how fast they respond to a grid contingency—the faster the response, the sooner the contingency can be managed. A recent analysis suggested a relationship between contingency reserve capacity

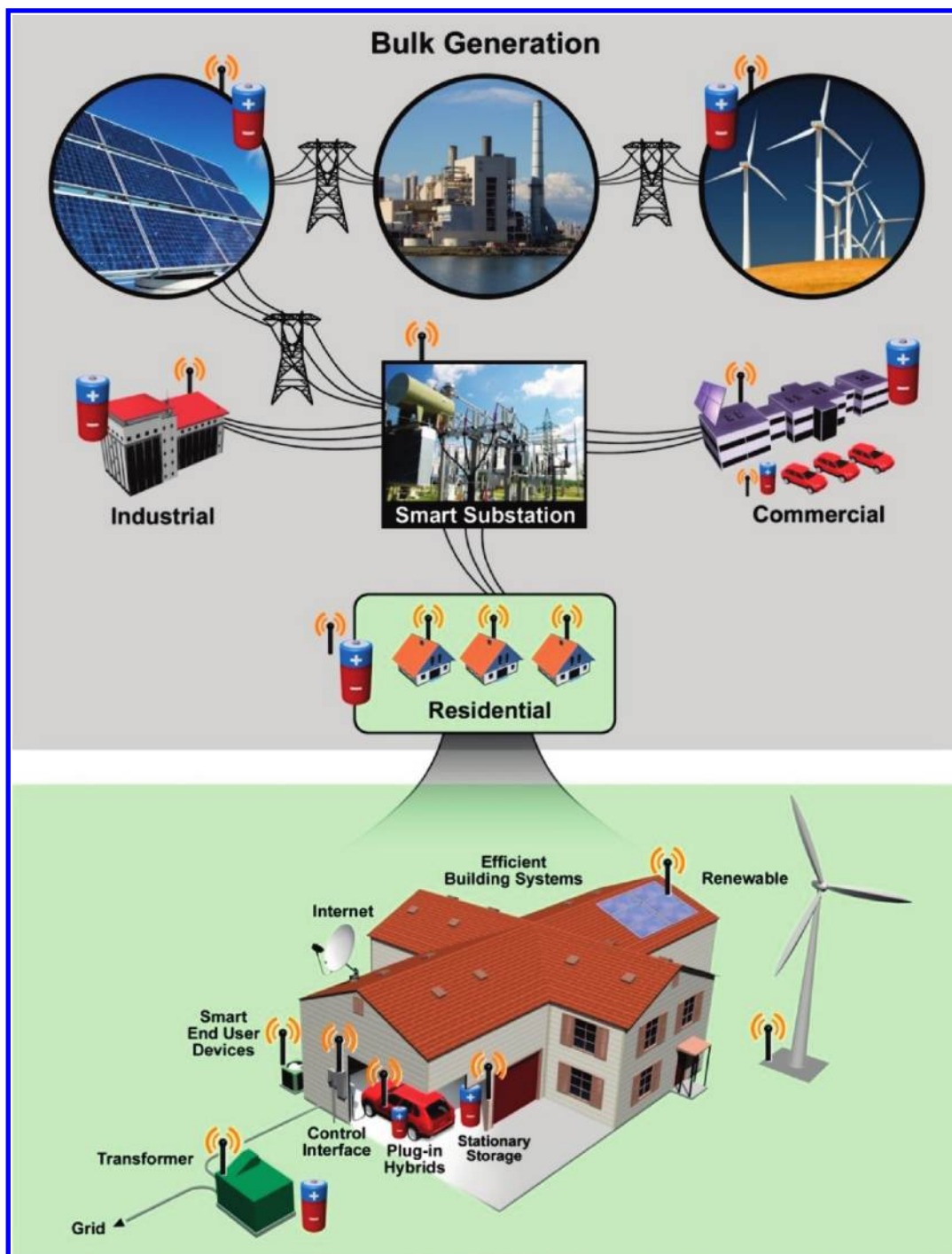


**Figure 2.** Schematic of applications of electricity storage for generation, transmission, distribution, and end customers and future smart grid that integrates with intermittent renewables and plug-in hybrid vehicles through two-way digital communications between loads and generation or distribution grids.<sup>10</sup>

requirements and reserve response time—the faster a grid asset responds, the less capacity the system needs.<sup>11</sup> This result suggests that a fast-responding EES unit may potentially provide a higher value to the grid than a conventional turbine unit of the same capacity size (MW). Furthermore, in addition to providing reliability service to the grid, EES can improve the economic efficiency of the electricity infrastructure by improving its utilization. On average, the entire electricity delivery system (T&D) is used to about 50%.<sup>12</sup> Designed for a peak load condition with some reserve

margin and load-growth expectations added to the peak load, the infrastructure is underused most of the time. From an economic efficiency point of view, this is less than optimal. To improve the entire use of the grid assets, the system will need to be more evenly loaded. EES can play an important role in that process by shifting electric energy from peak to off-peak periods. As shown in Figure 3, electrical energy is stored (via load leveling) when it can be produced cheaply (at off-peak times, for example) and released at peak times when it is more valuable.

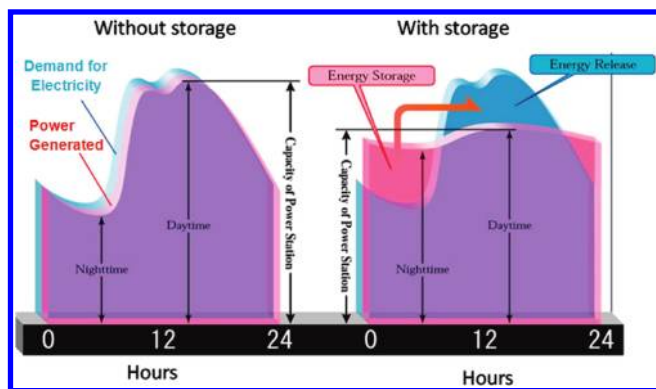


**Figure 3.** Schematic of balancing generation and demand via load leveling, a typical case of load shifting (Courtesy of NGK, Inc.).

To date, however, EES (almost exclusively pumped hydro-electric storage) contributes to only about 2% of the installed generation capacity in the United States. The percentages are higher in Europe and Japan, at 10% and 15%, respectively, largely because of favorable economics and government policies.<sup>13</sup> With little energy storage capability, the U.S. power grid has evolved by relying on redundant generation and transmission grid assets to meet the grid reliability requirements. While this power system design concept has provided grid operations with acceptable levels of reliability in the past, the future grid will face significant challenges by providing clean power from intermittent resources to a much more dynamic load. These challenges will not only be faced in the United States, but also internationally. With the general effort by many nations to lower their national carbon footprint, a greater reliance will be placed on the nation's electric power grids as their energy system backbone. With tighter constraints on carbon emissions, a general trend of electrification of fossil-fuel-based end uses is emerging. The most prominent is the electrification of transportation. Some estimates suggest that 30–50% of all new vehicle purchases in 2030 will be plug-in hybrid vehicles.<sup>14,15</sup> Other services, such as residential heating, which is generally provided by fuel oil and natural gas, may be electrified with tighter emission constraints. This places an increasingly growing importance and reliance on the power grids to support the nations' economies. But not only will the demand for electricity grow, the way the electricity is being used will also become much more dynamic as residential, commercial, and industrial electricity customers install onsite generators (such as PVs, fuel cell technologies, and other distributed generators) and become net-producers of electricity at certain times. On the large-scale power generation side, a significant new capacity of intermittent renewable energy is projected to decarbonize the electric power system.

While the absolute capacity of intermittent renewable energy resources that can be integrated into the existing power grids may vary from region to region, there is ample consensus that additional flexible grid assets are required to accommodate the increasing variability in power production. A doubling of the regulation service requirements to maintain 60-Hz grid frequency and safe grid operations has been reported to be necessary for California and the Pacific Northwest by 2020.<sup>16,17</sup> California will then have a contribution of renewable energy resources to the entire generation mix of 30%. The Pacific Northwest is estimated to have between 15 and 20% of electricity from renewable, nonhydro resources. At a national level, the U.S. Department of Energy (DOE) targets a 20% contribution of renewable energy to the total electric generation mix.

To meet this target would require about 300 GW of new capacity. The majority of this new capacity is likely to be wind and solar resources because of their technological maturity and economic characteristics. To integrate new wind and solar energy resources at this scale, significant investments will be required to upgrade the grid. And the need of grid investment is already felt. On February 26, 2008, a cold front moved through west Texas, and winds died in the evening just as electricity demand was peaking. Over a 2-h period the generation from wind power in the region plummeted rapidly from 1.7 GW to only 300 MW, while the power demand rose to a peak of 35612 MW from 31200 MW. The sudden loss of wind power and the lack of alternative electricity supply to ramp up as quickly forced the Electric Reliability Council of Texas (ERCOT) to curtail 1100 MW demand from industrial customers within 10 min and grid stability was restored within 3 h. To prevent a similar problem, ERCOT investigated the addition of EES. As a result, in April 2010 Electric Transmission Texas (ETT) installed a 4 MW sodium–sulfur utility scale battery system in Presidio, TX. EES will not only function as a buffer for the intermittency of renewable energy resources but also as a transmission resource if placed properly in the grid. As mentioned above, there are many other grid services that EES can provide to the grid, and several of them can be provided simultaneously. While EES can provide significant value to the grid today in the United States and internationally, it should be noted that other conventional and nonconventional technologies will compete for the same market share. For EES to be successful, it will need to compete on its own merits. Its cost and performance characteristics will need to be cost-competitive with the conventional technologies. In most cases, this is a natural gas combustion turbine. However, with the significant national and international investments in smart grid technologies, demand response or load-side control strategies are emerging as a new technology to offer some of the values that EES competes for. The U.S. Congress has recognized the potential of EES as an enabler for fully used smart grid technologies to integrate a large capacity of renewable energy resources in the Energy Independence and Security Act of 2007. This legislation authorized DOE to develop and demonstrate storage technologies for utility applications.<sup>18</sup> The American Recovery and Reinvestment Act of 2009 has made a significantly level of funding available for stationary energy storage demonstrations. Additionally, commercial interests have been generated to develop stationary energy storage technologies for utility applications. Several pilot projects are under way to test the performance and reliability of EES. Recently, California enacted a law requiring utilities to include energy storage systems in electricity distribution networks that can handle 2.25–5.00% of peak load. While EES may already be cost-competitive for some high-value niche markets, further cost reduction has to occur for EES to be more widely used. DOE is the key U.S. funding organization to address the science and technology research needs for the next generation of storage materials and storage systems.

## 2. POTENTIAL EES TECHNOLOGIES

### 2.1. Technical and Economic Considerations of EES

*Performance requirements* of EES for stationary use depend on the application markets that are broad and varied in power and energy ratings, the ratio of power to energy, the discharging time, etc. (Figure 4 shows power and energy rating zones of varied applications.) For example, to regulate frequency, the energy storage capacity may not need to be long-lasting — minutes can be sufficient — but it must have a long cycle life because the system

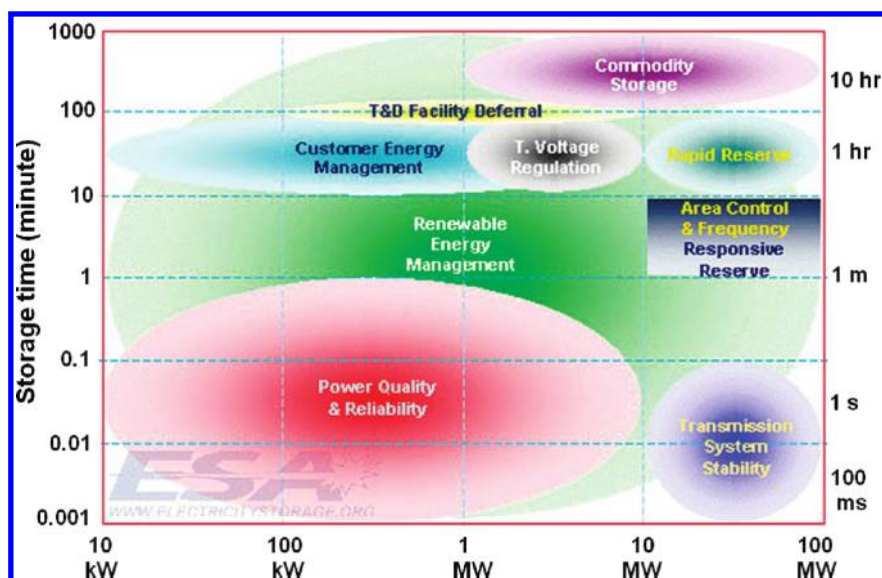


Figure 4. Power and discharge duration (or energy) requirements for varied applications<sup>20</sup> (Courtesy of Electricity Storage Association [ESA]).

is likely to encounter multiple daily discharge events. High discharge rates or high current densities are important, although the state-of-charge (SOC) of the storage system typically will not move over a wide range. In comparison, energy management, such as load shifting, requires systems of up to MWh or even GWh levels that are capable of discharge durations up to a few hours or more at designated power. For this type of application, high round-trip energy efficiency and a long deep-cycle life, along with low operation and maintenance costs, are principal drivers. Unlike vehicle applications that have constraints on weight and volume, high-energy densities may not be strictly required for stationary applications. Also, the grid and renewable applications often require a quick response from the storage that can bring the grid up to full power in a matter of a second.<sup>19</sup>

Cost is probably the most important and fundamental issue of EES for a broad market penetration. Among the most important factors are capital cost and life-cycle cost. The capital cost is typically expressed in terms of the unit cost of power (\$/kW) for power applications (e.g., frequency regulation) or the unit cost of energy capacity (\$/kWh) for energy applications (e.g., load leveling). The life-cycle cost is the unit cost of energy or power per cycle over the lifetime of the unit.

Different applications have different cost tolerances, for example, load shifting and renewable firming. In the authors' opinion, the cost of electricity storage probably needs to be comparable to the cost of generating electricity, such as from natural gas turbines at a cost as low as 8–10 ¢/kWh per cycle. Thus, to be competitive, the capital cost of storage technologies for energy applications should be comparable or lower than \$250/kWh, assuming a life cycle of 15 years or 3900 cycles (5 cycles per week), an 80% round trip efficiency, and “zero” maintenance. A capital cost of \$1,250/kWh or less is desired if the technology can last 5 h at name-tag power. Beyond the life-cycle cost is the social cost that considers the environmental impacts, such as the cost associated with reducing CO<sub>2</sub> emissions by deploying advanced storage systems.

The Reliability, durability, and safety of energy storage systems must be addressed for stationary applications. EES must have a long calendar life (e.g., >15 years) and a long cycle life (e.g., >4000 deep cycles for energy applications) as well as minimum

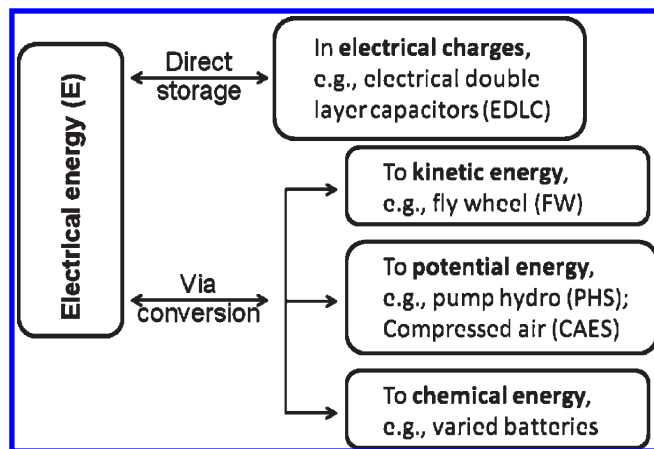


Figure 5. Classification of potential electrical storage for stationary applications.

maintenance and safety requirements for utility assets and for a low life-cycle cost. Given the amount of stored energy, safety is also an important issue. Many electric energy storage technologies, especially those that operate electrochemically, have the potential to release their energy rapidly if the structure fails, or certain temperature limits are exceeded. An uncontrolled energy release can range from a thermal runaway event that simply drains the storage system of its energy to an explosive discharge of energy. Better safety and reliability require the use of inherently safe materials/chemicals and better engineering of the storage systems against rapid, explosive releases of energy.

The aforementioned technical and economic considerations offer guides for the stationary applications and particular targets for some applications. There is still a need to develop the entire requirement matrices for every application or market.

## 2.2. Potential Technologies

Given the aforementioned requirements, a number of technologies can be potential candidates for renewable energy and utility applications. These technologies can be classified into two groups, as shown in Figure 5, depending on how the electrical energy is

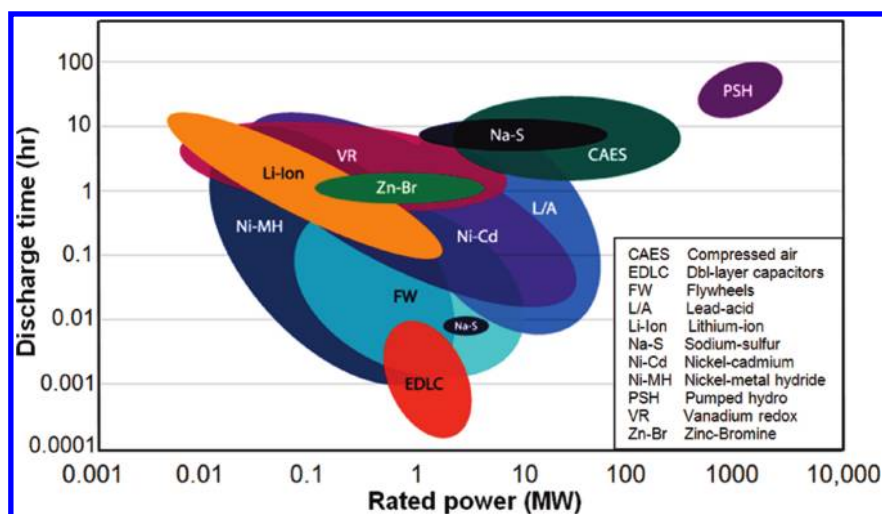


Figure 6. Power ratings and discharge times (i.e., energy ratings) of varied technologies<sup>23,24</sup> (Courtesy of Electrical Storage Association (ESA)).

stored. The first group of technologies stores electricity directly in electrical charges. Typical examples are capacitors or supercapacitors that are highly efficient (close to 100%) but have a low energy density and discharge typically in a short period of time (e.g., a few seconds). As such, these technologies are used for power management (e.g., frequency regulation). The power and energy ratings (or discharge times) of capacitors are shown in Figure 6, along with those of other technologies. The capacitance technologies have been demonstrated for grid power applications.<sup>21</sup>

Alternatively, electrical energy can be stored by converting electrical energy to another form of energy that can be kinetic, potential, or chemical energy. Typical examples involving conversion to kinetic energy are flywheels (FWs), which are mechanical devices that store energy by spinning their rotors at high speeds. The stored energy is directly proportional to the square of the speed and can be converted back to electrical energy by slowing down. The storage via conversion into kinetic energy offers high power but low energy. Like the direct storage technologies, FWs are typically useful for power management but are not truly energy storage devices. The first 1 MW system developed by Beacon Power completed the Independent System Operator (ISO) New England pilot testing for frequency regulation in September 2008 and currently is in service since November 2008.<sup>22</sup> FW is becoming a mature technology for grid power applications.

Electrical storage via potential energy, such as pumped hydro and possibly compressed air energy storage (CAES), can be an attractive option for bulk energy storage reaching up to GW levels. With a low life cycle cost, a number of pumped hydro storage (PHS) plants have been built and operated worldwide. The first PHS plant was built in Europe in the 1890s, and currently, the United States has 38 plants installed, supplying 19 GW of electricity.<sup>25</sup> But PHS is limited by site selection and requires a large initial investment and long construction periods up to 7 or 8 years as well as a reaction time up to 10 min. CAES plants use off-peak electricity to compress air into an air storage system. When the grid needs additional electrical power, air is withdrawn from the store, heated, and passed through an expansion turbine driving an electrical generator. A 290-MW facility in Huntorf, Germany, has been in operation since 1978, storing energy during off-peak hours and providing spinning reserves. Another is a 110-MW facility in McIntosh, Alabama, completed in 1991 after years of construction. This unit can start up and be on line within 14 min.<sup>25</sup> There have

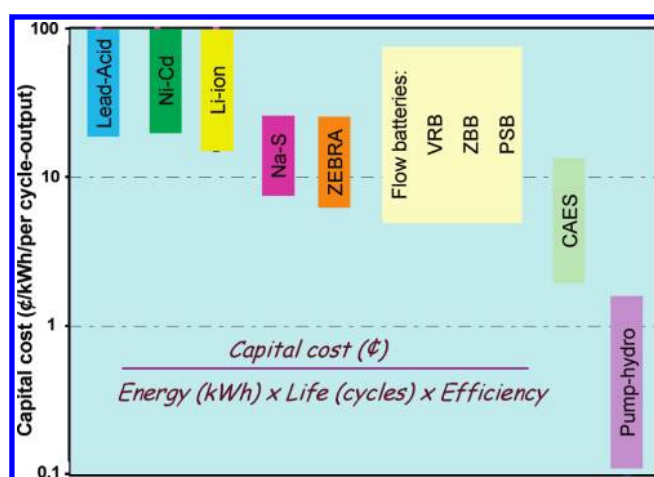


Figure 7. Comparison of varied electrical storage technologies: (a) discharge time (hours) vs power rating (MW); (b) approximation of capital cost per cycle. Note: carrying charges, operation and maintenance (O&M), and replacement costs are not included.<sup>23</sup>

been a few demonstration units, including one for the municipal utility CAES plant being developed in Iowa. However, CAES has geographic requirements such as depleted aquifers, salt domes, caverns, or other rock formations for air storage. Also, the effectiveness and economy of CAES has not yet been fully proved, and the technology is not truly “clean” because it consumes about 35% of the amount of premium fuel consumed by a conventional combustion turbine and thus produces about 35% of the pollutants on a per kWh basis when compared to it.

The largest group of technologies for stationary applications is probably electrochemical storage technologies or batteries that can efficiently store electricity in chemicals and reversibly release it according to demand. A number of battery technologies were developed for varied applications over the last century. Some of these have been demonstrated for grid applications. Among the earliest is the lead-acid battery that has dominated the market share in the past century. The largest installation is a 10-MW/40-MWh flooded lead-acid system that was built in 1988 in Chino, CA, which is used for load leveling at the Chino substation of Southern California Edison Company. In addition, a few other systems with

**Table 1. Technology Comparison of Potential Batteries<sup>a</sup> for Utility Applications<sup>13,23,26,27</sup>**

type	open circuit voltage (V)	specific energy (Wh/kg)	operating temperature (°C)	discharge time	self-discharge % per month (@20 °C)	cycle life (deep cycles)	round-trip DC energy efficiency (%)
LAB	2.1	25–40	−40–60	up to 8 h	4–50	1000	50–75
NCB	1.35	30–45	−10–45	up to 4 h	5–20	2000	55–70
VRB	1.4	10–20	10–40	4–12 h	3–9	5000	65–80
LCB	2.1	25–40	−40–60	up to 4 h		3000	
Na–S	2.1	150–240	300–350	4–8 h	negligible	4000	75–90
ZEBRA	2.6	95–120	300–350	4–8 h	negligible	3000	75–90
C-LC	3–4	155	−25–40	up to 4 h	2	1000	94–99
LT-LFP	1.7	50–70	−25–40	up to 4 h	2	4000	94–99

<sup>a</sup>LAB: lead-acid batteries; NCB: nickel–cadmium batteries; VRB: all-vanadium redox flow batteries; LCB: lead–carbon ultrabatteries; Na–S: sodium–sulfur batteries; ZEBRA: Zeolite Battery Research Africa; C-LC: Li-ion batteries of C anode and LiCoO<sub>2</sub> cathode; LT-LFP: Li-ion batteries of Li<sub>4</sub>Ti<sub>5</sub>O<sub>12</sub> anode and LiFePO<sub>4</sub> cathode.

power from 3 to 10 MW were also installed in Hawaii, Puerto Rico, and Germany. The primary advantage of the lead-acid batteries is their low capital cost and easy availability. The battery demonstrated the value of stored energy in the grid, but its limited cycling capability, along with high maintenance, made its life-cycle cost unacceptable. Figure 7 shows the life-cycle cost of the lead-acid battery in comparison with other technologies.

Ni-metal batteries were another early electrochemical energy storage technology that was demonstrated for stationary applications. These batteries all share the same cathode (nickel oxyhydroxide in the charged state) but a different anode that can be cadmium, zinc, hydrogen, metal-hydride, or iron. A nickel–cadmium system was commissioned in 2003 in Fairbanks, Alaska, to provide 27 MW ac power for a short period of time (up to 15 min) until back generation comes online. The Ni-metal batteries are susceptible to overcharge, and their direct current DC-to-DC round-trip efficiency is low (<70%, round-trip efficiency). For the Ni-cadmium in particular, cadmium is toxic and considered a serious environmental hazard that has to be handled with special disposal means. The use of high-cost metals makes it difficult to meet the cost targets for the stationary markets.

Recently, interest has been growing in technologies developed in the past few decades because of the high costs and limited performance of the early technologies. Systems up to multi MWs/MWhs have been demonstrated for redox flow batteries and sodium–sulfur batteries. Even Li-ion batteries that have been widely developed for mobile electronic and vehicle applications were stacked to a few MW levels for grid demonstration. Besides, a lead–carbon battery, a derivative of lead-acid by hybridizing with carbon super capacitors, is being demonstrated as well at large scales for the stationary markets.

Overall, however, most existing technologies cannot meet the economic requirements for most, if not all, utility markets even without accounting for carrying charges, operation/maintenance (O&M), and replacement costs. Particularly, ESSs for energy applications compared to power applications are probably facing even more challenges to meet economic targets for broad market penetration. With the exception of PHS and possible CAES, all others are higher than the target for broad market penetration (refer to Figure 7). The high cost is related to unsatisfactory performance and the high cost of raw materials and fabrication as well as the scale of production. Thus, cost reduction must rely on advances in technology to improve reliability, cycle life, efficiency, use of less expensive materials, etc. Some general

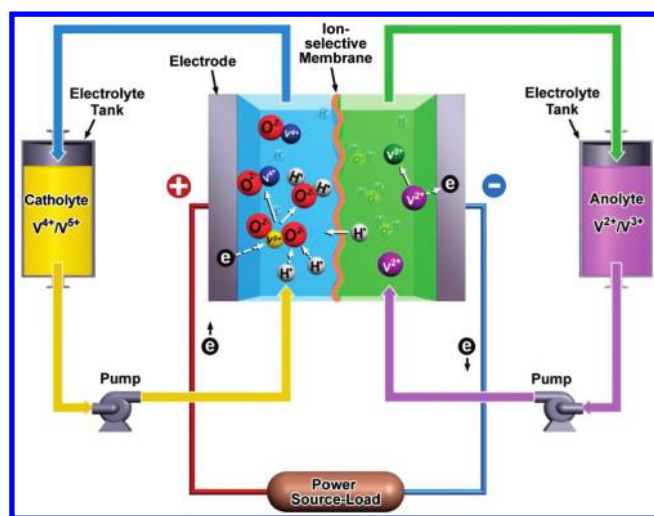


**Figure 8.** Schematic of an all vanadium redox flow battery as an example of redox flow batteries (or regenerative fuel cells).

performance characteristics of the existing technologies are summarized in Table 1.

To help the research community obtain a better understanding of stationary EESs, a relatively new area, and accelerate development efforts, we offer a comprehensive review on electrochemical energy storage technologies or batteries. This includes principles of operation as well as the status and challenges in materials, chemistries, and technologies. While there is no intention to cover all potential technologies, this paper focuses on redox flow, Na-solid oxide electrolyte, and Li-ion and lead–carbon batteries to illustrate the needs of research and development.

### 3. REDOX FLOW BATTERIES

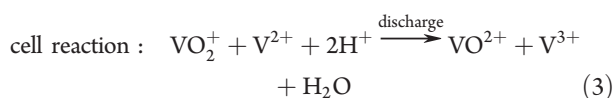
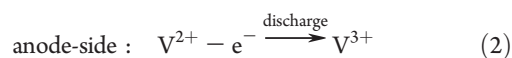
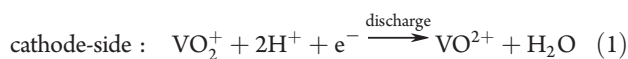
A redox flow battery (RFB), as schematically shown in Figure 8, is a type of rechargeable battery that stores electrical energy, typically in two soluble redox couples contained in external electrolyte tanks sized in accordance with application requirements. Liquid electrolytes are pumped from storage tanks to flow-through electrodes where chemical energy is converted to electrical energy (discharge) or vice versa (charge). The electrolytes flowing through the cathode and anode are often

different and are referred to as anolyte and catholyte, respectively. Between the anode and cathode compartments is a membrane (or separator) that selectively allows cross-transport of nonactive species (e.g.,  $H^+$ ,  $Cl^-$ ) to maintain electrical neutrality and electrolyte balance. Unlike traditional batteries that store energy in electrode materials, RFBs are more like regenerative fuel cells in which the chemical energy in the incoming fuels is converted into electricity at the electrodes. As such, the power and energy capacity of an RFB system can be designed separately. The power (kW) of the system is determined by the size of the electrodes and the number of cells in a stack, whereas the energy storage capacity (kWh) is determined by the concentration and volume of the electrolyte. Both energy and power can be easily adjusted for storage from a few hours to days, depending on the application, which is another important advantage for renewable integration. In addition, simplicity in cell and stack structure allows for building large systems based on module design. Also, the liquid electrolyte and intimate interfaces with electrodes make a quick response (in a matter of subseconds) possible for utility applications.

The RFB can be traced back to the zinc-chlorine system that was developed in 1884 by Charles Renard and used to power his airship "La France".<sup>28,29</sup> In this system, chlorine was generated by an onboard chemical reactor containing chromium trioxide and hydrochloric acid. The modern RFBs were first developed in the 1970s when the iron-chromium (Fe/Cr) redox flow battery was invented by Lawrence Thaller at National Aeronautics and Space Administration (NASA, USA).<sup>30–32</sup> Since then, a number of other RFB chemistries were reported or developed.<sup>33,34</sup> These RFBs can be classified as follows according to the anolyte and catholyte chemistries: all vanadium redox flow batteries (VRBs), polysulphide/bromine flow batteries (PSBs), iron/chromium flow batteries (ICB), zinc/bromine flow batteries (ZBB), vanadium/cerium flow batteries, soluble lead-acid batteries (refer the lead-carbon section), etc. Among the RFBs, VRB, ZBB, ICB, and PSB have been demonstrated at a few hundred kW and even multi-MW levels. In the following discussion, the VRB, as a model system, will be explained in terms of operational principles, key materials, chemistries and components, along with status and challenges of the technology. That will be followed by a brief overview of other flow batteries.

### 3.1. All Vanadium Redox Flow Batteries

VRBs exploit the capability of vanadium to exist in solution in four different oxidation states and use this property to make a flow battery that has only one active element in both anolyte and catholyte (see Figure 8). As such, the cross-contamination of the anolyte and catholyte in VRBs is significantly diminished. In a VRB, the energy conversions are realized via changes in vanadium valence states through the following electrode reactions:



The overall electrochemical reaction gives a cell voltage of 1.26 V at 25 °C and unit activities (i.e., standard voltage).

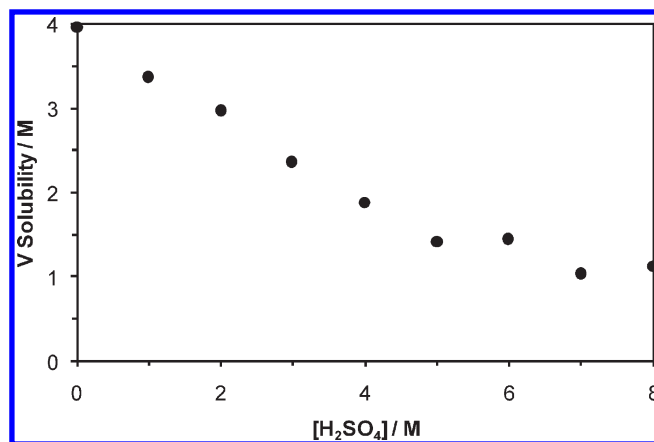


**Figure 9.** Dependence of the solubility of the V(IV)-H<sub>2</sub>SO<sub>4</sub> solution on the H<sub>2</sub>SO<sub>4</sub> concentration at 25 °C.<sup>47</sup>

The chemistry of vanadium redox couples was first studied with cyclic voltammetry (CV) by NASA researchers in the 1970s.<sup>35</sup> The operational VRB was invented and pioneered by Maria Skyllas-Kazacos and co-workers at the University of New South Wales.<sup>36–38</sup> They successfully demonstrated the first ever VRB in the late 1980s.<sup>39</sup> Since then, research and development activities have been increasing around the world. As a promising technology for storing intermittent renewable energy,<sup>40–45</sup> VRB systems (VRB-EES) up to multi-MW/MWhs have been demonstrated. The largest system installed is a 4.0-MW/6.0-MWh VRB on a 32-MW Tomamae Wind Villa farm on the northern island of Hokkaido in Japan. This system delivered a pulse power of 6 MW for up to 30 s for wind power regulation.

**3.1.1. Electrolytes.** In a VRB, the anolyte is a solution of V(III)/V(II), and the catholyte is a solution of V(V)/V(IV). H<sub>2</sub>SO<sub>4</sub> has been the most-used supporting electrolyte in both the anolyte and catholyte. The concentration of vanadium and total SO<sub>4</sub><sup>2-</sup> is usually controlled at less than 2 and 5 M, respectively, because of the stability of vanadium species and the solubility of VOSO<sub>4</sub> (as starting electrolytes). The solution of V(IV) ions is prepared by dissolving VOSO<sub>4</sub> in H<sub>2</sub>SO<sub>4</sub> solutions. The solubility of VOSO<sub>4</sub> has been confirmed to decrease with increasing H<sub>2</sub>SO<sub>4</sub> concentration,<sup>46</sup> as shown in Figure 9.<sup>47</sup> The solubility of VOSO<sub>4</sub> increased with temperature, and the effect was more significant at a lower H<sub>2</sub>SO<sub>4</sub> concentration.<sup>46</sup>

In the media of H<sub>2</sub>SO<sub>4</sub>, less than 4 M of V(IV) was reported to exist in noncomplexing acidic solutions as the blue oxovanadium ion [VO(H<sub>2</sub>O)<sub>5</sub>]<sup>2+</sup> (an aqua cation of VO<sup>2+</sup>),<sup>48,49</sup> and its radius is roughly estimated as 0.28 nm based on crystallographic data (V–O interatomic distance for VO<sup>2+</sup> plus radius of O<sup>2-</sup>).<sup>47</sup> The structure was described as a tetragonal bipyramid with four equatorial waters having a residence time of 1.35 × 10<sup>-3</sup> s and the axial water being more weakly held with a residence time of 10<sup>-11</sup> s.<sup>50</sup> Figure 10 depicts the molecular structure of V(IV) that was proved recently by a nuclear magnetic resonance (NMR) study.<sup>51</sup> The study further indicated that the structure is stable in the temperature range of –33 to 67 °C with the vanadium concentration up to 3 M. The same work also concluded that the sulfate anions are weakly bound to vanadyl ions forming the second coordination sphere of a vanadyl ion, as shown in Figure 11. These sulfate anions may affect the redox reactions of V(IV) solution by playing a role in the proton and water exchange kinetics of vanadyl ions. When the H<sub>2</sub>SO<sub>4</sub> concentration is higher than 5 M, VO<sup>2+</sup> tends to form ion pairs with anions (such as SO<sub>4</sub><sup>2-</sup> and HSO<sub>4</sub><sup>-</sup>), resulting in a larger complex.

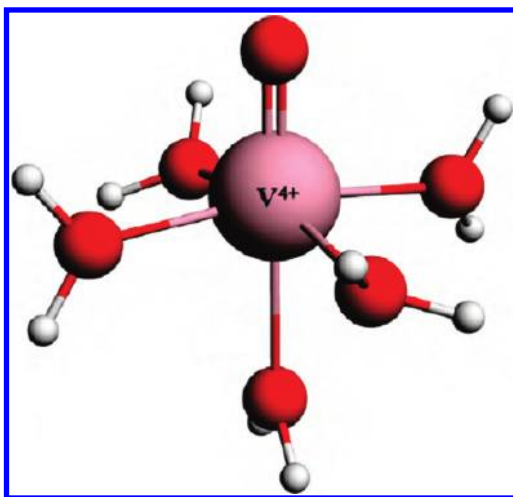


**Figure 10.** Structure of hydrated form vanadyl ion  $\text{VO}_2^{2+}$  in noncomplexing acidic solutions.<sup>48–51</sup>

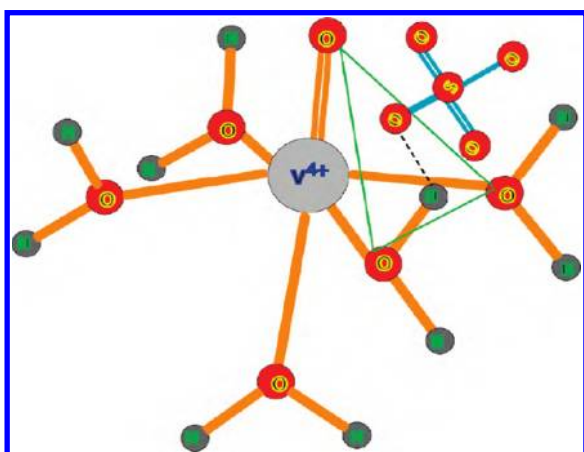


**Figure 11.** Schematic view of vanadyl ion with sulfate anions occupying second coordination sphere of the hydrated vanadyl ion. The dashed line represents the formation of new hydrogen bonds leading to proton exchange between sulfate anion and equatorial water molecule.<sup>51</sup>

In strong acid solution, the V(V) ion exists as the yellow dioxovanadium ion  $\text{VO}_2^+$  in its hydrated form of  $[\text{VO}_2(\text{H}_2\text{O})_4]^+$ .<sup>48,50</sup> This is a coordinated octahedral structure with two oxygen atoms coordinating in cis-configuration along with four complexed water molecules. Vijayakumar et al.<sup>52</sup> reported that the V(V) ions likely exist as a more stable structure of  $[\text{VO}_2(\text{H}_2\text{O})_3]^+$  (as shown in Figure 12, compound A) compared to the octahedral structure. With the increase in temperature and vanadium concentration, the compound A tends to turn to compound B, as shown in Figure 12, which eventually precipitates out as solid  $\text{V}_2\text{O}_5$  by protonation, limiting the solubility of V(V). In the solutions with high vanadium and sulfuric acid concentrations, complex species, such as  $[\text{V}_2\text{O}_3]^{4+}$ ,  $[\text{V}_2\text{O}_4]^{2+}$ ,<sup>53</sup> and complexes with sulfate and bisulfate,<sup>54,55</sup> tend to form. In concentrated  $\text{H}_2\text{SO}_4$  and  $\text{HClO}_4$ , except the dimer species, the  $\text{VO}_2^+$  ions also polymerize into chains of vanadate octahedra.<sup>56,57</sup>

The energy density of VRBs depends on the concentration of vanadium species: the higher the concentration, the higher the energy capacity. As previously discussed, however, the concentration of vanadium is limited by the precipitation of solid vanadium oxide phases. For example, increasing the concentration over 2 M in an

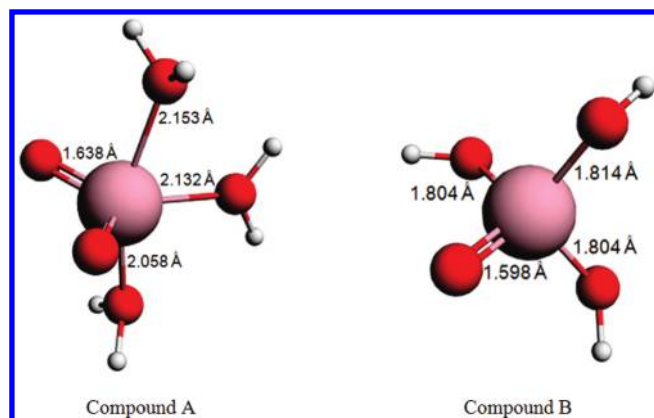


**Figure 12.** Geometry-optimized structures for  $[\text{VO}_2(\text{H}_2\text{O})_3]^+$  (compound A) and the neutral  $\text{VO}(\text{OH})_3$  (compound B).<sup>52</sup> The vanadium, oxygen, and proton atoms are represented as pink, red, and white spheres. Calculated bond lengths are indicated alongside the respective bonds.

$\text{H}_2\text{SO}_4$  supporting electrolyte led to the formation of  $\text{V}_2\text{O}_5$  precipitates in the V(V) electrolyte at a temperature above 40 °C and VO in V(II) or V(III) solutions below 10 °C.<sup>58,59</sup> The extent and rate of formation of the precipitate depend on temperature, the concentration of vanadium, and the concentration of sulfuric acid as well as the state-of-charge (SOC) of the electrolyte (ratio of V(V) to V(IV) ions).<sup>55,58,60</sup> Thus, it is important to optimize the operating conditions to improve the stability of both positive and negative solutions. Some studies reported that the stability of vanadium electrolyte with sulfuric acid could be improved to some extent by adding some organic or inorganic chemicals as stabilizing agents.<sup>61–64</sup> However, even with the positive effects of the additives, the vanadium concentration is still limited to under 2 M for most practical VRB systems in the temperature range of 10–40 °C.

The electrochemical behavior of vanadium redox couples in aqueous electrolytes is closely dependent on electrodes (to be further discussed in the next section) and operational conditions. The early work at NASA<sup>35</sup> showed a better reversibility of V(III)/V(II) than that of Cr(III)/Cr(II) on a  $\text{B}_4\text{C}$  electrode, while the V(V)/V(IV) and V(IV)/V(III) redox couples appeared irreversible. Sum and Skyllas-Kazacos reported a poor reversibility of V(V)/V(IV)<sup>65</sup> and V(III)/V(II)<sup>66</sup> redox couples at the glassy carbon electrode (area = 0.07  $\text{cm}^2$ ). One study<sup>67</sup> also found that the V(V)/V(IV) reaction turned from irreversible to reversible when the exchange current density ( $i^0$ ) was increased by 2 orders of magnitude at a graphite felt electrode. Figure 13 shows the cyclic voltammogram obtained at a glassy carbon electrode in 1 M  $\text{VOSO}_4/2$  M  $\text{H}_2\text{SO}_4$  solution with different scan rates.<sup>68</sup> The anodic peak at about 1000–1100 mV corresponds to the oxidation of V(IV) to V(V) (i.e., eq 1). The corresponding reduction peak occurs at about 700 mV during a negative scan. The anodic peak at about –400 mV and the cathodic peak at about –750 mV correspond to the oxidation and reduction of the redox couple of  $\text{V}^{2+}/\text{V}^{3+}$ , respectively (i.e., eq 2). The large peak separation between anodic and cathodic peaks (>200 mV even at a low scan rate of 100 mV/s) suggested a slow kinetics for the electrochemical reactions of both the V(V)/V(IV) and (VIII)/V(II) redox couples. Thus, electrodes are often optimized to maximize the electrochemical activity of redox electrolytes.

In a practical system, single VRB cells are electrically connected by bipolar plates (see Figure 14) to build up a voltage. To reduce electrical resistance, electrodes are often integrated with a bipolar plate into one component. The electrodes/bipolar plates,

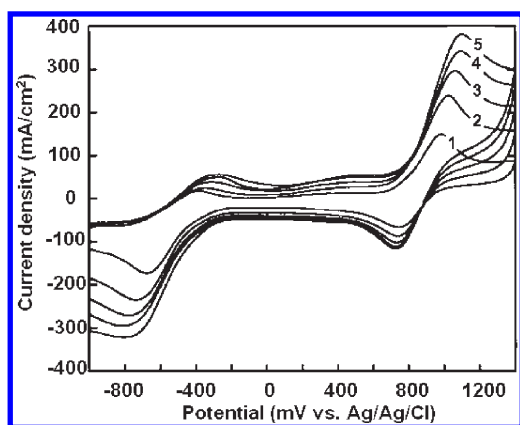


**Figure 13.** Cyclic voltammogram obtained at a glassy carbon electrode in 1 M  $\text{VOSO}_4$ –2 M  $\text{H}_2\text{SO}_4$  solution; scan rates: (1) 100, (2) 200, (3) 300, (4) 400, and (5) 500  $\text{mV s}^{-1}$ .<sup>68</sup>

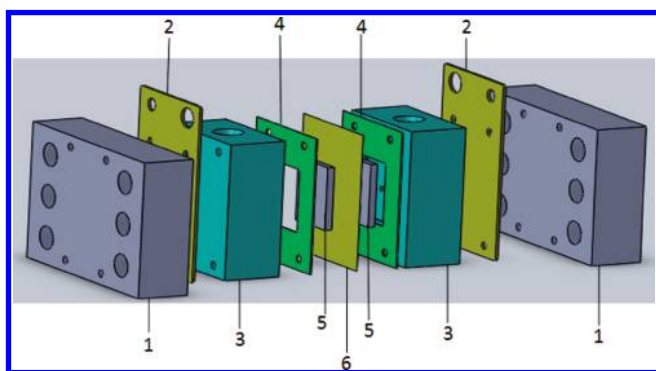


**Figure 14.** Hardware of a single all-vanadium redox flow battery. 1-end plate, 2-current collector, 3-bipolar plate, 4-gasket, 5-electrode, and 6-membrane.

along with electrolyte and membrane, are discussed in detail in the following sections.

**3.1.2. Electrodes/Bipolar Plates.** As mentioned previously, electrodes are often integrated with a bipolar plate into one component in a VRB. One early combination was graphite felts as electrodes mechanically compressed to graphite plates. The bipolar plate functions as a current collector, separating the anolyte on one side and the catholyte on the other. Additionally, it supports the porous electrode and directs the flow of electrolytes. As such, the bipolar plates are often fabricated with flow channels on both sides. They must demonstrate low bulk and contact resistance while at the same time being structurally and mechanically stable and chemically compatible with electrolytes during operation. Given the strong acidic conditions, the choices of materials are very limited. Currently, the materials used in VRBs include polymer-impregnated graphite plates, conductive carbon-polymer composites,<sup>69,70</sup> and polymer-impregnated flexible graphite.<sup>71,72</sup> The polymer-impregnated graphite plate is widely used because of its low electronic resistance and good fabricability. But its relatively high cost and brittleness may limit its practical use. In recent years, a conductive carbon-polymer composite has become an attractive alternative for the VRB bipolar plates because of its low cost, lightweight, and flexibility.<sup>69,70,73–77</sup>

For optimized performance, the electrodes are required to have a high surface area, suitable porosity, low electronic resistance, and high electrochemical activity toward the reactions

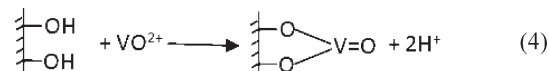
between vanadium species. Again due to the corrosive environment in a VRB, there are limited choices of materials to make electrodes. Inert, high-surface-area, graphite- or carbon-based materials in forms such as felt or porous structures have been the most common materials for electrodes.<sup>66,67,69,70,76–89</sup> However, the graphite or carbon-based electrodes often show inadequate electrochemical activity and kinetic reversibility toward the electrochemical reactions between the vanadium species.

Given that electrochemical activity closely depends on their structure, surface chemistry, surface area, etc., varied approaches have been employed to optimize the graphite or carbon electrodes for improved electrochemical properties.<sup>85,86,90–92</sup> The methods that have been developed to modify the graphite felt mainly include heat treatment,<sup>86,89,93</sup> chemical treatment,<sup>69,85,90</sup> electrochemical oxidation,<sup>92,94–96</sup> and doping by depositing other metals on carbon fibers.<sup>87,91,97</sup>

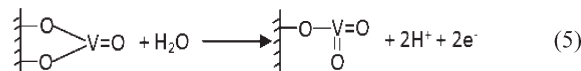
Sun and Skyllas-Kazacos<sup>86</sup> employed heat treatment at 400 °C for 30 h to improve the electrochemical activity of graphite felt. An improvement in energy efficiency of vanadium redox cells from 78% to 88% was reported. The increased activity was attributed to the increased surface hydrophilicity and the formation of the functional groups of C–O–H and C=O on the surface of the graphite felt. They suggested that the C–O groups on the electrode surface behave as active sites and catalyze the reactions of vanadium species. The proposed mechanisms for reactions are as discussed below.<sup>85,86</sup>

In the positive half cell, the electrode reaction (i.e., eq 1) involves oxygen transfer. The charging involves the following processes:

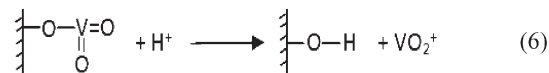
- (a) First,  $\text{VO}^{2+}$  ions transport from the solution to the electrode surface, exchange protons with phenolic groups on the electrode surface, and thus bond onto the electrode surface:



- (b) Second, electrons transfer from  $\text{VO}^{2+}$  to the electrode along the C–O–V bond, and one oxygen atom on the C–O functional group transfers to the  $\text{VO}^{2+}$ , forming a surface  $\text{VO}_2^+$ :



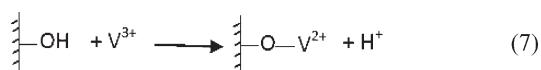
- (c) Third, the  $\text{VO}_2^+$  exchanges with an  $\text{H}^+$  from the solution and diffuses back into the bulk solution:



During discharge, the reactions are the reverse of the charge processes. The formation of the C–O–V bond facilitates the electron-transfer and oxygen-transfer processes and thus reduces the activation overpotential for the V(IV)/V(V) redox process.

In the negative half cell, the reaction (i.e., eq 2) involves electron transfer. During charging, the  $\text{V}^{3+}$  diffuses from the bulk

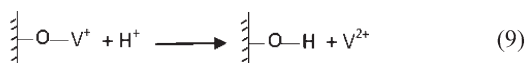
solution to the surface of the electrode and combines with the hydrogen of the phenol groups:



And then, the electrons transfer from the electrode surface to the  $\text{V}^{3+}$  along the  $-\text{C}-\text{O}-\text{V}$  bond to form  $\text{V}^{2+}$ .



Finally, the  $\text{V}^{2+}$  ions exchange with protons and then diffuse into the bulk solution:



For the discharge process, the reactions are reversed. The formation of a  $\text{C}-\text{O}-\text{V}$  bond facilitates the transfer of electrons and thus reduces the activation overpotential for the  $\text{V}^{2+}/\text{V}^{3+}$  process.

*Chemical treatment* is another method to activate carbon materials. It was found that a strongly acidic carboxyl group was formed at room temperature after the carbon was treated with  $\text{NaOCl}$ ,  $\text{KMnO}_4$ , or  $(\text{NH}_4)_2\text{S}_2\text{O}_8$  solutions. Sun and Skyllas-Kazacos<sup>85</sup> investigated the electrochemical properties of the carbon felt after it was treated with concentrated  $\text{H}_2\text{SO}_4$  or  $\text{HNO}_3$ . A significant improvement in both Coulombic and voltage efficiencies of VRB was achieved with graphite felt treated with concentrated  $\text{H}_2\text{SO}_4$ . The increased activity of the VRB was attributed to the increased concentrations of surface functional groups, such as  $\text{C}=\text{O}$  and  $\text{C}-\text{OOH}$ , that formed during acid treatment. These functional groups not only led to an increase in the hydrophilicity of the graphite felt but also behaved as active sites for the electrochemical reactions.

Additionally, Li et al.<sup>90</sup> investigated the electrochemical behavior of vanadium redox couples at the graphite felt electrode that was modified by combining acid treatment and heat treatment. The graphite felt was treated first in 98% sulfuric acid for 5 h and then kept at 450 °C for 2 h. The acid and heat synergistic effects from the process increased the  $-\text{COOH}$  functional groups on the graphite felt surface and its surface area from 0.31  $\text{m}^2/\text{g}$  to 0.45  $\text{m}^2/\text{g}$ . As a result, the electrode activity was greatly improved, which was mainly ascribed to the increase of the  $-\text{COOH}$  groups that behave as active sites, catalyzing the reactions of vanadium species and accelerating both electron and oxygen transfer processes.

*Electrochemical oxidation* was employed recently to modify the graphite felts to improve their electrochemical activity toward the electrochemical reactions between vanadium species in VRBs. Li et al.<sup>94</sup> investigated the characteristics of graphite felt oxidized electrochemically for VRBs, and Tan et al.<sup>92</sup> studied the activation mechanism of electrochemical-treated graphite felt. The studies indicated the formation of  $-\text{COOH}$  functional groups on the graphite felt, leading to an increased surface area and the O/C ratio. AC impedance data showed a reduction in resistance to the reactions of the vanadium species. The mechanism of the improvement in the electrochemical activity of graphite felt was attributed to the formation of a  $\text{C}-\text{O}-\text{V}$  bond, which facilitated the electron transfer for the reactions on both positive

and negative electrodes and the oxygen transfer for the reactions on the positive electrode.

*Metal-doping* is an alternative method for improving the electrochemical activity of carbon electrodes in VRBs. Sun et al.<sup>87</sup> reported chemical modification of graphite fibers by impregnating them in solutions containing  $\text{Pt}^{4+}$ ,  $\text{Pd}^{2+}$ ,  $\text{Au}^{4+}$ ,  $\text{Ir}^{3+}$ ,  $\text{Mn}^{2+}$ ,  $\text{Te}^{4+}$ , or  $\text{In}^{3+}$  and found that electrodes modified by  $\text{Ir}^{3+}$  exhibited the best electrochemical performance. Wang et al.<sup>91</sup> investigated the Ir-modified carbon felt as the positive electrode for vanadium redox flow batteries. The Ir-modified carbon electrode led to a reduction in the cell internal resistance and the overpotential for a  $\text{V(IV)}/\text{V(V)}$  redox reaction. The improved activity was attributed to the formation of active functional groups of Ir. However, this method is not cost-effective because it involves the deposition of Ir, a noble metal. Also, the long-term stability of deposited Ir on graphite felt in vanadium electrolyte solutions is still questionable.

**3.1.3. Membranes and Separators.** The membrane in a VRB system is a key component that separates the cathode and anode compartments while allowing the transport of charge carriers ( $\text{H}^+$ ,  $\text{SO}_4^{2-}$ , etc.) to keep its electrical neutrality. To minimize resistance and power loss, the membrane is required to have a high ionic conductivity. Also, the fast ionic transport must be highly selective: the transport of vanadium cations as active species must be minimized to reduce the capacity and energy loss. In addition, water transport across the membrane should be limited as well to maintain catholyte and anolyte balance and ease maintenance. Exposed to a strong acidic environment and strong oxidative  $\text{V}^{5+}$  ions in the positive half-cell electrolyte in VRB, the membrane must demonstrate satisfactory chemical stability. Operated with a relatively low current density (typically 50  $\text{mA}/\text{cm}^2$ ), the VRB stacks have a much larger size than those of fuel cells. As such, the mechanical and structural stability can be another challenge in practical systems. Finally, a membrane with a low cost is critically important for commercializing the technology.

Both cation and anion exchange membranes have been investigated for VRB applications. In addition to the traditional dense membrane, microporous membranes (or separators) were also explored for VRB chemistries.<sup>98,99</sup>

Among the most widely studied are probably the Nafion membranes that are commonly used in low-temperature proton exchange membrane (PEM) fuel cells. The Nafion membranes are generally highly conductive to protons and are chemically stable in strong acid and oxidation conditions.<sup>100</sup> However, the vanadium ions with different oxidation states tend to transport from one-half-cell to its opposite half-cell and react with other vanadium ions, leading to loss of cell capacity and reduction of energy efficiency in VRB systems.<sup>101–105</sup> The vanadium ion's cross-transport appears complicated because of (in part) the varied chemical coordination of vanadium ions in the solution electrolytes (described in section 3.1.1). The transport rate of the vanadium ions mainly depends on the concentrations of vanadium ions and sulfuric acid, the SOC of the electrolyte, membrane properties (such as thickness, pore size), and temperature. One study<sup>105</sup> found the diffusion coefficients of the vanadium ions across the Nafion 115 membrane on the order of  $\text{V}_2^+ > \text{VO}_2^+ > \text{VO}^+ > \text{V}_3^+$ . Besides, the water transfer across the membrane is accompanied with the transport of selective and balancing ions that carry water as well as being driven by the osmotic pressure difference between the positive and negative electrolyte solutions. The net water transfer causes the negative and positive half-cell electrolyte solutions to go out of balance,

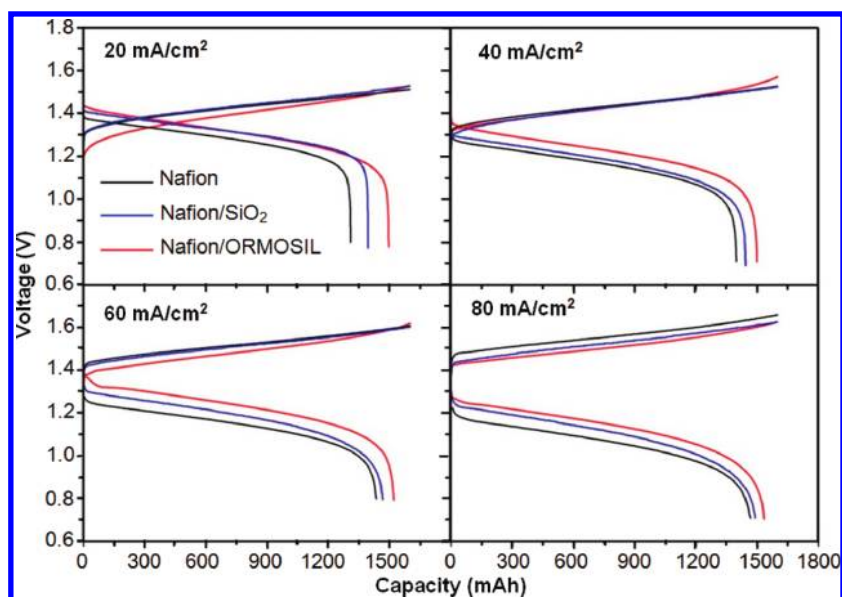


**Figure 15.** Charge–discharge curves of VRB with Nafion, Nafion/SiO<sub>2</sub>, and Nafion/ORMOSIL hybrid membranes at different current densities. The charge capacity was controlled to be 1600 mAh, corresponding to a redox couples utilization of 75%. Mixtures of 40 mL of 2 M V<sup>3+</sup>/V<sup>4+</sup> and 2.5 M H<sub>2</sub>SO<sub>4</sub> solutions were used as the starting anolyte and catholyte.<sup>82,118</sup>

resulting in a loss in the capacity of flow batteries. Efforts by Skyllas-Kazacos and colleagues in the 1990s indicated that in the case of cation exchange membranes, a large amount of water transferred with V<sub>2</sub><sup>+</sup> and V<sub>3</sub><sup>+</sup> as hydration water from the negative side to the positive side across the membrane.<sup>106–108</sup> In the case of anion membranes, a net water transfer came with the penetration of neutral VOSO<sub>4</sub> and negative VO<sub>2</sub>SO<sub>4</sub><sup>−</sup> through the membrane from the positive side to the negative side.<sup>106</sup> The water transfer appeared also to be dependent on the SOC of the electrolyte: toward the positive half-cell in 100% to 50% SOC and the negative half cell in 50% to 0% SOC.<sup>109</sup> The most significant level of water transfer occurred during overdischarging.<sup>109</sup> A similar observation was confirmed during a recent study that also indicated an important role of osmosis on the water transfer across a Nafion membrane.<sup>105</sup>

To improve their selectivity and minimize the cross-water and vanadium transport, varied approaches were taken to modify the membranes. The early work was carried out by Skyllas-Kazacos and colleagues, starting in the 1990s.<sup>98,107,110–114</sup> One way was to make Nafion-based hybrid membranes. The reported hybrid structures include a Nafion/pyrrole membrane,<sup>115</sup> a Nafion/sulfonated poly(ether ether ketone) (SPEEK) layered composite membrane,<sup>116</sup> a Nafion/polyethylenimine (PEI) composite membrane,<sup>117</sup> and a Nafion-(polycation poly(diallyldimethylammonium chloride-polyanion poly(sodium styrene sulfonate) [PDDA-PSS]<sub>n</sub>) membrane.<sup>104</sup> The last one is a multilayer composite Nafion membrane made by alternate adsorption of PDDA and PSS where “n” is the number of multilayers. The hybrid membranes led to a reduced permeability of vanadium ions and improved Coulombic efficiencies and energy efficiencies of the VRB cells over the Nafion membranes.

Alternatively, Nafion membranes were furnished with non-organic layers. An in situ sol–gel method was employed to synthesize Nafion/SiO<sub>2</sub><sup>82</sup> and a Nafion/organically modified silicate (Nafion/ORMOSIL)<sup>118–119</sup> hybrid membrane. Tests on the synthesized membranes in the VRB cells observed vanadium ion permeability that was greatly minimized compared to the Nafion 117 membrane. As shown in Figure 15, the sulfate VRBs with the

Nafion/ORMOSIL membrane exhibited the highest discharge capacity and voltage, while the one with the unmodified Nafion membrane was the lowest.<sup>82,118</sup> Teng et al.<sup>120</sup> synthesized and evaluated a composite membrane from a Nafion and organic silica-modified TiO<sub>2</sub> (Nafion/Si/Ti hybrid membrane). Tests found both a lower permeability of vanadium ions and water across the Nafion/Si/Ti hybrid membrane than that of the unmodified Nafion membrane. The use of the composite membrane led to a slightly higher columbic and energy efficiency of VRB cells over those with the Nafion 117 membrane. Additionally, Sang et al.<sup>121</sup> fabricated and characterized the Nafion 1135/zirconium phosphate (ZrP) hybrid membranes with the impregnating method. The ZrP hybrid membrane demonstrated a diffusivity of VO<sup>2+</sup> that is an order of magnitude lower than that of the unmodified Nafion membrane.

Besides the aforementioned cation membranes, others that have been investigated recently for VRBs include (1) the polyethylene (PE-X) membrane and the asymmetric membrane (MH-X),<sup>122</sup> (2) the sulfonated poly(arylene thioether ketone) (SPTK) and sulfonated poly(arylene thioether ketone) (SPTKK) membranes,<sup>123</sup> (3) the poly(vinylidene fluoride) (PVDF)-based,<sup>101,124,125</sup> poly(tetrafluoroethylene) (PTFE)-based,<sup>126</sup> and poly(ethylene-co-tetrafluoroethylene) (ETFE)-based<sup>127</sup> fluorinated or partly fluorinated membranes, (4) the sulfonated poly(phenylsulfone) membrane,<sup>128</sup> and (5) the sulfonated poly(flourenyl ether ketone) (SPFEK)<sup>129</sup> and SPEEK<sup>130,131</sup> based nonfluorinated membranes. All of these membranes exhibited more or less improvement in VRB performance. For example, a novel sandwich-type composite membrane made from a layer of polypropylene membrane between two layers of SPEEK/tungstophosphoric acid (TPA) membrane led to stable VRB performance, as shown in Figure 16, over 80 cycles (>350 h).<sup>130</sup> The improved performance was attributed to the reduction in vanadium cross-transport and a good chemical stability in the strong acidic and oxidative vanadium solutions.

In addition to the cation membranes, anion exchange membranes were also investigated for applications in VRB systems. Rychcik et al.<sup>88</sup> first reported a sulphonated polyethylene

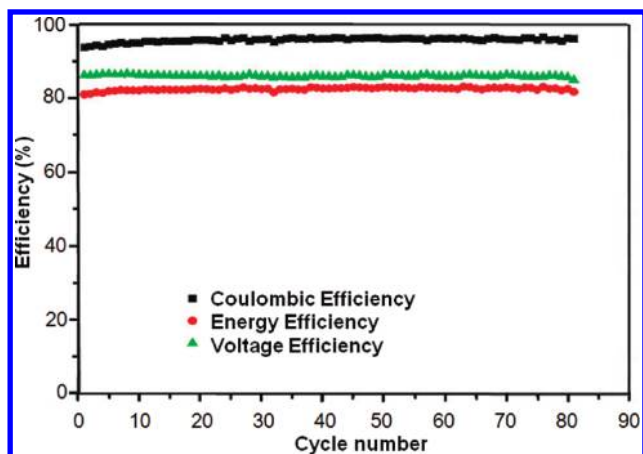


**Figure 16.** The cycle performance for a VRB single cell with a SPEEK/TPA/polypropylene (PP) membrane at the current density of 35.7 mA/cm<sup>2</sup>. Carbon felt with an active area of 28 cm<sup>2</sup> served as electrode materials for both negative and positive sides. The negative and positive electrolytes consisted of 1.5 mol L<sup>-1</sup> VOSO<sub>4</sub> in 2.0 mol L<sup>-1</sup> H<sub>2</sub>SO<sub>4</sub>.<sup>130</sup>

membrane that allowed the cross-transport of SO<sub>4</sub><sup>2-</sup>, HSO<sub>4</sub><sup>-</sup>, neutral VOSO<sub>4</sub>, and VO<sub>2</sub>SO<sub>4</sub><sup>-</sup>. To reduce the permeability of the vanadium ions and water, the anion exchange membranes were modified by cross-linking or incorporating cation exchange groups, resulting in improved performance and energy efficiency of VRBs.<sup>102,111,132</sup> Other anion membranes explored include the quaternized poly (phthalazinone ether sulfone ketone) (QPPEK)<sup>133</sup> and poly (phthalazinone ether sulfone ketone) (QPPE).<sup>134</sup> The QPPEK membrane demonstrated a good chemical stability in the VO<sub>2</sub><sup>+</sup> solutions for 20 days. The results of VRB single-cell tests showed a higher energy efficiency (88.3%) from the cell with the QPPEK membrane than that with the Nafion 117 membrane (82.9%).<sup>133</sup> Qiu et al.<sup>135</sup> prepared an ETFE-based anion exchange membrane (AEM) to reduce the permeability of vanadium ions in vanadium redox flow batteries. Experimental results indicated a high ion exchange capacity, lower area resistance, and much lower vanadium ion permeability of the ETFE-based AEM membranes compared to the Nafion 117 membranes.

Another type of potential membrane for VRBs is the Daramic membranes or separators that are characterized with a low electrical resistance but a high puncture resistance. In comparison with the Nafion membranes, the porous separators generally demonstrate higher ionic transport, but their selectivity is relatively lower. To minimize the permeability of vanadium ions, the Daramic separators were modified and optimized for VRBs.<sup>98,100,107,110,112,113,136</sup> For example, the Daramic/Nafion composite separator/membrane was made by soaking a Daramic separator in a 5-wt% Nafion solution.<sup>136</sup> The composite separator exhibited a low area resistance and suppressed the vanadium ions' permeability for VRBs. The improved properties, along with the significant advantage of a low cost over the traditional membrane, make the porous separators attractive for the flow batteries. However, there remain challenges in the cross-transport of vanadium species and chemical stability in the highly oxidative V<sup>5+</sup> electrolytes.

**3.2. Other RFB Chemistries.** In addition to the all-vanadium redox couples, there are a number of others that can be potentially combined into an RFB. Figure 17 compiles varied redox couples and their standard potentials (except the H<sup>+</sup>/H<sub>2</sub> couple

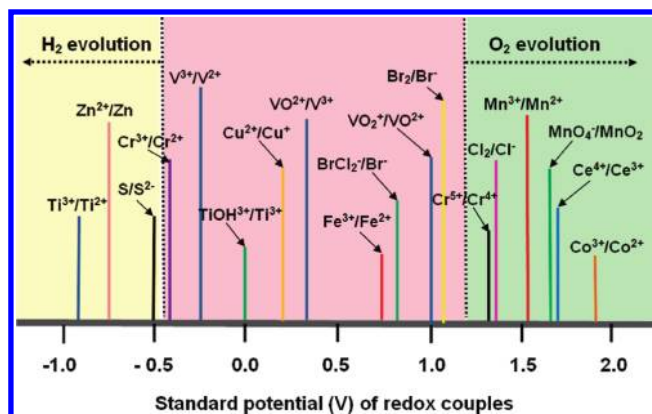
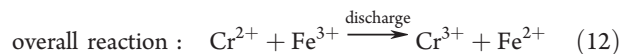
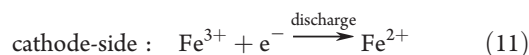
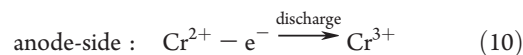


**Figure 17.** Standard potentials (verse the standard hydrogen electrode) of redox couples,<sup>149</sup> except the H<sub>2</sub> evolution potential that is the overpotential on carbon electrodes.

that is based on the overpotential on carbon electrodes). Their combinations for a useful voltage are, however, limited by hydrogen and oxygen evolutions in an aqueous system. In addition to VRBs, other flow battery chemistries that were explored include V<sup>2+</sup>/V<sup>3+</sup> vs Br<sup>-</sup>/ClBr<sub>2</sub><sup>-</sup>,<sup>137-139</sup> Br<sub>2</sub>/Br<sup>-</sup> vs S/S<sup>2-</sup>,<sup>13,34,140</sup> Fe<sup>3+</sup>/Fe<sup>2+</sup> vs Cr<sup>3+</sup>/Cr<sup>2+</sup>,<sup>141,142</sup> Br<sup>-</sup>/Br<sub>2</sub> vs Zn<sup>2+</sup>/Zn,<sup>143,144</sup> Ce<sup>4+</sup>/Ce<sup>3+</sup> vs V<sup>2+</sup>/V<sup>3+</sup>,<sup>145</sup> Fe<sup>3+</sup>/Fe<sup>2+</sup> vs Br<sub>2</sub>/Br<sup>-</sup>,<sup>146</sup> Mn<sup>2+</sup>/Mn<sup>3+</sup> vs Br<sub>2</sub>/Br<sup>-</sup>,<sup>147</sup> Fe<sup>3+</sup>/Fe<sup>2+</sup> vs Ti<sup>4+</sup>/Ti<sup>3+</sup>,<sup>148</sup> etc.<sup>33</sup> Among these RFBs that were not all vanadium, PSBs with Br<sub>2</sub>/Br<sup>-</sup> vs S/S<sup>2-</sup> redox couples, ICBs with Fe<sup>3+</sup>/Fe<sup>2+</sup> vs Cr<sup>3+</sup>/Cr<sup>2+</sup>, and ZBBs with Br<sup>-</sup>/Br<sub>2</sub><sup>-</sup> vs Zn<sup>2+</sup>/Zn were also demonstrated at scales up to 100 kW and even MW levels. These demonstrated flow batteries are briefly reviewed in the following sections.

In the early 1970s, Thaller at NASA invented an electrochemical storage system that employs the redox couples of Fe<sup>3+</sup>/Fe<sup>2+</sup> and Cr<sup>3+</sup>/Cr<sup>2+</sup> in an acid medium (usually hydrochloric acid solution) as catholyte and anolyte, respectively.<sup>31,32,150</sup> The ICB was the earliest storage device that used two fully soluble redox couples that were pumped through a power conversion cell. During the 1970s<sup>32,151</sup> and 1980s,<sup>152-154</sup> a systematic work was carried out by NASA on the ICB system. The electrode and cell reactions are as follows:



The cell reaction offers a standard voltage of 1.18 V. The ICB operates with either a cation or anion exchange membrane/separator and typically employs carbon fiber, carbon felt, or graphite as electrode materials. The Fe<sup>3+</sup>/Fe<sup>2+</sup> redox couple exhibits a very high reversibility and fast kinetics on the carbonaceous electrodes (carbon or graphite). In comparison, the Cr<sup>3+</sup>/Cr<sup>2+</sup> redox couple shows a relatively slow kinetics with the electrode materials. Thus, catalysts were employed for the Cr<sup>3+</sup>/Cr<sup>2+</sup> redox couple to enhance its electrode kinetics.<sup>150,155</sup> Additionally, it is desirable that these catalysts have a high overpotential for hydrogen to mitigate hydrogen evolution during the reducing process of Cr<sup>3+</sup> to Cr<sup>2+</sup>. The hydrogen evolution appears to be a competitive reaction to the Cr<sup>3+</sup>/Cr<sup>2+</sup>

**Table 2. Technical Comparison of All Vanadium VRB with Other Chemistries**<sup>13,23,24,176</sup>

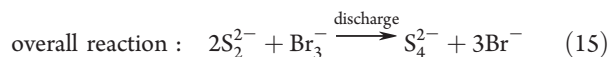
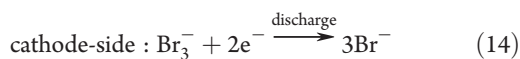
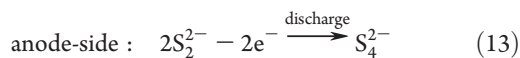
type	open circuit voltage (V)	specific energy (Wh/kg)	characteristic discharge time, hours	self-discharge % per month, at 20 °C	cycle life (cycles) <sup>c</sup>	round-trip DC energy efficiency
VRB	1.4	15 (29) <sup>a</sup>	4–12	5–10	5000	70–80%
PSB	1.5	20 (41)	4–12	5–10	2000	60–70%
ICB	1.18	<10	4–12		2000	70–80% <sup>b</sup>
ZBB	1.8	65 (429)	2–5	12–15	2000	65–75%

<sup>a</sup>Theoretical specific energy. <sup>b</sup>Depending on operating temperatures. <sup>c</sup>Commonly reported cycle numbers under deep charging/discharging, usually 20–80% SOC.

anode during charging. Catalysts including Au,<sup>155</sup> Pb,<sup>156</sup> Tl,<sup>157</sup> Bi,<sup>158</sup> or their compounds were studied. The deposition of Pb and Bi on the electrode surface in HCl solutions not only enhanced the rate of the Cr<sup>3+</sup>/Cr<sup>2+</sup> reaction but also increased the hydrogen overpotential.<sup>155</sup> Lopez-Atalaya et al.<sup>155</sup> investigated the behavior of the Cr<sup>3+</sup>/Cr<sup>2+</sup> reaction on gold-graphite electrodes and concluded that the use of gold as a catalyst for Cr<sup>3+</sup>/Cr<sup>2+</sup> in an Fe/Cr redox cell is unnecessary for the acceptable behavior of the cell. An outstanding issue with the early ICBs was the cross-transport of iron and chromium active species. A significant reduction in the cross-transport was achieved by using mixed electrolytes at both the cathode and anode sides.<sup>159</sup> The mixed electrolytes allowed for the use of a cost-effective microporous separator, leading to a reduction in resistance.<sup>160</sup> The single cells demonstrated much improved performance at 65 °C.

There were extensive attempts<sup>141,142,153,161–166</sup> to optimize and scale-up the ICB system for the applications in energy storage. NASA licensed its Fe/Cr flow battery technology to Sohio (Standard Oil of Ohio, Cleveland, OH) in the mid 1980s and that was later bought by British Petroleum. Currently, Deeya Energy of California is developing ICBs at relatively small scales as backup powers. Enervault of California is supported by DOE in developing and demonstrating multi-MW systems for grid applications.

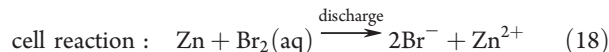
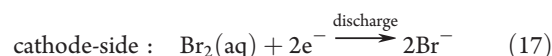
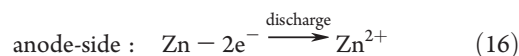
PSBs employ electrolytes of sodium bromides and sodium polysulfides.<sup>13,34,140</sup> These chemicals are abundant and soluble in aqueous media and are of reasonable cost. A standard cell voltage of 1.36 V is given by the following electrochemical reactions:



During the charging cycle, the bromide ions are oxidized to bromine and complexed as tribromide ions in the cathode side; the soluble polysulfide anion is reduced to sulfide ion in the anode side. On discharge, the sulfide ion is the reducing agent, and the tribromide ion is the oxidizing agent. The open-circuit cell voltage is around 1.5 V, depending on the activity of the active species. The electrolyte solutions are separated by a cation-selective membrane to prevent the sulfur anions from reacting directly with the bromine, and the electrical balance is achieved by transporting Na<sup>+</sup> across the membrane. Nafion membranes were used in PSB cells.<sup>34,167</sup> Electrodes reported were made from materials including high-surface-area carbon/graphite, a nickel foam, and even sulfide nickel.<sup>168–171</sup>

The full concept of PSB was documented by Zito,<sup>172</sup> an independent inventor in North Carolina, who assigned his invention rights to Regenesys Technologies Ltd. (RGN), a wholly owned company of Innogy of UK. The company developed systems with ratings from kWh to MWh, including a 1-MW station installed and tested at the Aberthaw Power Station in South Wales, UK. A 15-MW/120-MWh system with a round-trip efficiency of 60–65% had been planned before RGN was bought by VRB Power Systems in 2006.<sup>34</sup>

In addition to the traditional RFBs, ZBBs (invented 100 years ago<sup>173</sup>) are often classified with the redox flow battery categories. The charge and discharge of the ZBB cells proceed via the following electrode reactions:



The cell reaction gives a standard voltage of 1.85 V. The ZBB employs an aqueous solution of zinc bromides that is added with agents.<sup>143,144</sup> During operations, the electrolyte is pumped through positive and negative electrode surfaces that are separated by a microporous plastic film as the separator, or alternatively, there is an ionic membrane that selectively allows the transport of zinc and bromide but not the aqueous bromine, polybromide ions, or complex phase. At the positive cathode, bromide ions are converted to bromine during charging or vice versa during discharging. Complexing agents are used to reduce the evolution of bromine that is a serious health hazard. At the negative anode, zinc is reversibly deposited from the ions. Thus, ZBBs are not truly redox batteries and are often referred as a “hybrid” RFB. The power/energy relationship of a ZBB is more fixed than that of the traditional redox flow systems because its total available energy is limited by the available electrode area for plating zinc. The electrodes are generally made from high-surface-area, carbon-based materials.<sup>174,175</sup>

ZBB cells, which have a high degree of reversibility, offer a higher voltage and energy density than do VRBs and PSBs (see Table 2). Also of interest are the abundant, low-cost chemicals that are employed in the flow batteries. In a well-designed system and in consistently manufactured systems, the DC-DC efficiency can be up to 70–75%. In the mid-1980s, Exxon licensed the technology to a number of companies that included Johnson Controls, JIC, who in 1994 sold their interest to ZBB Energy Corporation. Since then, ZBB has developed 50-kWh and 500-kWh systems based on a 50-kWh battery module. Meidisha, another company that licensed Exxon's technology, demonstrated a 1-MW/4-MWh ZBB battery

in 1991 at Kyushu Electric Power Company in Japan.<sup>13</sup> In the United States, a 400-kWh system was installed in Lum, Michigan, by Detroit Edison for load management.<sup>25</sup> In addition to ZBB, Premium Power is supported by DOE in developing and demonstrating a multi-MW system for renewable integration.

Performance parameters of the aforementioned major FRB technologies are compared in Table 2.

**3.3. Challenges and Future R&D Needs for RFBs.** With all the stated advantages and the successful demonstration of systems up to MWh levels, all RFB technologies have, however, not seen broad market penetration. The current technologies are still expensive in capital cost and life-cycle cost. A VRB, for example, has operating cost about \$500/kWh or higher,<sup>177</sup> which is obviously still too high for broad market penetration. The high cost is attributed to the high cost of materials/components and performance parameters, including reliability, cycle/calendar life, energy efficiency, system energy capacity, etc. While the all vanadium redox couples demonstrate excellent electrochemical reversibility, the vanadium cost is high with the price fluctuating from \$7 to \$14 per pound. Another expensive component is the Nafion-based membranes that also need further improvement in selectivity and chemical stability. The high reactivity of  $V^{5+}$  as a strong oxidant makes it challenging to select materials in terms of the long-term durability in VRBs. Hydrocarbon and anion membranes/separators are potential alternatives to the Nafion membranes. However, these materials must demonstrate adequate ionic conductivity, selectivity, and chemical stability in the strong acidic and oxidative solutions of vanadium. It is critical to further optimize materials and develop advanced materials, along with cell/stack engineering and design, to further reduce cost and improve performance.

Other flow chemistries, such as ZBB, ICB, PSB, etc., have potential advantages in using more cost-effective materials/components. Issues in performance, reliability, and durability still remain. For example, an ICB requires suitable catalysts to improve the electrochemical activity of the  $Cr^{3+}/Cr^{2+}$  electrode. ZBB development has been hindered by issues related to the formation of zinc dendrites upon deposition and the high solubility of bromine in the aqueous zinc bromide electrolyte.<sup>178</sup> A uniform current distribution is preferred to mitigate dendrite growth. In addition, any system, such as ZBBs, involving the evolution of hazardous gases may lead to health and environmental concerns.

The current RFBs are mainly operated in an aqueous electrolyte. To avoid gas evolution, their operation voltage, and thus their energy density, are limited (refer to Figure 15). While not critical to some stationary markets, increasing the energy capacity of electrolytes would reduce the system footprint and the use of materials, cutting down the overall system cost. Attempts have been made to search for new redox couples and electrolytes that can lead to new RFBs with improved energy density and performance over the existing technologies. The General Electric (GE) Global Research Center is currently supported by DOE in investigating organic flow chemistries.

In addition to materials/components and electrolyte chemistries, cell, stack, and system design and engineering are critical to improve the performance and economy of the RFB technologies. A major issue in dealing with RFBs is the shunt or parasitic currents that lead to self-discharge and energy loss. The current loss occurs because all anode or cathode sides of the cells of an RFB stack are fed with pumped electrolyte in parallel. The voltage difference over different cells creates the shunt current

that flows through the conductive electrolyte fed commonly to the cells. Optimum designs are critical to minimize the shunt current and improve other performance parameters so that the overall system life-cycle cost can be reduced.

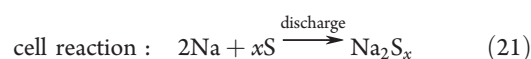
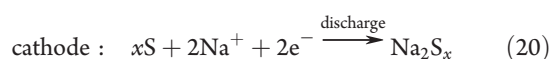
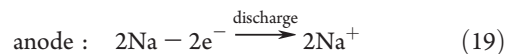
## 4. SODIUM-BETA ALUMINA MEMBRANE BATTERIES

With its abundant resources and low cost, along with its low redox potential, sodium (Na) is a favorable material to make anodes of batteries. As to its sensitivity to oxygen and water, the Na anode is often separated with a cathode by a  $Na^+$  conducting solid membrane in sealed electrochemical devices. A widely used membrane is  $\beta''\text{-Al}_2\text{O}_3$  (beta-alumina) that demonstrates an excellent  $Na^+$  conductivity, particularly at elevated temperatures. As such, batteries built from the beta alumina electrolyte are required to operate at elevated temperatures.

### 4.1. Cell Structure and Electrochemistry

Sodium-beta alumina batteries (SBBs) reversibly charge and discharge electricity via sodium ion transport across a  $\beta''\text{-Al}_2\text{O}_3$  solid electrolyte (or BASE) that is doped with  $Li^+$  or  $Mg^{2+}$ .<sup>179</sup> To minimize electrical resistance and achieve satisfactory electrochemical activities, SBBs typically operate at moderate temperatures (300–350 °C). The anode is metallic sodium in a molten state during battery operation. The cathode can be either molten  $S/Na_2S_x$ , which is known as a sodium–sulfur (Na–S) battery, or solid metal halides or Zeolite Battery Research Africa (ZEBRA) batteries. The Na-beta batteries are commonly built in tubular designs, as schematically shown in Figure 18.

**4.1.1. Sodium–Sulfur Batteries.** Sodium–sulfur (Na–S) batteries convert electrical energy to chemical potential via the following reactions:



The Na–S battery offers a voltage of 1.78–2.208 V at 350 °C, depending on the cell chemistry ( $x = 3\text{--}5$ ). Figure 19 is a schematic showing the cell structure of a Na–S battery. The Na–S battery was initially developed by Ford in the late 1960s and 1970s for electrical vehicle applications,<sup>181</sup> and it was halted in the mid 1990s with the emergence of battery technologies such as Ni-metal hydride and later Li-ion. By the early 1980s, the Tokyo Electric Power Company collaborated with NGK Insulator, Inc. to develop Na–S technologies for utility energy storage. By the late 1990s, varied systems up to the MWh scale had been developed. A number of MWh systems were demonstrated on the electrical grid. The largest system currently under construction is a 34-MW/238-MWh (7 h) Na–S storage for the Rokkasho wind farm in northern Japan.

**4.1.2. Sodium–Metal Halide Batteries.** Sodium (Na)-metal halide batteries are built with a semisolid cathode that is made from porous metal/metal halide structures impregnated with molten  $NaAlCl_4$  as a second electrolyte. Similar to the Na–S battery, the Na-metal halide batteries are commonly constructed on a tubular  $\beta''\text{-Al}_2\text{O}_3$  membrane. The energy

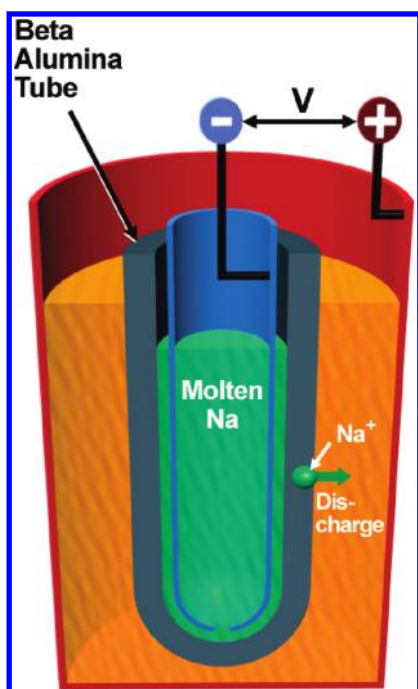


Figure 18. Single-cell and tubular design of a Na-beta battery.<sup>10,180</sup>

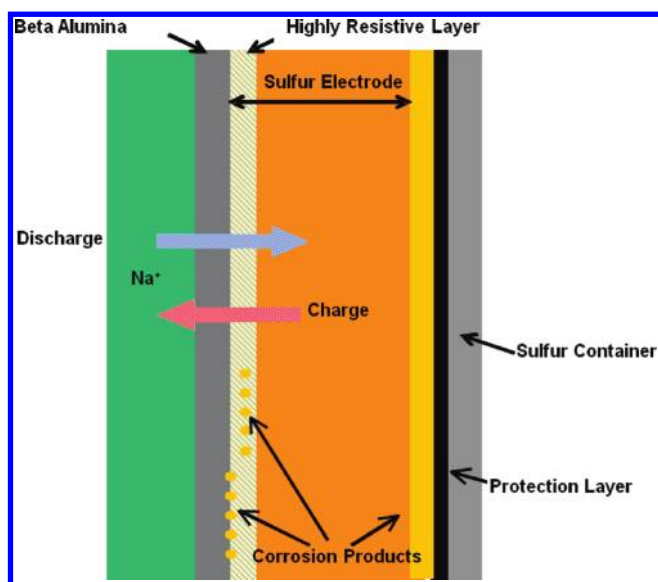
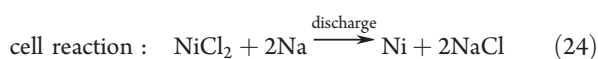
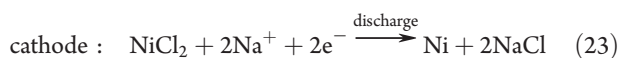
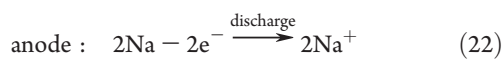


Figure 19. Schematic of cell structure and  $\text{Na}^+$  transport during charge and discharge in a Na-S Battery (Courtesy of NGK Insulator, Inc.).

conversion is carried out via the following reactions:



The Na-halide batteries offer a standard voltage of 2.58 V at 300 °C, slightly higher than that of Na-S batteries. During discharge, sodium ions are transported through the BASE from the anode

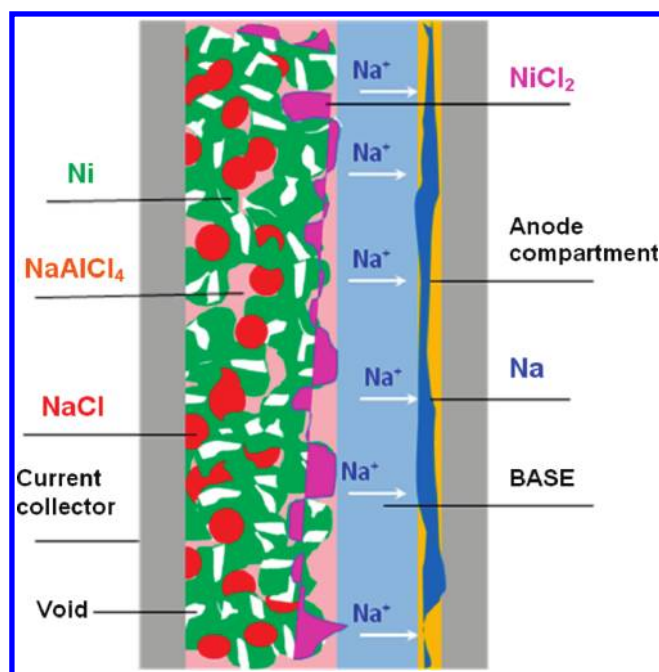


Figure 20. Schematic of cell structure and  $\text{Na}^+$  transport during a charge process in Na-metal halide battery.

to the cathode, reducing  $\text{NiCl}_2$  to Ni via the migration of sodium ions in the molten  $\text{NaAlCl}_4$  (eutectic of  $\text{NaCl}$  and  $\text{AlCl}_3$ ) as the second electrolyte. Figure 20 shows the cell structure and microstructure of electrodes during a charge process. The concept of ZEBRA was proposed in 1978 and further developed by BETA Research and Development Ltd. in England.<sup>182,183</sup> MES-DEA acquired the ZEBRA technology and has since been involved in commercialization efforts. Now FIAMM Energy LLC has joined with MES-DEA in forming a new company, FZ Sonick SA, to manufacture the Na-halide batteries. The use of solid or semisolid cathodes makes Na-metal halide batteries intrinsically safer and less corrosive than Na-S batteries. The high voltage of Na-metal halide batteries may also help energy density. As such, the battery was considered and demonstrated for transportation applications, although further improvement in power, reliability, etc. is needed. Recently, some prototypes have been designed for stationary applications.

Major components, including the BASE and the electrodes of Na-Beta batteries (NBBs), are discussed in the following sections.

#### 4.2. Beta-Alumina Solid Electrolyte (BASE)—Structure, Chemistry, Processing, and Properties

The membrane of NBB is made from  $\beta''\text{-Al}_2\text{O}_3$ , which is characterized with alternating, closely packed slabs and loosely packed layers, as shown in Figure 21. The loosely packed layers contain mobile cations (typically sodium) and are called conduction planes or slabs in which the cations are free to move under an electric field. The closely packed slabs are layers of oxygen ions with aluminum ions sitting in both octahedral and tetrahedral interstices. These layers are referred to as a spinel block, which is bonded to two adjacent spinel blocks via conduction planes or slabs. The mobile cations diffuse exclusively within the conduction layers perpendicular to the  $c$  axis. There are two distinct crystal structures in the group:  $\beta\text{-Al}_2\text{O}_3$  (hexagonal:  $P6_3/mmc$ ;  $a_0 = 0.559$  nm,  $c_0 = 2.261$  nm)<sup>184,185</sup>

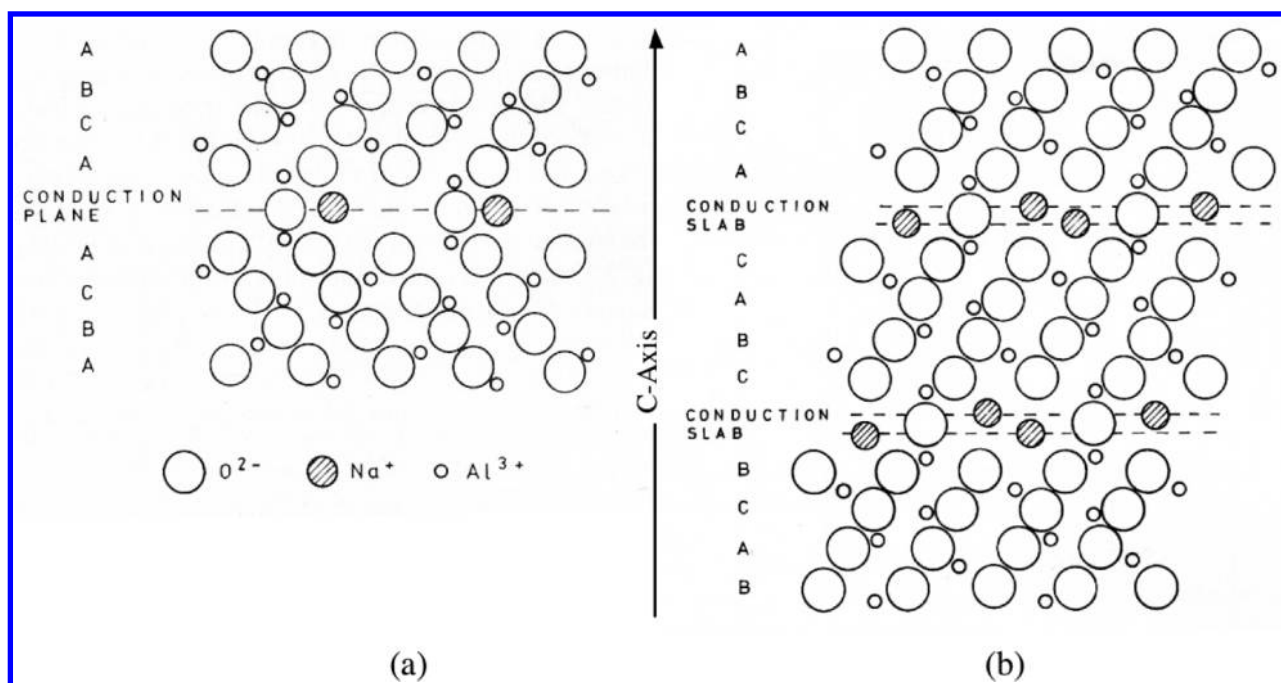


Figure 21. Projection of (a)  $\beta$ - and (b)  $\beta''$ -alumina unit cells on  $(11\bar{2}0)$  showing stacking sequence.<sup>179</sup>

and  $\beta''$ - $\text{Al}_2\text{O}_3$  (rhombohedral:  $R3m$ ;  $a_o = 0.560$  nm,  $c_o = 3.395$  nm).<sup>186,187</sup> They differ in chemical stoichiometry and the stacking sequence of oxygen ions across the conduction layer (see Figure 20). At  $300$  °C,  $\beta''$ - $\text{Al}_2\text{O}_3$  exhibits a  $\text{Na}^+$  conductivity, typically,  $0.2\text{--}0.4$  S  $\text{cm}^{-1}$ ,<sup>188,189</sup> and is thus a favorable solid-state  $\text{Na}^+$  conducting membrane.

Stoichiometric  $\beta$ - $\text{Al}_2\text{O}_3$  has the formula  $(\text{Na}_2\text{O})_{1+x}\text{Al}_2\text{O}_3$ , where  $x = 0$ . Practically, however, it has never been stoichiometrically prepared, and  $x$  could be as high as  $0.57$  for  $\beta$ - $\text{Al}_2\text{O}_3$  (undoped).<sup>179</sup> The depletion in aluminum or enrichment in sodium in the nonstoichiometric  $\beta$ - $\text{Al}_2\text{O}_3$  leads to a higher  $\text{Na}^+$  conductivity over that of stoichiometric  $\beta$ - $\text{Al}_2\text{O}_3$ . A further step to improve the  $\text{Na}^+$  conductivity of  $\beta$ - $\text{Al}_2\text{O}_3$  is to substitute aluminum ions in the spinel blocks with mono- or divalent ions (e.g.,  $\text{Li}^+$ ,  $\text{Mg}^{2+}$ ). The substitution or doping allows significant departure from the  $\beta$ - $\text{Al}_2\text{O}_3$  stoichiometry, resulting in a higher sodium content and conductivity in  $\beta''$ - $\text{Al}_2\text{O}_3$ .<sup>179,190</sup> In addition, the mono- or divalent dopants help stabilize the beta-alumina structure that tends to decompose at temperatures  $>1600$  °C. Two favorable doping elements have been Li and Mg.<sup>179</sup> Thus, two ideal  $\beta''$ - $\text{Al}_2\text{O}_3$  stoichiometries are  $\text{Na}_{1.67}\text{Al}_{10.33}\text{Mg}_{0.67}\text{O}_{17}$  ( $\text{Mg}^{2+}$  doped) and  $\text{Na}_{1.67}\text{Al}_{10.67}\text{Li}_{0.33}\text{O}_{17}$  ( $\text{Li}^+$  doped).

A variety of  $\beta''$ - $\text{Al}_2\text{O}_3$  powders can be synthesized via a conventional solid-state reaction,<sup>188,191–193</sup> the sol–gel process,<sup>194–199</sup> the coprecipitation technique,<sup>195,200</sup> the spray-freeze/freeze-drying method,<sup>201,202</sup> etc. The solid-state reaction technique is typically carried out with the starting materials  $\alpha$ - $\text{Al}_2\text{O}_3$ ,  $\text{Na}_2\text{CO}_3$ , and a small amount of  $\text{MgO}$  or  $\text{Li}_2\text{CO}_3$ . This approach involves multiple ball-milling and calcination steps with final sintering at above  $1600$  °C. The solid-state approach is at a disadvantage in controlling sodium loss and grain growth during high-temperature sintering. It is difficult to obtain a uniform product: the synthesized  $\beta''$ - $\text{Al}_2\text{O}_3$  is often mixed with  $\beta$ - $\text{Al}_2\text{O}_3$  and with remnant  $\text{NaAlO}_2$  distributed along grain boundaries. In comparison to the solid-state reaction route, the solution-based chemical methods may produce powders with a higher degree of

homogeneity and purity, along with a surface area that facilitates the subsequent sintering. Similar to the solid-state approach, however,  $\beta$ - $\text{Al}_2\text{O}_3$  cannot be completely eliminated from the final products via the chemical approach.<sup>194,196,198</sup> Alternatively, cheap abundant raw materials from the hydroxyl alumina group, such as boehmite and bayerite, were used to prepare  $\beta''$ - $\text{Al}_2\text{O}_3$ .<sup>203,204</sup> With the starting precursors of boehmite,  $\text{Na}_2\text{CO}_3$ , and  $\text{Li}_2\text{CO}_3$ , pure  $\beta''$ - $\text{Al}_2\text{O}_3$  was obtained at temperatures as low as  $1200$  °C without  $\alpha$ - $\text{Al}_2\text{O}_3$ ,  $\text{NaAlO}_2$ , or  $\beta$ - $\text{Al}_2\text{O}_3$  side products. To achieve a high density, adequate mechanical strength, and good electrical performance, the synthesized powders have to be sintered at temperatures  $\geq 1600$  °C. The high sintering temperatures require that the  $\beta''$ - $\text{Al}_2\text{O}_3$  samples be encapsulated in a platinum or magnesia container to minimize sodium evaporation. For the same purpose, zone sintering was also employed to shorten dwelling time in the high-temperature zone and thus reduce sodium loss.<sup>205,206</sup> Another issue to deal with when sintering at high temperatures is the tendency for a duplex microstructure to form with large grains ( $50\text{--}500$   $\mu\text{m}$ ) in a fine-grained matrix.<sup>188,189,207</sup> To suppress grain growth, the period of sintering is limited to under 30 min.

In addition, the vapor phase method was used to synthesize  $\beta''$ - $\text{Al}_2\text{O}_3$ .<sup>208–210</sup> It started with high-purity  $\alpha$ - $\text{Al}_2\text{O}_3$  or  $\alpha$ - $\text{Al}_2\text{O}_3/\text{YSZ}$  (Ytria-stabilized zirconia). First, the powders were fired at  $1600$  °C in air to achieve a full density ( $>99\%$ ). The dense  $\alpha$ - $\text{Al}_2\text{O}_3$  sample was then packed in  $\beta''$ - $\text{Al}_2\text{O}_3$  packing powders and heat-treated at elevated temperatures ( $\sim 1450$  °C) in air to convert  $\alpha$ - $\text{Al}_2\text{O}_3$  to  $\beta''$ - $\text{Al}_2\text{O}_3$ . The vapor phase approach offers advantages that include (1)  $\alpha$ - $\text{Al}_2\text{O}_3$  can be fully converted to  $\beta''$ - $\text{Al}_2\text{O}_3$ ; (2) encapsulation is not required because the conversion temperature is lower than the conventional process; (3) the grain size of the converted  $\beta''$ - $\text{Al}_2\text{O}_3$  is in the same level as that before conversion,<sup>208</sup> as seen in Figure 22; and (4) the converted  $\beta''$ - $\text{Al}_2\text{O}_3$  is resistant to moisture attack.

As the membrane in the SBB,  $\beta''$ - $\text{Al}_2\text{O}_3$  is first and foremost required for a satisfactory  $\text{Na}^+$  conductivity. Table 3 lists the typical

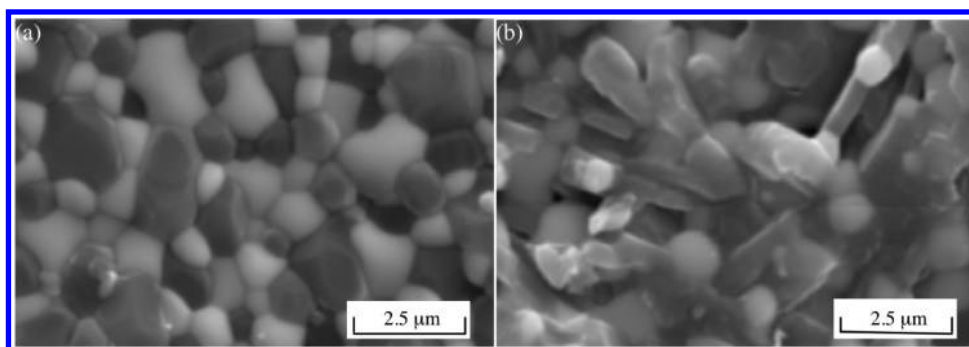


**Figure 22.** SEM images of (a)  $\alpha$ - $\text{Al}_2\text{O}_3$  and (b)  $\beta''$ - $\text{Al}_2\text{O}_3$ . The  $\beta''$ - $\text{Al}_2\text{O}_3$  was obtained via the vapor phase conversion process by heat treating  $\alpha$ - $\text{Al}_2\text{O}_3$  at  $\sim 1450$  °C in air for 2 h in  $\beta''$ - $\text{Al}_2\text{O}_3$  packing powders.<sup>208</sup>

**Table 3.** Ionic Conductivity of Single Crystal and Polycrystalline  $\beta$ - and  $\beta''$ - $\text{Al}_2\text{O}_3$

	$\sigma$ ( $\text{S cm}^{-1}$ )		$E_a$ (eV)	ref
	25 °C	300 °C		
single crystal $\beta$ - $\text{Al}_2\text{O}_3$	0.036			218
	0.024		0.16	219
	0.035	0.21	0.13	220
	0.03		0.16	221
	0.014		0.16	222
	0.03		0.17	190
	0.025		0.15	223
	0.03	0.27	0.14	224
Polycrystalline $\beta$ - $\text{Al}_2\text{O}_3$	0.0012	0.065	0.27 (25–200 °C) 0.15 (>200 °C)	220
	single crystal $\beta''$ - $\text{Al}_2\text{O}_3$	0.04	0.22 (25–250 °C) 0.17 (250–650 °C)	190
	0.1	0.20 (–80~150 °C) 0.12 (150–500 °C)	223	
	0.014	0.31 (–80~150 °C) 0.09 (150–500 °C)	223	
		1 0.33 (25–150 °C) 0.10 (>150)	211	
	0.01	1 0.33 (<200 °C)	212	
polycrystalline $\beta''$ - $\text{Al}_2\text{O}_3$		0.22–0.35	0.15–0.26	189
		0.21	0.24 (285–330 °C) 0.22 (330–375 °C)	188
		0.36	0.18 (285–330 °C) 0.16 (330–375 °C)	188
		0.2		213

ionic conductivity of a single crystal and polycrystalline  $\beta$ - and  $\beta''$ - $\text{Al}_2\text{O}_3$ . In general, single crystal materials show much higher conductivity than polycrystalline materials. For example, single crystal  $\beta''$ - $\text{Al}_2\text{O}_3$  was reported to have a  $\text{Na}^+$  conductivity about  $1 \text{ S cm}^{-1}$  at 300 °C,<sup>211,212</sup> which is almost 5 times that for polycrystalline  $\beta''$ - $\text{Al}_2\text{O}_3$ .<sup>188,189,213</sup> The high conductivity in a single crystal is attributed to the absence of a grain-boundary and the anisotropic  $\text{Na}^+$  conduction in beta-alumina crystals. The ionic conductivity of polycrystalline  $\beta''$ - $\text{Al}_2\text{O}_3$  closely depends on its composition and the ratio of  $\beta''/\beta$  and the microstructure (grain size, porosity, impurities, etc.). As aforementioned, doping elements sitting at interstitial sites can significantly improve the

conductivity.<sup>179,189</sup> The presence of impurities such as calcium and silicon also influences the conductivity of  $\beta/\beta''$ -alumina.<sup>214,215</sup> Calcium in  $\beta$ -alumina electrolyte led to the formation of intergranular calcium aluminate phases, which were likely to block ion transport and cause an exponential increase in resistance. The smaller average grain size and a larger portion of the  $\beta$ -phase likely led to lower conductivity.<sup>213,216,217</sup>

Another important property for the  $\beta''$ - $\text{Al}_2\text{O}_3$  membrane is its mechanical strength that is strongly affected by the microstructure, such as grain size and porosity. Dense  $\beta''$ - $\text{Al}_2\text{O}_3$  with an average grain size less than  $10 \mu\text{m}$  exhibits a much higher fracture strength (e.g.,  $> 200 \text{ MN/m}^2$ )<sup>216,217</sup> while that of the completely coarse-grained ones with a grain size larger than  $200 \mu\text{m}$  is as low as  $120 \text{ MN/m}^2$ .<sup>217</sup> The strength with a duplex structure varies from 120 to  $170 \text{ MN m}^{-2}$ , depending on the size and the amount of large grains in the matrix.<sup>213,216,217</sup> The smaller average grain size results in a higher fracture strength.<sup>213,216,217</sup>

Besides, the strength and fracture toughness can be enhanced by incorporating  $\text{ZrO}_2$  into the  $\beta/\beta''$ - $\text{Al}_2\text{O}_3$  matrix.<sup>192,225–230</sup> The typical fracture strength value for  $\beta''$ - $\text{Al}_2\text{O}_3$  with the addition of  $\text{ZrO}_2$  is above  $300 \text{ MN m}^{-2}$ , which is almost 50% higher compared to that for pure  $\beta''$ - $\text{Al}_2\text{O}_3$  ( $\sim 200 \text{ MN/m}^2$ ). It clearly demonstrates the significant strengthening effect of  $\text{ZrO}_2$  addition into  $\beta''$ - $\text{Al}_2\text{O}_3$ . As such,  $\beta''$ - $\text{Al}_2\text{O}_3$  is often incorporated with  $\text{ZrO}_2$  as the ceramic electrolyte in real batteries. Another benefit of  $\text{ZrO}_2$  addition is to mitigate the sensitivity of pure  $\beta''$ - $\text{Al}_2\text{O}_3$  to water moisture that tends to disintegrate the ceramic structure through penetration and reaction along grain boundaries. It must be noted, however, that adding of  $\text{ZrO}_2$  into  $\beta''$ - $\text{Al}_2\text{O}_3$  might deteriorate the electrical performance because  $\text{ZrO}_2$  is not a sodium-ionic conductor at battery operating temperatures ( $< 450$  °C). One study<sup>229</sup> found that the amounts of  $\text{ZrO}_2$  could be up to 10 wt % ( $\sim 6$  vol%) before a significant increase in resistivity was observed. The resistivity remains less than  $10 \Omega \cdot \text{cm}$  at 300 °C with up to 15 vol% of  $\text{ZrO}_2$  addition. Satisfactory electrical conductivity along with excellent mechanical strength makes it acceptable for use as a ceramic electrolyte.

#### 4.3. Negative Electrodes or Sodium-Anodes (for both Sodium–Sulfur and Sodium–Metal Halide Batteries)

Both Na–S and Na–metal halide batteries employ an anode of sodium (melting point, 98 °C), which is in a liquid state during cell operation. As the sodium is consumed during discharge, and the volume decreases accordingly, it is critical that the sodium keeps in contact with the full active area of the BASE. The same is true during charge. Typically, there are three ways to achieve good contact between the anode and the BASE: feeding sodium by

gravity from a top reservoir, wicking sodium to the BASE surface, or forcing sodium from a reservoir by gas pressure.<sup>180</sup> Among the three methods, the second one is most widely used for tubular design, and the wicking approach facilitates simplification in sealing, high sodium utilization, and compact cell design.

In addition to a good physical contact between the molten sodium and the BASE, the interfacial resistance has to remain stable and low throughout the life of battery operation. Unfortunately, a few abnormalities regarding the polarization at the sodium/BASE interface have been observed,<sup>231–233</sup> which are probably related to incomplete wetting of the BASE by sodium. The incomplete wetting is likely caused by impurities at the sodium/BASE interface. One of the impurities is calcium. It was believed that calcium might be oxidized and form a surface film, which impedes sodium dissolution as well as sodium ion transport.<sup>234</sup> The problem could be addressed via treatments of both the BASE and sodium electrodes. Coating the surface of the BASE with a thin layer of lead was proved to significantly improve initial wettability.<sup>234,235</sup> Another treatment is to add titanium or aluminum into the liquid sodium, which serves as an oxygen getter that can minimize the amount of calcium oxidized at the interface.<sup>234,236</sup> The combination of both treatments was demonstrated to completely eliminate the interfacial effects. The negative effects of calcium oxide at the interface can also be alleviated by modifying the electrolyte composition, such as the amounts of  $\text{Li}^+$  and  $\text{Na}^+$ .<sup>237</sup> In addition to the calcium impurity at the interface, a surface layer of sodium oxide, which results from sodium reaction with moisture, might also be responsible for the incomplete wetting of the BASE.<sup>235,238</sup>

#### 4.4. Positive Electrodes or Cathodes

**4.4.1. Sulfur Cathodes in Sodium–Sulfur Batteries.** In a Na–S battery, sulfur reacts with sodium ions to form sodium polysulfides during discharge and is reformed during recharge. As both sulfur and sodium polysulfides are electrical insulators, carbon felt is typically inserted in the molten cathode as an electronic conductor to facilitate electron transfer. A main issue with the sulfur/polysulfide melts is that they are highly corrosive, leading to the formation of highly resistive product interface layers (refer to Figure 17). This limits the selection of materials for current collectors and containers. Molybdenum, chromium, and some super alloys have been used for the current collectors.<sup>179,239</sup> However, these materials are either expensive or difficult to fabricate. Alternatively, more cost-effective corrosion-resistant alloys, such as stainless steels, are applied with a thin corrosion-resistant layer.<sup>179</sup> The coating could be the above-mentioned metals and alloys, nonmetals such as carbon, doped  $\text{TiO}_2$  and  $\text{CaTiO}_3$ , etc. Even though the nonmetal materials show higher electrical resistivity, a thin layer of coating only contributes a minor portion of the overall cell resistance. Another issue with the Na–S battery is the cell failure mode. When the BASE is broken, the melts are in direct contact with liquid sodium, and the reactions between them are inherently vigorous, potentially causing fire and even explosion. Furthermore, when the cell fails, resistance increases significantly and renders the entire series of cells open-circuited.

**4.4.2. Metal–Halide Cathodes in Sodium–Metal Halide Batteries.** As attractive alternatives to molten sulfur, metal halides can be employed as cathodes in NBBs. As the BASE and most of the metal halides are solid, a secondary molten electrolyte of  $\text{NaAlCl}_4$  is typically needed to serve as a sodium ion transport medium between the BASE and the reaction zone in the

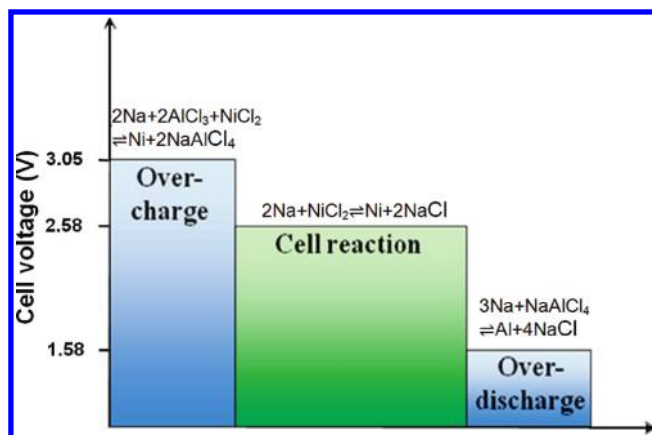


Figure 23. Cell reactions in sodium–nickel chloride battery at 300 °C.<sup>180</sup>

cathode.<sup>240</sup> The metal halide cathodes are less corrosive than sodium polysulfides and, thus, make it easier to select materials for current collector and cell case. So far, among various metal halides, nickel<sup>241,242</sup> and ferrous<sup>243,244</sup> chlorides have been widely used. Ferrous chloride is a much more cost-effective alternative to nickel chloride. However, ferric chloride tends to form during overcharge, and  $\text{Fe}^{3+}$  might transport and penetrate into the BASE, causing degradation of the electrolyte.<sup>180</sup> As such, only a limited amount of ferrous chloride can be added. The open-circuit voltages of cells with nickel and ferrous chlorides are 2.58 and 2.35 V, respectively, at 300 °C (see Figure 23 for nickel chloride).

Another major advantage of the Na–metal halide battery over the Na–S chemistry is the safe, low-resistance cell failure mode. If the BASE is broken, liquid  $\text{NaAlCl}_4$  reacts with sodium, producing sodium chloride and metallic aluminum. The reaction is less violent compared to that in a Na–S battery. The aluminum shorts the current pathway between the anode and cathode and eventually leads to a low cell resistance. The entire battery can be further operated with only the loss of voltage associated with the broken cell. Another advantage of the batteries is their tolerance to overcharge and/or overdischarge. For example, in a sodium–nickel chloride battery, the cathode can be excessively charged at a higher voltage than the normal charge with the cost of the current collector and the  $\text{NaAlCl}_4$  melt, which can serve as a useful “end of charge” indicator so that the risk of a BASE breakdown can be avoided. The overdischarge reaction, which is similar to the cell failure reaction, happens at a much lower voltage without an electrolyte failure.<sup>180</sup>

In addition to nickel and ferrous chlorides, a number of other transition metal chlorides have been investigated as potential cathode materials.<sup>245,246</sup> Among them, only molybdenum and cobalt chlorides appeared to be insoluble in the molten electrolyte, and they appear promising as cathode materials. Virkar et al.<sup>208,209</sup> explored the possibility of using zinc chloride and tin(IV) iodide as cathodes. Immersion tests with the BASE in corresponding molten salts revealed that no ion exchange occurred. But the presence of an applied electric field likely affects the charge transport, which requires further research and understanding.

Chemical additives play important roles in improving the metal halide cathode performance. Particularly, the additives were found to be effective in overcoming several performance issues with the metal halide cathodes. During charge, nickel chloride forms and grows into a layer on the nickel surface, increasing electrical resistance.<sup>247–249</sup> Once the layer reached a certain thickness, further charge was suppressed. As a result, the

use of both nickel and cell capacity was reduced. The second issue is related to the solubility of nickel chloride in  $\text{NaAlCl}_4$  melt at elevated temperatures, causing a loss in discharging capacity.<sup>250</sup> The third problem is capacity loss during cycling due to grain growth and coarsening of nickel<sup>242</sup> and/or  $\text{NaCl}$ .<sup>251</sup> During charge, small particles of these two phases are consumed, and large ones are reduced into small particles. During the subsequent discharge, the small particles that remain become the nuclei of inhomogeneous growth of the newly formed phases. The excessive growth of  $\text{Ni}$  and  $\text{NaCl}$  phases over cycling reduces the accessibility of the materials and eventually results in capacity loss with time. Modifying the molten electrolyte and cathode with certain chemical additives led to promising results. According to Prakash et al.,<sup>248</sup> adding small amounts of sodium bromide, sodium iodide, and sulfur into the molten electrolyte led to much higher nickel utilization and lower impedance compared to that without additives. Prakash et al.<sup>248</sup> also found that adding sodium bromide, sodium iodide, and sulfur into the molten electrolyte could dramatically reduce the solubility of nickel chloride in the melt. Adding 1–5 wt % sulfur into the melt was also observed to dramatically suppress the coarsening of nickel grains during cycling. The mature cell with a sulfur-doped nickel chloride cathode was demonstrated to achieve a long cell life (>2000 cycles) with capacity retention >75% and no resistance increase.<sup>242</sup> Other solutions to improve the cell performance include incorporating small amounts of aluminum, iron, and iron sulfide into the nickel chloride electrode.<sup>183,252</sup>

#### 4.5. Challenges and Future Trends in the Development of the Na-Batteries

Because of their excellent properties (refer to Table 1), such as high theoretical energy density, high round-trip efficiency, and good cycle life, NBBs have gained much interest for stationary and transportation applications. However, a broad market penetration requires further advances in performance, safety, and cost-reduction via the use of new materials along with novel component/cell designs and engineering. Currently, the capital cost of NBBs stands at \$500–600/kWh, and that is still high for broad market penetration.

One trend is to reduce the operating temperatures, which can allow for improvement in materials durability, the use of more cost-effective cell and stack materials, and easier thermal management. This may be realized by reducing the solid oxide membrane thickness. The state of the art of BASE is 1.0–2.0 mm thick. Reduction to less than 1.0 mm thickness, as shown in Figure 24, would lead to a lower resistance. But the thinner BASE has to demonstrate satisfactory structural and mechanical stability. Alternatively, a sodium ion conductor membrane that can demonstrate facile sodium ion transport at the reduced temperatures can reduce operating temperatures. In addition to  $\beta''\text{-Al}_2\text{O}_3$ , the sodium superionic conductor (NASICON), with the nominal composition  $\text{Na}_{1+x}\text{Zr}_2\text{Si}_x\text{P}_{3-x}\text{O}_{12}$  ( $x = 0\text{--}3$ , typically 2–2.5), was investigated for solid-state, Na-batteries.<sup>253,254</sup> Recently, Ceramtec has built Na-batteries from a NASICON membrane and with a sodium anode and sulfur cathode. The batteries were claimed to operate satisfactorily at temperatures even lower than the melting point of sodium.

Reducing operating temperatures potentially opens a door to employ organic materials, such as ionic liquids, in the electrodes. There have been limited attempts<sup>255,256</sup> involving tetracyanoethylene (TCNE) as the cathode that exhibited an energy density as high as 620 Wh/kg with a potential of  $\sim 3.0$  V vs  $\text{Na}^+/\text{Na}$ .

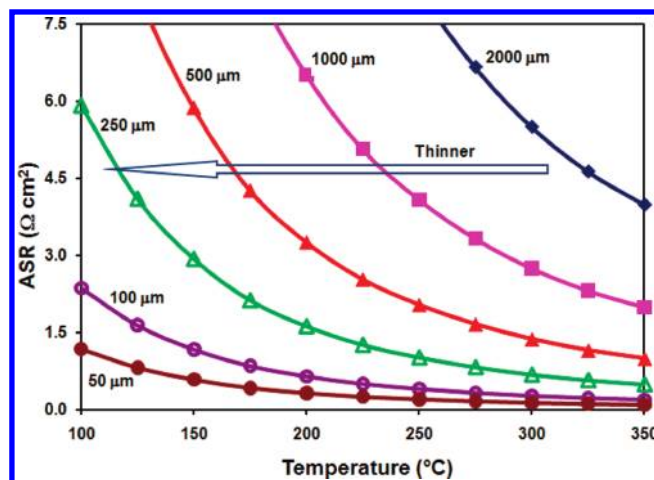


**Figure 24.** Area specific resistance ( $\Omega \text{ cm}^2$ ) of  $\beta''\text{-Al}_2\text{O}_3$  as a function of temperature and thickness of the samples. The resistance was measured by AC impedance using a sodium–sodium cell configuration (both electrodes are sodium).

However, there may be concerns regarding the stability of organic materials at these elevated temperatures.

Additionally, optimizing the design, probably by modifying component materials and chemistries, can lead to improved performance and reduced cost. For example, a ZEBRA cell was optimized with the cross section from a round to a clover-leaf-shaped BASE,<sup>183,252</sup> which significantly increased the available electrolyte surface area, reduced the thickness of the cathode, and eventually improved the power density of the cell. More substantially, NBBs constructed on a planar electrolyte have recently been developed.<sup>257,258</sup> DOE's Advanced Research Projects Agency-Energy (ARPA-E) program is currently funding Eagle-Pitcher Technologies, LLC and Pacific Northwest National Laboratory to develop a planar Na-metal halide battery. The drastic changes in design will potentially lead to improved energy/power densities and ease of manufacturing, but this demands that materials and chemistries for electrodes and stack components be optimized, such as by sealing. It is worthy of note that attempts to develop batteries that operate at intermediate temperatures may be leveraged from existing progress that has been achieved in developing solid oxide fuel cells, another electrochemical system based on a solid oxide electrolyte ( $\text{Y}_2\text{O}_3$  stabilized  $\text{ZrO}_2$ ).<sup>259</sup>

## 5. LI-ION BATTERIES

### 5.1. Concept of Li-Ion Batteries and Traditional Chemistries

Li-ion batteries store electrical energy in electrodes made of Li-intercalation (or insertion) compounds. During charge and discharge,  $\text{Li}^+$  ions transfer across an electrolyte between one host structure and the other, with concomitant oxidation and reduction processes occurring at the two electrodes. While the electrolyte can be a liquid, a gel, or a solid polymer, the majority of Li-ion batteries use liquid electrolytes containing a lithium salt such as  $\text{LiPF}_6$ ,  $\text{LiBF}_4$ ,  $\text{LiClO}_4$ ,  $\text{LiBC}_4\text{O}_8$  (LiBOB), and  $\text{Li}[\text{PF}_3\text{-}(\text{C}_2\text{F}_5)_3]$  (LiFAP), which dissolves in a mixture of organic alkyl carbonate solvents like ethylene, dimethyl, diethyl, and ethyl methyl carbonate (EC, DMC, DEC, EMC, respectively). Additionally, a variety of additives have been introduced, including vinylene carbonate (VC), to stabilize the electrolyte/electrode

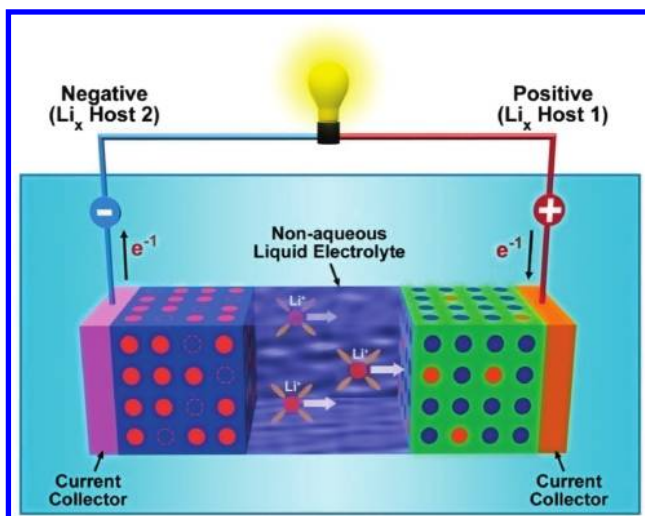
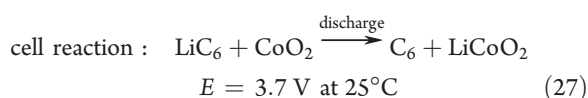
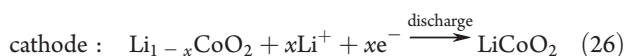
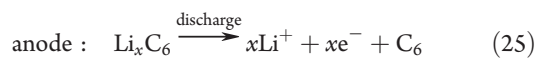


**Figure 25.** Schematic of a traditional Li-ion battery cell in which, during discharge,  $\text{Li}^+$  ions migrate through the electrolyte, and electrons flow through the external circuit, both moving from the anode (negative) to the cathode (positive).

interfaces.<sup>260–262</sup> Figure 25 illustrates the operation of a lithium-ion battery in discharge mode.

The Li-ion technologies started with discovery of intercalation compounds, such as  $\text{Li}_x\text{MO}_2$  ( $M = \text{Co}, \text{Ni}$ ), that were initially proposed by Goodenough and are still widely used today.<sup>263,264</sup> The discovery of highly reversible, low-voltage Li-intercalation carbonaceous materials led to the commercialization of  $\text{Li}_x\text{C}_6/\text{Li}_{1-x}\text{CoO}_2$  cells by Sony in 1991.<sup>265,266</sup> The energy storage in the so-called “rocking-chair” cells is completed via the following reactions:



The Li-ion cells operate with 3.7 V and demonstrate a capacity and power about 150 Ah/kg and over 200 Wh/kg, respectively.<sup>266</sup> The favorable electrochemical performance in energy and power densities and advances in system design and manufacturing have made the early Li-ion a great success for mobile electronics in spite of the remaining challenges. Among these is that the early Li-ion chemistries are inherently unsafe. The lithiated-graphite electrode operates at a potential close to that of metallic lithium, leading to Li-dendrite growth and potential electrical shorting. In the presence of flammable organic electrolyte solvents currently in use, there is a risk of heat generation, thermal runaway, and fire. An additional challenge is the high cost that may not be critical to small portable electronic applications but is very important for scaled-up applications.

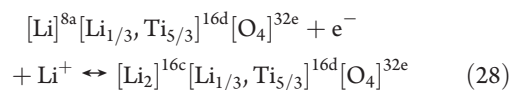
The most notable scaled-up application so far has been for hybrid electrical vehicles (HEVs), plug-in hybrid electrical vehicles (PHEVs), and electrical vehicles (EVs). The advantages in high energy capacity and power over other technologies (refer to Table 1) have made Li-ion batteries the most promising

option for transportation applications. As such, extensive research and development were carried out in this past decade. Substantial progress has been made in materials and chemistries to improve the battery technologies for the applications.

On the anode-side, graphite is the material of choice for most lithium-ion candidate chemistries. It has a theoretical capacity of 372 Ah/kg and an observed capacity of 280–330 Ah/kg, depending on the type of graphite. The potential of  $\text{LiC}_6$  against the  $\text{Li}/\text{Li}^+$  reference electrode is practically zero; this implies that the battery’s open circuit voltage completely depends on the reduction potential of the coupled positive material. But unfortunately, this could cause lithium deposition at the negative electrode surface during fast charging (especially at cold temperatures) without proper controls. This process degrades the performance of the battery and, in a worst-case scenario, could lead to a thermal runaway. Graphite is readily available naturally or as a byproduct of petroleum, but the price varies, depending on the heat-treatment process. At the initial cycle, all types of carbon-based anodes show irreversible capacity loss at  $\sim 0.8$  V because of electrolyte decomposition and the formation of a solid electrolyte interface (SEI) layer. In the following cycles, the irreversible capacity is much reduced and shows stable cyclic properties. Among many different types of carbon electrodes, well-ordered graphites are currently becoming one of the representatives for an industrial standard because of their long plateau in voltage profile and their low electrode potential relative to lithium metal. However, the graphite system has a limited capacity of about 310 mAh/g. On the other hand, soft carbons (heat-treated at 500–1000 °C) give a reversible capacity of nearly 700 mAh/g with a characteristic plateau in discharge/charge properties at about 1.0 V; hard carbons ( $\sim 1100$  °C) give a reversible capacity of 600 mAh/g, but with small irreversible capacity loss and polarization. In the commercial cells, well-ordered graphites, such as mesocarbon microbeads (MCMB) heat-treated at 3000 °C, natural graphite and nongraphitizing carbons (hard carbon) have been mainly used.<sup>267</sup> These different anodes show different output properties with a constant and slightly inclined discharge potential profile in the commercial cell, which is more suitable for cellular phones and EV battery applications, respectively.

Alternative alloys and/or intermetallic materials, such as Si (4200 mAh/g), Sn (992 mAh/g), or  $\text{SnO}_2$  (782 mAh/g) based anodes, have been extensively investigated as options for high specific capacity. While promising progress has made with the high-capacity alloy anodes, structural stability issues ascribed to large-volume expansion (300–400 vol%) during alloying with lithium still remain.<sup>266,268,269</sup> In addition, with potentials close to that of the Li electrode, the metallic anodes have the same issue in safety as the carbon-based negative electrodes.

Because of the aforementioned challenges to the carbon- and metallic-based negative electrodes, metal oxides and other compounds have been explored as alternative anodes. For example, lithium titanate spinel  $\text{Li}_4\text{Ti}_5\text{O}_{12}$  was found to be a safe replacement for the graphite anode.<sup>270,271</sup> The titanate anode operates at 1.55 V vs  $\text{Li}^+/\text{Li}$  and can accommodate Li with a theoretical capacity of 175 mAh/g, based on the following reaction:



where the superscripts stand for the number of equivalent sites

with the space group  $Fd\bar{3}m$ . While sacrificing energy density to some extent, the relatively high potential versus Li makes titanate electrodes intrinsically safer than graphite. In the lithium titanate spinel, the  $O_4$  framework provides a three-dimensional network of channels for facile  $Li^+$  diffusion ( $10^{-8}$ – $10^{-6}$   $cm^2/s$ <sup>272,273</sup>) and exhibits little or no volume expansion, even during lithiation.<sup>274</sup> Accordingly, good reversibility and the capability to resist structural change during lithium insertion/extraction make it an attractive anode for applications that require a long cycling life. There are no, or few, side reactions with electrolytes directly related to the irreversible capacity and power loss. This allows for the use of nanostructures to improve rate capability, and thus power, without side reactions with electrolytes. The good chemical compatibility, along with the relatively high potential vs  $Li^+/Li$ , makes the lithium titanate anode much safer than the carbon-based anodes.

In addition to lithium titanates, various  $TiO_2$  polymorphs, including anatase, rutile,  $TiO_2$ -B, etc., have been tested as an active Li-host, and some of their nanostructures have demonstrated promising electrochemical properties.<sup>21,275–278</sup> The anatase in particular, as shown in Figure 26, demonstrates a flat charge/

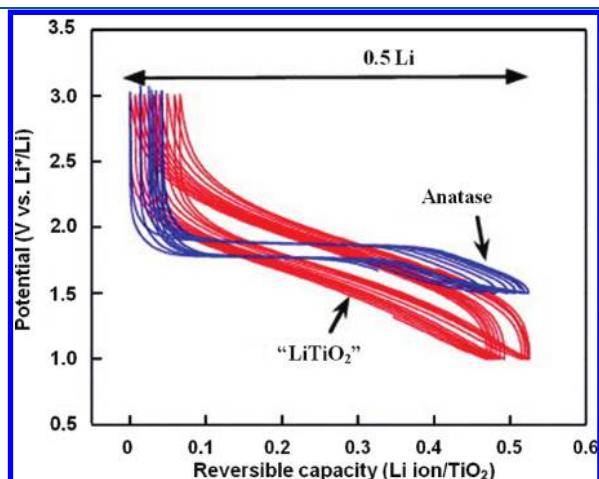


**Figure 26.** Comparison between the electrochemical behavior of rutile-(nanorod) and anatase type  $TiO_2$  after the first reduction in a galvanostatic mode with 30 mA/g between 3 and 1 V in 1 M  $LiPF_6$ , EC/DMC electrolyte at 20 °C.<sup>279</sup>

discharge curve and capability to accommodate  $>0.5$  Li per  $TiO_2$ .<sup>279</sup> Nanostructuring further enhances its Li-activity and capacity.<sup>278</sup> With the advantage in further reduction in materials cost over the lithium titanate spinel, the electrochemical activity of  $TiO_2$  is, however, negatively impacted by its low electronic conductivity. Therefore, conductive additives, along with nanostructuring, have been employed to enhance the electrochemical performance of  $TiO_2$ -based anodes. Recently, a novel self-assembled metal oxide/graphene hybrid nanostructure has been developed where anionic sulfate surfactants assist the stabilization of graphene in aqueous solution and facilitate the self-assembly process of an in situ grown nanocrystalline metal oxide with graphene.<sup>280</sup> Figure 27 shows schematically the formation of the self-assembled nanostructured composites. Nanostructured anatase  $TiO_2$ /graphene hybrid materials show significantly enhanced Li-ion insertion/extraction kinetics in  $TiO_2$ . The specific capacity of 110 mAh/g was delivered at a high charge rate of 30 C, which is more than doubled, as compared with the pure  $TiO_2$  phase.

On the cathode-side, a few alternatives to the  $LiCoO_2$  cathode have been developed. Among these are layered compounds with hexagonal/symmetry based on the  $\alpha$ - $NaFeO_2$  structure with a space group of  $R\bar{3}m$ , such as  $LiNiO_2$ ,  $LiNi_xCo_yO_2$ ,  $LiMn_xCo_yO_2$ ,  $LiMn_xNi_yO_2$ ,  $LiNi_xCo_yAl_zO_2$ ,  $LiNi_{1/3}Mn_{1/3}Co_{1/3}O_2$ , etc. as shown in Figure 28.<sup>281–283</sup> Many different elements (such as Co, Mn, Ni, Cr, Al, or Li) can be substituted into the  $\alpha$ - $NaFeO_2$  structure, and they influence the electronic conductivity, the ordering of the layer, the stability on delithiation, and the cycling performance. Various combinations have been tried to reduce the cost and to make a more stable layered structure cathode. Interestingly, the element that helps to make a stable layered structure and suppress the migration of a transition metal to the lithium site are on the order of  $Co > Ni > Mn$ , which coincides with the cost of the elements.<sup>284–287</sup> The layered cathode material is currently commercially used in Li-ion batteries that offer  $<180$  Ah/kg capacity with a reasonably long cycle and service life, but safety concerns still remain because the material is prone to a thermal runaway, especially when the battery is overcharged.

Another mature alternative cathode is spinel-type  $LiMn_2O_4$  (see Figure 28), originally proposed by Thackeray et al., and its derivatives have a voltage of over 4.0 V versus Li and a capacity about 10% less than that of  $LiCoO_2$ . The  $LiM_2O_4$  ( $M = Ti, V, Mn$ ) materials are normal spinels with the space group  $Fd\bar{3}m$  in which the lithium ions occupy tetrahedral sites (8a), and the transition metal ions reside at

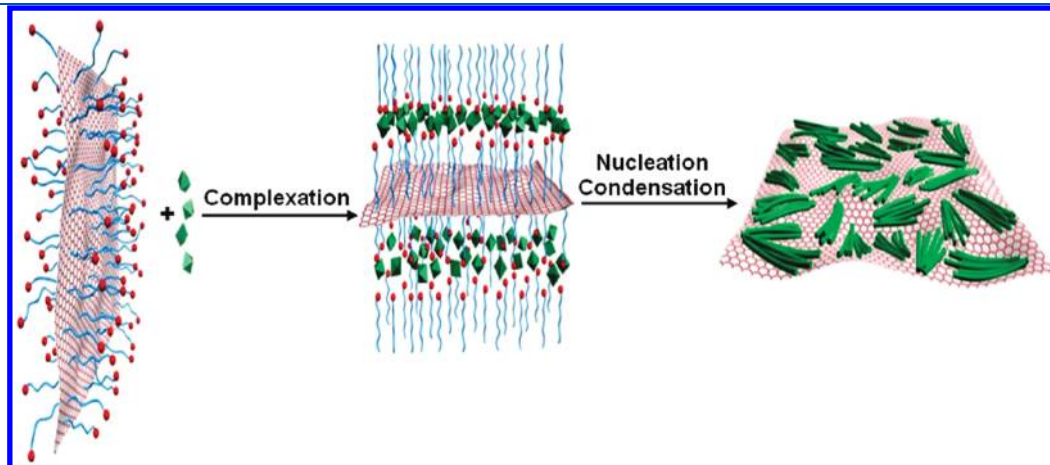


**Figure 27.** Schematic drawing of self-assembly of anatase  $TiO_2$ /graphene nanocomposite.<sup>280</sup>

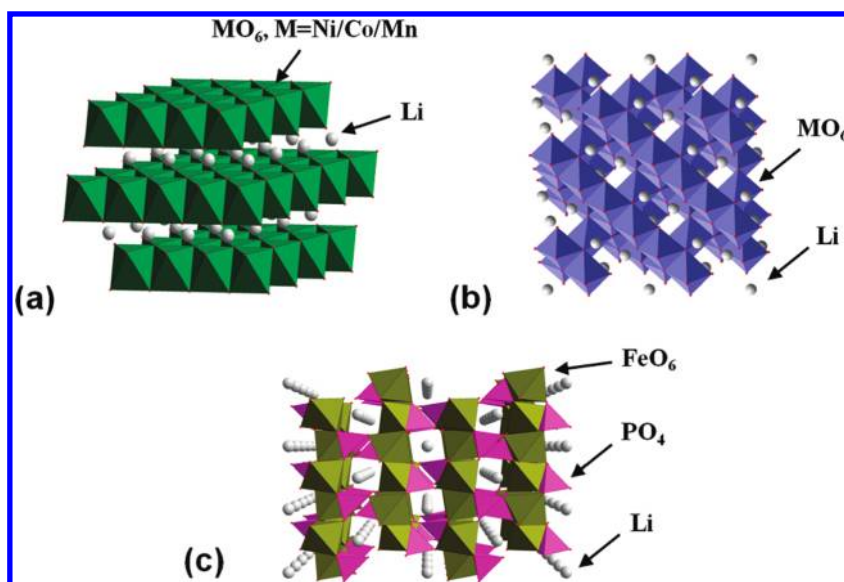


**Figure 28.** Structures of cathode materials: (a) Layered structure ( $\text{LiMn}_x\text{Ni}_y\text{Co}_z\text{O}_2$ ); (b) spinel structure ( $\text{LiMn}_2\text{O}_4$ ); (c) olivine structure ( $\text{LiFePO}_4$ ).

octahedral sites (16d). The spinel lattice also contains empty tetrahedral (8b, 48f) and octahedra (16c) sites. Spinel materials offer a three-dimensional lattice for the insertion of lithium ions because of their cubic structure. When  $0 \leq x \leq 1$ ,  $\text{Li}_x\text{Mn}_2\text{O}_4$  cells discharge at 4 V versus lithium, whereas when  $1 < x \leq 2$ , the cells discharge at 3 V. The 4-V redox is significantly more stable to cycling than the 3-V redox because the cubic symmetry of the  $\text{Li}_x\text{Mn}_2\text{O}_4$  spinel structure is maintained at 4 V, which allows the electrode to expand and contract isotropically during Li insertion/extraction reactions. When Li is inserted into  $\text{Li}_x\text{Mn}_2\text{O}_4$  at 3 V, the average Mn-ion valency falls  $< 3.5$ , and a Jahn–Teller distortion transforms the crystal symmetry from cubic to tetragonal  $\text{Li}_2\text{Mn}_2\text{O}_4$  (space group  $I4_1/amd$ ), accompanied by a 16% increase in the  $c/a$  ratio, which is too large to maintain its structural integrity during cycling. Although only the stable 4-V plateau is used for cycling, a slow capacity fade has been encountered in the high-voltage range, which can be attributed to several possible factors, such as an instability of the organic-based electrolyte at the high voltages, a slow dissolution of the  $\text{Mn}^{2+}$  from the  $\text{LiMn}_2\text{O}_4$  electrode into the electrolyte due to the disproportionation reaction ( $2\text{Mn}^{3+} = \text{Mn}^{2+} + \text{Mn}^{4+}$ ), and the onset of the Jahn–Teller effect in deeply discharged  $\text{Li}_x\text{Mn}_2\text{O}_4$  electrodes (i.e., at  $x \approx 1$ ). Although much more cost-effective than  $\text{LiCoO}_2$ , the spinels have aforementioned issues that degrade battery performance and reduce battery life.<sup>266,288</sup>

Among the high-voltage cathode materials, doped spinels  $\text{LiMn}_{2-x}\text{M}_x\text{O}_4$  ( $M = \text{Ni, Fe, Cr, Co, Cu, Al, or Li}$ ) (e.g.,  $\text{LiNi}_{0.5}\text{Mn}_{1.5}\text{O}_4$ ) have shown promising results and are currently the best candidates for future EV applications. Among these doped transition-metal spinels,  $\text{LiMn}_{1.5}\text{Ni}_{0.5}\text{O}_4$  (LMNO) with a potential plateau of 4.7 V where charge neutrality is maintained by oxidizing  $\text{Ni}^{2+}$  to  $\text{Ni}^{4+}$  is one of the most attractive compositions because it provides a specific capacity of 147 mAh/g with good cycling and rate capabilities at room temperature. However, the LMNO spinel demonstrates a significant capacity loss at an elevated temperature, which is a critical environment for HEV/EV applications.<sup>284–287</sup>

Lithium iron phosphate ( $\text{LiFePO}_4$ ), particularly in nanosizes, is another promising positive electrode material.<sup>289</sup> In the late 1990s, Padhi et al. proposed olivine-structured  $\text{LiFePO}_4$  with the space group  $Pnma$ , which exhibits a lower voltage ( $\sim 3.45$  V vs Li) but a higher capacity of around 170 mAh/g, compared to

$\text{LiCoO}_2$ .<sup>290</sup> This is the first cathode material using low cost, plentiful, and environmentally benign elements such as Fe or Mn that could have a major impact in electrochemical energy storage. It has a tunnel structure (as shown in Figure 26) with the Li diffusion path along the [010] direction and a flat potential of 3.45 V against  $\text{Li}/\text{Li}^+$  (the reference electrode) because of two-phase  $\text{LiFePO}_4/\text{FePO}_4$  transition and is considered very stable. The 3.45 V potential vs  $\text{Li}^+/\text{Li}$ , which is higher than previously known iron-based cathode materials, comes from the inductive effect of the  $(\text{PO}_4)^{3-}$  phosphate polyanions that lowers the energy of the  $\text{Fe}^{3+}/\text{Fe}^{2+}$  redox couple in the olivine structure environment. In addition to its low cost and being environmentally benign, the olivine structure is highly stable and allows for long cycles of Li-insertion/extraction. The strong bonding between the iron and oxygen prevents the release of oxygen that could fuel a typical thermal runaway at high temperatures. However, the material exhibits low Li-ion and electronic conductivity. Introducing nanostructuring, carbon coatings, and doping shortens the Li-diffusion distance and enhances electron conduction, substantially improving the performance of the olivine-structured chemistry as cathodes.<sup>291–294</sup> Nanostructured  $\text{LiFePO}_4$  has gained commercial success in Li-ion batteries.

In addition to the aforementioned cathode compositions, there is a significant amount of ongoing research and development on advanced and thermally stable cathode materials of a higher capacity. However, with all the progress made in recent years, there are no compositions coming close to commercialization.

Different combinations of anodes and cathodes give varied cell voltages and performance. As required of a high-energy density caused by volume and weight constraints, transportation applications prefer those combinations that offer a high voltage and high specific capacity. Some common combinations are listed in Table 4. It is noted that, with a high potential vs  $\text{Li}^+/\text{Li}$ , titanate-based anodes have to couple with a high-voltage cathode for the applications to make sure of a relatively high voltage and thus a high energy density.

## 5.2. Challenges of Traditional Li-Ion Chemistries for Stationary Applications

Given their high energy/power density and nearly 100% Coulombic efficiency and anticipated mass production, Li-ion

**Table 4. Demonstrated Combinations of Negative and Positive Electrodes in Li-Ion Batteries**

chemistry	charged composition	Ah/kg (theoretical)	Ah/kg (observed)	potential vs Li/Li <sup>+</sup>	open circuit voltage (V)
LiCoO <sub>2</sub>	LiC <sub>6</sub> (-)	370	<300	100 mV	3.9
	LiCoO <sub>2</sub> (+)	~295	160+	3.9 V	
LiNi <sub>x</sub> Co <sub>y</sub> Al <sub>z</sub> O <sub>2</sub>	LiC <sub>6</sub> (-)	370	<300	100 mV	3.6
	LiNi <sub>x</sub> Co <sub>y</sub> Al <sub>z</sub> O <sub>2</sub> (+)	~300	180	3.6 V	
LiMn <sub>2</sub> O <sub>4</sub>	LiC <sub>6</sub> (-)	370	<300	100 mV	3.8
	LiMn <sub>2</sub> O <sub>4</sub> (+)	148	~120	3.8 V	
LiFePO <sub>4</sub>	LiC <sub>6</sub> (-)	370	<300	100 mV	3.3
	LiFePO <sub>4</sub> (+)	178	160	3.3 V	
Li <sub>4</sub> Ti <sub>5</sub> O <sub>12</sub>	Li <sub>4</sub> Ti <sub>5</sub> O <sub>12</sub> (-)	233	~170	1.5 V	2.4
	LiMn <sub>2</sub> O <sub>4</sub> (+)	148	~120	V	

technologies have gained increasing interest for stationary applications. Altairano developed a Li-ion battery based on nanotitanate anodes and demonstrated up to 2.0-MW systems. Operating with a relatively lower voltage (2.3 V) and a lower energy density than conventional Li-ion chemistries, the Altairano technology offered a great range of safety ( $-40$ – $260$  °C), long calendar and cycle life ( $>15$  years and  $>10000$  cycles), and high power (4 kW/kg). The system demonstrated a quick response, in a matter of milliseconds, to control commands and a round-trip efficiency of about 90%. However, it could only last up to 15 min at the name-tag power. In the A123 system, a Li-ion battery was developed based on a nanostructured LiFePO<sub>4</sub> cathode, and it demonstrated up to 2.0-MW systems for power management. Similarly, the A123 system lasted only 15 min at the same power. Heat management appears among the major challenges for better technologies. Overall, Li-ion technologies have not yet been fully demonstrated to meet the performance and economic matrix for the utility sector. Additionally, there has been discussion on the use of the Li-ion battery stacks after their service life on hybrid or electrical vehicles. This would extend the values of the batteries that are initially developed for transportation applications. It remains questionable, however, whether these batteries can meet the performance and economic matrix for stationary applications.

For stationary applications, the Li-ion chemistries of current interest for vehicle applications may face a few challenges. First and foremost, the cost of the Li-ion batteries that are targeted for vehicle applications is a factor of 2–5 times higher on a kWh basis than that of the stationary applications.<sup>295,296</sup> The high cost is mainly attributed to the materials cost. For the energy form of the 18650 cell, cathode materials account for 40–50% of the overall battery cost, whereas the anode and electrolyte take up about 20–40%. To reduce cost demands, it is necessary to use cost-effective electrode materials and electrolyte. Additionally, the targeted performance parameters of the Li-ion batteries may not be good enough for stationary applications. For example, stationary applications generally require a longer cycle and calendar life than that for vehicle applications.

A further challenge of Li-ion batteries for stationary applications is in safety and reliability. As for transportation applications, the Li-ion batteries must be safe and reliable. This becomes particularly important for grid applications at scales up to MW levels. The heat generated during charge/discharge must dissipate quickly to avoid heating and promote the effective use of the designed capacity of the batteries. In a Li-ion battery pack, proper thermal management plays a significant role in extending the cycling life of a battery because of the thermal instability of the widely used liquid electrolyte and its compatibility with the electrodes. Thermal

management strongly depends on the power/energy (P/E) ratio requirement of the application. High power utilization of the Li-ion battery leads to larger polarization and resistance, which converts into heat energy that needs to dissipate efficiently to prevent thermal runaway. However, thermal management becomes more critical and difficult for a larger battery pack because the surface area/volume ratio of batteries decreases with increasing battery size, resulting in a lower heat transfer rate per unit rate of heat generation compared to smaller cells for portable applications.<sup>297</sup> While the irreversible heat generation rate due to internal resistance can be minimized by suitable electrode and cell design, the reversible heat generation rate is an inherent property of the electrode materials, which plays a significant role, especially when internal resistance has been minimized. Therefore, selecting electrode materials with low reversible heat is a key factor for improving the cycle life of the Li-ion battery.

Measuring individual electrode and full cell entropy changes for LiCoO<sub>2</sub>, LiCoO<sub>2</sub> modified with Ni, spinel LiMn<sub>2</sub>O<sub>4</sub>, LiFePO<sub>4</sub>, graphite, spinel Li<sub>4</sub>Ti<sub>5</sub>O<sub>12</sub>, and LiCoO<sub>2</sub>-graphite full cells showed that certain cathode/anode couples can be conducive to a lower rate of reversible heat generation because of cathode and anode entropy changes canceling out each other at a given SOC across the desired SOC range.<sup>297</sup> In particular, a combination of an LiFePO<sub>4</sub> cathode and an Li<sub>4</sub>Ti<sub>5</sub>O<sub>12</sub> or TiO<sub>2</sub> anode led to the lowest internal heat generation because both electrode materials experience minimum crystal structural change during Li insertion/extraction. Additionally, LiFePO<sub>4</sub>, Li<sub>4</sub>Ti<sub>5</sub>O<sub>12</sub>, and TiO<sub>2</sub> redox potentials lie within the stable window of a conventional electrolyte where an SEI layer and dendrite formation are prevented.

### 5.3. Long Life, Low Cost, Safe Li-Ion Batteries for Stationary Applications

In contrast to vehicle applications that are constrained by volume and weight, the specific energy and energy density of storage technology may not be strictly required for stationary applications. Instead, capital cost and life are critical to the stationary markets. Before finding an ideal Li-ion battery that could meet the requirements for both stationary and transportation applications, efforts may focus on cost-effective, Li-ion technologies that can also provide a long calendar and cycle life. It would be of particular interest to combine cost-effective electrodes, along with the electrolyte, in batteries that can demonstrate satisfactory performance at a low cost, even though that may mean the sacrifice of energy density and specific energy.

One favorable combination is a LiFePO<sub>4</sub> cathode and Li-titanate or a simple TiO<sub>2</sub>-based anode, along with a low cost electrolyte, as schematically shown in Figure 29.<sup>280,298</sup> The

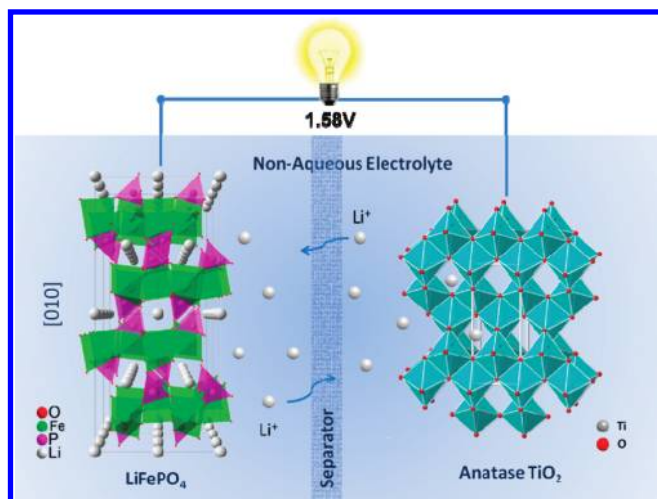


**Figure 29.** Li-ion batteries made from “zero” straining electrodes.

combination of a  $\text{LiFePO}_4$  cathode and anatase  $\text{TiO}_2$  anode gives a full cell voltage of 1.58 V; that of the  $\text{LiFePO}_4$  cathode and  $\text{Li}_4\text{Ti}_5\text{O}_{12}$  anode offers 1.8 V. Both full cells deliver a capacity of  $\sim 120$  mAh/g at a 1C rate, where the C value is based on the weight of the capacity-limiting electrode. After several initial charge/discharge cycles, the batteries show no fade in capacity over 700 cycles in a coin cell setup with the coulombic efficiency reaching close to 100% (see Figure 30). Recently, Hydro-Québec claimed to achieve >20000 charging cycles ( $\sim 50$  years) at a 5 C rate using a  $\text{LiFePO}_4/\text{Li}_4\text{Ti}_5\text{O}_{12}$  electrode combination in an 18650 cell.<sup>299</sup>

In addition to the liquid electrolyte, a solid polymer or solid-state electrolyte of high Li-ion conductivity and stability can be advantageous for stationary applications. The solid-state, Li-ion batteries are potentially safer and last longer. A commonly used material for such an electrolyte is polymer. The solid polymer electrolytes are made from ionically conductive polymers such as polyethylene oxides (PEOs) containing a lithium salt ( $\text{LiPF}_6$  or  $\text{LiAsF}_6$ ) and are often mixed with liquid electrolytes or inorganic oxide nanoparticles (e.g.,  $\text{Al}_2\text{O}_3$ ,  $\text{TiO}_2$ ,  $\text{SiO}_2$ , or  $\text{ZrO}_2$ ). This creates a more amorphous polymer matrix by inhibiting chain crystallization and attracting Li from its salt. Solid polymer electrolytes are low-cost, nontoxic, and can also retain contact over an electrode/electrolyte interface during modest changes of the electrode volume with the SOC of the battery. Li-ion polymer electrolytes have good chemical stability, but the Li-ion conductivity ( $\sigma_{\text{Li}} < 10^{-5}$  S/cm at room temperature) is still inferior to that of the carbonate electrolytes.<sup>262,286</sup> Under the support of the American Recovery and Reinvestment Act (ARRA) fund, SEEO Inc. of Berkeley, CA, is developing and demonstrating a 25-kWh prototype battery system for community storage, based on its proprietary nanostructured polymer electrolytes. The technology is expected to offer improvements in energy density, battery life, safety, and cost.

Alternatively, Li-ion conductive inorganic solids are also used as the solid-state electrolyte of Li-ion batteries.<sup>301–303</sup> The inorganic solid-state electrolytes demonstrate high potential stability but poor low-temperature  $\text{Li}^+$  ion mobility. Although solid electrolytes eliminate the risk of thermal runaway and the need for separators, assembling battery cells to obtain acceptable electrochemical activity is difficult and can be expensive and impractical. There is need for further basic and applied research into the technologies.

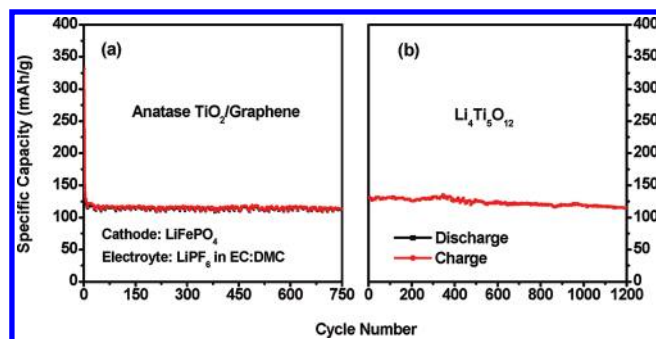


**Figure 30.** Cycling performance of Li-ion batteries made from  $\text{LiFePO}_4$  cathode and (a) self-assembled anatase  $\text{TiO}_2$ /graphene composite anode and (b)  $\text{Li}_4\text{Ti}_5\text{O}_{12}$  anode.<sup>280,298,300</sup>

#### 5.4. Li-Ion Battery Design for Stationary Applications

Recently, the Li-ion battery is being designed for stationary energy storage and is being tested for residential and community applications. The Li-ion battery design comes in a coin cell, a pouch cell, a prismatic cell, and a cylindrical cell. A standard cylindrical cell, the so-called “18650 cell” (W: 18 mm, L: 65 mm), has an exterior stainless steel can as its package, and it is the most common form of Li-ion cell package used today where an ultracompact size is not required. This cell design is easier to manufacture, and with a sealed can exterior and a resealable vent to release pressure under excessive charge, it has the capability to withstand high internal pressures. The prismatic cell design with rectangular packaging provides thinner cell geometries that are exclusively used for lithium polymer batteries and can be custom designed for various applications. Whereas the cylindrical and the prismatic cell designs use expensive metallic enclosures, a heat-sealable, multilayer foil is used in the pouch cell design. The pouch cell has the advantage of being lighter and cheaper and can make the most efficient use of the available space. However, the most suitable application for the pouch cell is the portable consumer electronics requiring ultrathin enclosures. For stationary applications, the most widely used battery pack unit consists of a number of prismatic cells (6–8) with or without an integrated cooling system. A number of battery pack units are integrated, depending on the size of the energy storage, ranging from few kW to MW level. A cooling system is not preferred for low maintenance cost, but air cooling is more accepted over a liquid-to-air or a liquid cooling system. Additionally, electric circuitry optimized for a battery pack is added to the energy storage system for effective performance and safety.

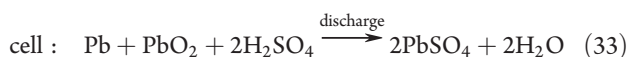
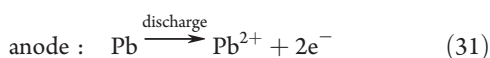
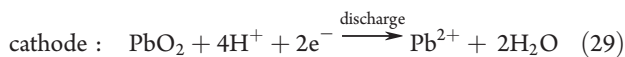
## 6. LEAD–CARBON BATTERIES

Recently, traditional lead-acid batteries have evolved into versions in which the lead-anode is partially or fully replaced by carbon, a common material in carbon supercapacitors. The carbon addition or replacement in the negative electrodes has led to improve performance and potentially reduced life-cycle cost over the traditional lead-acid batteries for stationary storage. To help understand the evolution of the oldest battery technologies, first we consider the traditional lead-acid batteries.

### 6.1. Lead-Acid Batteries: Chemistries, Design, and Application Challenges

Today’s lead-acid batteries originated from the lead-acid cell setup by Gaston Planté in 1860.<sup>304–306</sup> In the Planté cell, two long strips of lead foil and intermediate layers of coarse cloth

were spirally wound and immersed in a solution of 10% sulfuric acid. The early lead-acid cells stored electricity via corrosion of a lead foil to lead oxide to form the positive electrode, and similarly, the negative electrode was formed by roughening of the other lead foil. To increase the energy capacity over the original cell, Camille Fauré applied the pastes of lead oxides and sulfuric acid to conductive lead foil or a lead (or alloy) “grid” as the positive electrode. In the subsequent 150 years, the principle elements of the battery have not undergone much, if any, further radical changes. During discharge, both electrodes are converted to lead sulfate and the process reverses on charge:



The cell reaction offers a standard voltage of 2.105 V. The recommended end-of-discharge voltage for lead-acid battery cells is 1.75 V, always keeping the open terminal voltage at 2.10 V and higher. The early designs of lead-acid batteries had electrodes immersed in mobile electrolyte (so-called “flooded” design). Hydrogen and oxygen gases generated during overcharge were released freely into the atmosphere, necessitating regular water maintenance. In addition, the early batteries also suffered failure due to (1) positive-plate expansion, (2) acid stratification, (3) incomplete charging, and (4) corrosion.

Toward the end of the 20th century, the lead-acid battery underwent a significant functional revision by introducing a valve-regulated design. As shown in Figure 31, the valve-regulated lead-acid (VRLA) battery was designed to operate by means of an “internal oxygen cycle” (or “oxygen-recombination cycle”). As opposed to flooded lead-acid batteries (VLAs), a VRLA cannot spill its electrolyte if it is inverted. The reward is a battery that requires no maintenance, presents no threat of acid spill, sits in a reduced footprint, and is capable of delivering improved performance. The battery has been demonstrated to have a reasonable specific energy (35 Wh/kg and 70 Wh/L) and power and energy efficiency (90% and 75%, respectively). The self-discharge is limited to 5% per month. And the shelf- and cycle-life reach up to 8 years and over 1000 cycles, respectively, under a recommended depth of discharge (DOD) of <30% and a low charge rate (0.07 C). Gel electrolyte (GEL) and absorbed glass mat (AGM) are two common types of VRLA designs that find wide applications. The performance of the lead-acid batteries can be described by Peukert’s Law:

$$tI \times I^{n-1} = \Lambda \quad (34)$$

where  $t$  is the time of discharge,  $I$  is the discharge current, and  $\Lambda$  is the Peukert constant, which equals the capacity,  $C_p$ , for the rated time of discharge, assuming the discharge occurs under constant current. The Peukert number  $n$  increases with the age of batteries but generally ranges from 1.2 to 1.6 for a flooded battery, 1.1 to 1.25

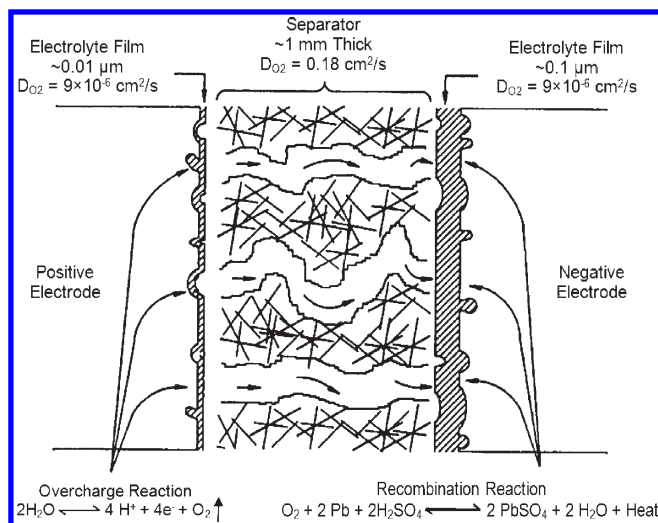


**Figure 31.** Construction of Sealed or VRLA, and conceptual view of internal oxygen cycle in a VRLA cell.<sup>305</sup>

for a GEL battery, and 1.05 to 1.15 for an AGM battery with enhanced efficiency when  $n$  is close to 1.

Given the low capital cost (<\$150/kWh), along with a well-established manufacturing and distributing network, the traditional lead-acid batteries have found wide applications, including some attempts for stationary applications. In the 1870s, magnetolectric generators became available to Planté, and about the same time, the Siemens dynamo began to be installed in central electric plants.<sup>304</sup> The early lead-acid batteries were employed to provide load leveling and to average out the demand peaks. Since then, numerous stationary systems up to multi-MW/MWh (see details in the section under Potential Technologies) were installed, which demonstrated the value of the lead-acid batteries in the grid. However, the limited cycle life incurs a high life-cycle cost (see Figure 7) because of the corrosion of the battery’s positive plate/grid and the sulfation of the battery’s negative plate/grid. During high-rate discharge, a compact layer of lead sulfate can form on the surface of the negative plate, which is difficult to recharge.<sup>304,307</sup> The accumulation of lead sulfate reduces markedly the effective surface-area and limits its performance. On the other hand, a high-rate charge promotes an early evolution of hydrogen, reducing the charging efficiency of the plate. As such, the VRLA is limited to 30–70% SOC at high rates and under a partial SOC. In addition, it takes about 5 times as long to recharge a lead-acid battery to the same charge capacity as it does to discharge. Measures were taken to overcome the performance limitations of the lead-acid battery.<sup>308,309</sup> While some improvement was achieved, the degree of the improvement does not meet the desirable targets required by many applications.

## 6.2. Lead–Carbon Electrochemical Storage Devices or Batteries

One way to further improve the cycle-life of a VRLA battery is to connect the battery with a supercapacitor in parallel. In such a combination, the supercapacitor provides the high power (or current) and, in turn, helps protect the battery from being discharged and charged at high rates. However, an electronic control is required to regulate the current flow between the lead-acid battery and supercapacitor because of the quite different operating voltages between these two devices. This will add significant extra complexity and cost to the system. Alternatively, the negative lead electrode is modified by adding carbon or, more

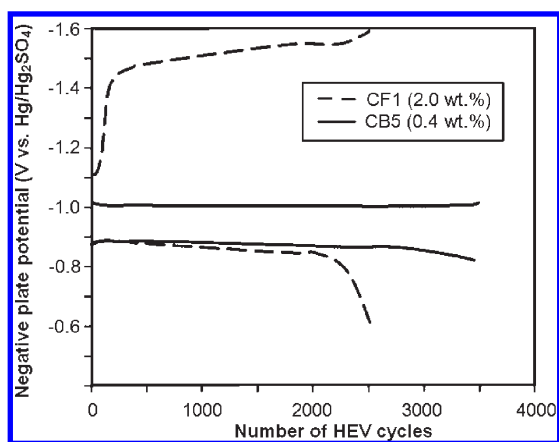


**Figure 32.** Changes in negative-plate potential during simulated HEV service for prototype cells containing different types and amounts of carbon materials in their negative plates. Upper curves are for potentials measured at the end of each charging step; lower curves are for potentials measured at end of each discharging step. Two sets of curves for cells containing 0.4 wt % carbon black with a very high surface area (CB5,  $1400 \text{ m}^2 \text{ g}^{-1}$ ) sustain their potentials far better than curves for a cell containing 2 wt % of carbon fibers with a low surface area (CF1,  $0.4 \text{ m}^2 \text{ g}^{-1}$ ).<sup>315</sup>

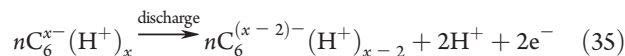
drastically, replacing it with a carbon electrode in a carbon supercapacitor.

**6.2.1. Effects of Carbon Additives.** Carbon, in the form of carbon black, is commonly added in a small amount (0.15–0.25 wt %) into the negative paste.<sup>310</sup> The primary function of the minor carbon additive was thought to “clear the negative plates during formation” and to improve performance.<sup>311</sup> In the mid 1990s, the Japan Storage Battery Company investigated the effects of carbon black that was added into the negative electrode to resist the accumulation of lead sulfate on the lead plate.<sup>312,313</sup> It was found that the increase in lead sulfate concentration per cycle fell from 0.1% to 0.05% and 0.03% after being added with  $3\times$  and  $10\times$  black carbon over the base level. Scientists at the Commonwealth Scientific and Industrial Research Organization (CSIRO) of Australia further confirmed the positive effects of increased levels of carbon to improve the cycle life of high-rate-partial-state-of-charge (HRPSoC), a common scenario of HEV operation. As shown in Figure 32, raising the concentration of a standard carbon black from 0.2% to 2.0 wt % significantly improved the cyclability of the lead-acid battery.<sup>314</sup> Other types of carbon of a higher surface area appeared more effective in inhibiting the formation of the sulfate and in improving the cycle life.<sup>315</sup>

It was concluded<sup>310,314</sup> that the carbon additives at increased levels resist the accumulation of sulfate and improve the cycle life of HRPSoC via the following two ways: first, as a stable second-phase material separating individual crystallites of  $\text{PbSO}_4$  and thus facilitating access of the electrolyte for the dissolution stage of the recharge reaction and second, as a facilitator for extending the electronically conducting surface available for the precipitation of lead. Moseley et al.<sup>310</sup> further suggests that these two functions, in principle, should be performed by two different materials, for example, a high-surface-area material such as silica for the first and a highly conductive form of carbon for the second.

**6.2.2. Lead–Carbon (PbC) Asymmetric Electrochemical Capacitors.** A more drastic change to the carbon addition is to completely replace the negative lead electrode with one made from high-surface-area carbon in carbon–carbon ultracapacitors. The new device is essentially a PbC asymmetric capacitor or a hybrid

electrochemical device that still employs the standard lead oxide positive electrode. During charge and discharge, the positive electrode undergoes the same chemical reactions that occur in a conventional lead-acid battery, that is, the  $\text{PbO}_2$  reacts with acid and sulfate ions to form  $\text{PbSO}_4$  and  $\text{H}_2\text{O}$  as described in eqs 29 and 30. The main difference in the lead–carbon battery is the replacement of the lead negative electrode with a high-surface-area carbon electrode that does not undergo any chemical reaction at all. Instead, the energy storage is realized by a double-layer (nonfaradic) storage, along with a possibly  $\text{H}^+$  pseudocapacitance (faradic) storage that has not yet been understood clearly. The storage process at the anode was expressed as<sup>316</sup>



$\text{H}^+$  stored in the carbon negative electrode in the fully charged state moves to the positive electrode during discharge where they are neutralized to form  $\text{H}_2\text{O}$ . As such, the nucleation and growth of  $\text{PbSO}_4$  are eliminated in the negative electrodes, leading to a prolonged cycle life. The result is also reduced acid concentration swings from the charged to discharged state, which reduces grid corrosion on the positive electrode and leads to a long life.

To provide a longer cycle life and a stable voltage, the  $\text{PbO}_2$  positive electrode is often overbuilt by a factor 3–10.<sup>310</sup> The anode is preferably made from high-surface-area carbon, such as activated carbon of a high surface area. Given that the carbon negative electrode is very efficient for operating the oxygen-recombination cycle, an AGM separator, a starved-electrolyte configuration, and a valve-regulated design are often employed. The stability of the positive electrode voltage results in a higher operating voltage for the cell as a whole and a greater utilization of the negative capacitance. With all these combined, the lead–carbon hybrid device offers substantial improvement in energy output, compared with equivalent carbon–carbon ultracapacitors. In comparison to the traditional lead-acid battery, the lead–carbon asymmetric capacitor is advantageous in power and cycle life because it completely avoids sulfate formation, although the discharge duration may be shortened. Therefore, the lead–carbon hybrid devices can be a promising storage technology for intro-hour applications.

The PbC asymmetric capacitor was first patented in 2001.<sup>317</sup> Currently, Axion International is developing and commercializing the PbC hybrid technologies.<sup>316,318</sup>

**6.2.3. Lead–Carbon (PbC) Ultrabatteries.** An alternative to carbon addition or full replacement with a carbon electrode is a split design of the negative electrode where half of it is lead, and the other half is carbon. The lead–carbon battery with a split negative electrode is known as an ultrabattery, which was invented by CSIRO in Australia.<sup>309,319</sup> As shown in Figure 33, the ultrabattery integrates a lead-acid cell and a PbC asymmetric capacitor into one unit without external electronic control. The device is composed of one lead-dioxide plate as the positive electrode to both a sponge lead negative plate (i.e., lead-acid anode) and a carbon-based negative anode (i.e., the asymmetric capacitor anode). Essentially, the lead-acid negative plate and the ultracapacitor carbon electrode are internally connected in parallel to act as the anode of the ultrabattery. In such a device, the total discharge or charge current of the combined negative plate is composed of two components: the capacitor current and the lead-acid negative plate current. Accordingly, the capacitor electrode can now act as a buffer to share the discharge and

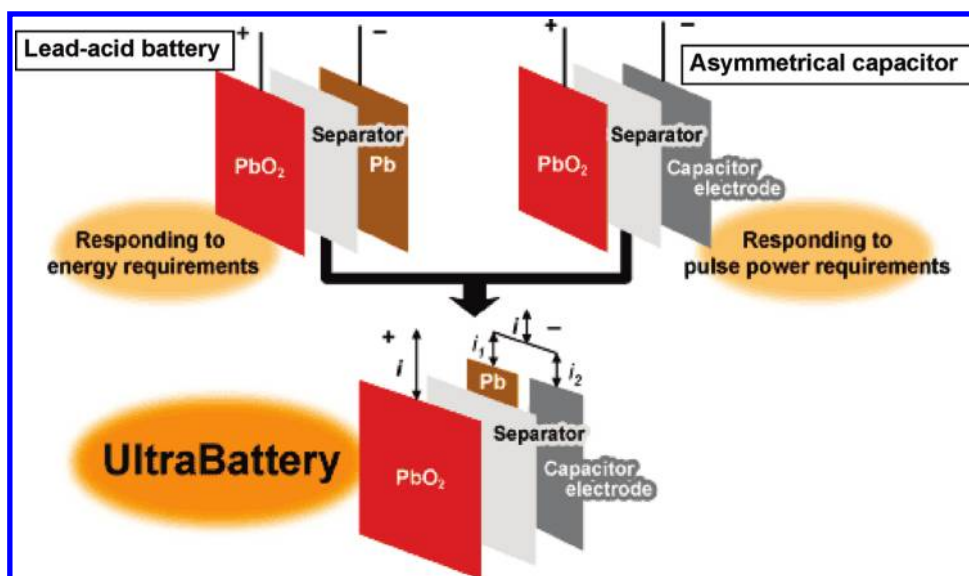


Figure 33. Schematic of an ultrabattery that integrates a lead-acid battery and lead-carbon asymmetric supercapacitor into a single unit<sup>320</sup> (Courtesy to The Furukawa Battery Co., Ltd.).

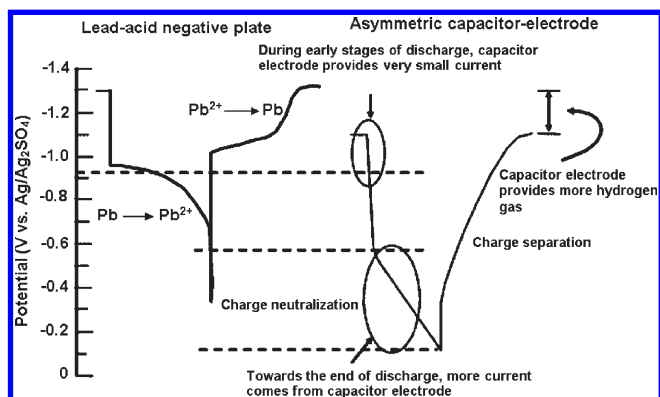


Figure 34. Operational potentials of a lead-acid negative plate and a carbon-based capacitor electrode during discharge and charge.<sup>309</sup>

charge currents with the lead-acid negative plate, and this prevents it from being discharged and charged at the high rates.

One issue with the unique integration of the lead-carbon battery and a PbC asymmetric capacitor is the large difference in operational voltage of these two devices, as shown in Figure 34. As explained by Lam et al.,<sup>309</sup> the lead negative starts to convert to lead sulfate at a potential of about  $-0.98$  V during discharge, and that converts back to sponge lead at a potential less than  $-1.0$  V. On the other hand, the charge neutralization on the capacitor electrode occurs at a potential greater than  $-0.5$  V during discharge, and subsequently, the charge separation occurs at a potential less than  $-0.3$  V during charge. As such, during the early stages of discharge, the current would mainly come from the lead-acid negative plate and only little from the capacitor electrode owing to its higher charge-neutralization potential. During charging, the current flows to the capacitor electrode first and then to the lead-acid negative plate. This would lead to significant hydrogen evolution at the lead negative-plate when it approaches toward the end of the charge. To solve the issue, the carbon electrode was modified via additives to such an extent that the hydrogen evolution on this electrode during charging has

been reduced significantly to a level close to that of the lead-acid negative plate.<sup>309</sup> The modified electrode also provided a high capacity and significantly long cycle-life.

By partnering with CSIRO, the Furukawa Battery Company of Japan and the East Penn Manufacturing Company of the United States are actively developing and commercializing the ultrabatteries.

### 6.3. Electrochemical Performance and Challenges for Grid Applications

Figure 35a shows the discharge and charge power behavior of an ultrabattery in comparison with that of a lead-acid battery (in simulating vehicle acceleration and regenerative braking). A total of 50% and 60% improvement in the discharge and charge power, respectively, was achieved over the traditional technology. It was indicated that the ultracell can be operated at a wider depth-of-discharge window, but still can provide and receive similar power levels to that of the conventional VRLA battery. Figure 35b shows the cycling performance of an ultrabattery, in comparison with a conventional lead-carbon cell. The ultracell with negative plates doped with carbon black and graphite completed 4000 cycles, which is about 2.7 times longer than that of the conventional lead-acid batteries. In comparison, the ultracell achieved  $\sim 17000$  cycles (light charge/discharge). Stacks that were provided by East Penn Manufacturing were tested at Sandia National Laboratory for grid applications. As shown in Figure 36, the HRPSoC cycle-life testing has indicated a superior HRPSoC cycle-life of the ultrabatteries over that of VRLA batteries.<sup>321</sup> Within  $\sim 70$  to 30% HRPSoC, the ultrabattery exhibited good power and efficiency. The current ultrabattery is recommended for a relatively deep depth of discharge, 30–70% (compared to that of  $<30\%$  lead-acid battery), which is a slight self-discharge per week (1% with a relatively flat cell voltage of 2 V). Under the support of the American ARRA fund, East Penn is demonstrating economic and technical viability with 3-MW frequency regulation and 1-MW/1-h demand management with the UltraBattery technology.

The significantly improved performance and prolonged life of the ultrabattery over the traditional lead-acid technology make it a

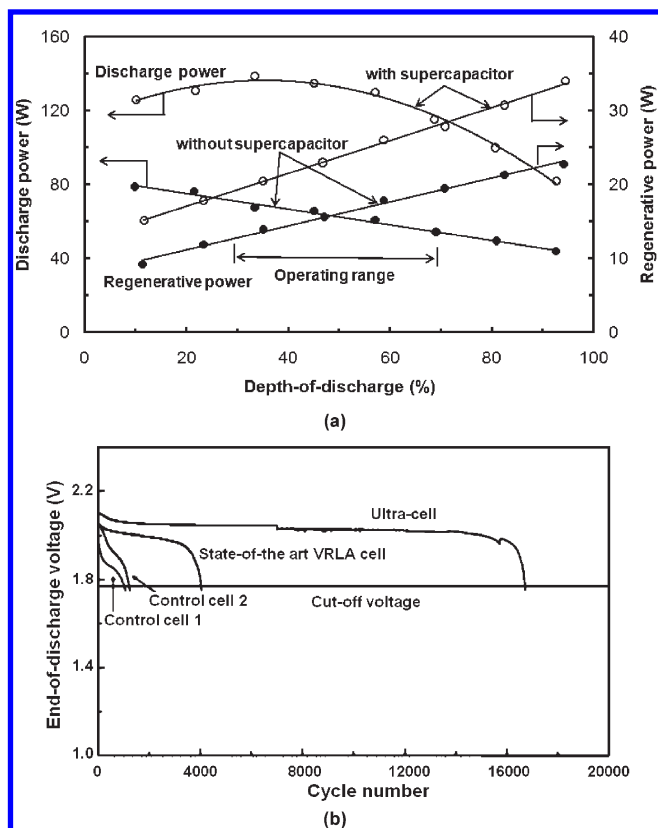


**Figure 35.** (a) Power performance and (b) cycling performance of a PbC ultracell, in comparison with that of a VRLA battery with negative plates doped with carbon black and that of two traditional lead-acid batteries (i.e., control cell).<sup>309</sup> The cycling tests were carried out with a discharge at 2.5C<sub>5</sub> A for 30 s and a charge at a constant voltage of 2.5 V with maximum current of 2.5C<sub>5</sub> A for 31 s. There are two rest times of 6.8 s each in between discharge and charge or charge and discharge. The cells were subjected repetitively to this profile at 40 °C until the voltage of each cell reached 1.77 V.

promising technology for grid applications. Before any deployment, however, there is need for further demonstration and field tests to understand its feasibility and the issues for the particular applications. The feedback from the field tests would help optimize materials/chemistries along with the design for the grid applications. One current challenge is that its capital cost of \$500/kWh is higher than the \$150/kWh of the VLA and the \$200/kWh of the VRLA. Advances in cell technology and the increasing scale of production hopefully will help to reduce its cost. In addition, its slow ramp rate may be an issue that would be a limit for uptake of wind or solar renewable energy and network stability. Furthermore, it remains unclear whether the ultrabattery offers a satisfactorily long deep cycle life. The deep-cycle cells likely require thicker plates that may deliver less peak current, but they have to withstand frequent discharging. Finally, the lead-carbon asymmetric capacitor and ultrabattery may be limited for applications that do not require a long discharge duration. An increased duration would make the technologies available for not only power management, but also energy applications. Scientifically, there is need of further basic study to understand the effects of carbon on electrode reactions, which involve the interaction and interfacial phenomenon between H<sup>+</sup> and high-surface-area carbon.

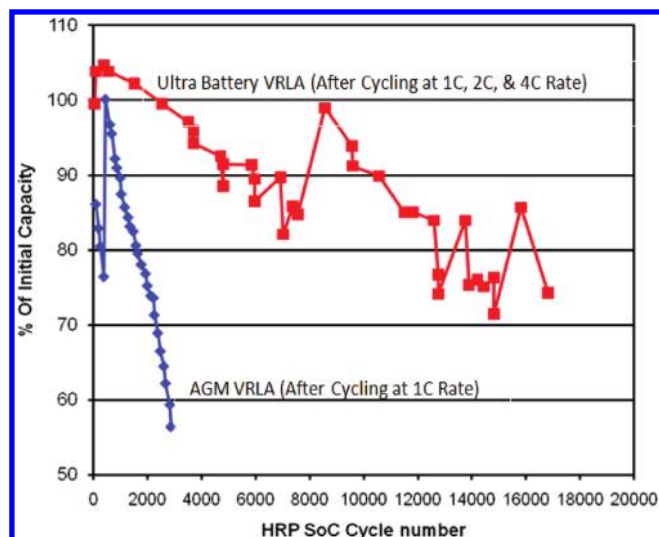


**Figure 36.** Cycling performance of lead-carbon ultrabattery compared to VRLA. The tests were carried out by Sandia National Laboratory (Courtesy of Sandia National Laboratory).

In addition to the promising lead-carbon batteries, it has to be noted that there have been attempts to develop membrane-free, lead flow batteries.<sup>322–327</sup> The flow concept appears potentially cost-effective in providing an independent power management and energy storage with a long-duration cycle. Nevertheless, there remain issues in durability, reliability, low energy densities, etc.

## 7. PERSPECTIVES

There appears to be general agreement on the needs of EES for the electrical grid, given the current trend toward increasing penetration of renewable energy, demands to improve power reliability and quality, along with implementation of smart grids. Nevertheless, the applications in terms of capacity, sitting, performance parameters, etc. need to be further refined.

A number of potential technologies for EES exist and can be potential technologies for varied stationary markets. Some of these technologies have been demonstrated for utility applications. However, these technologies are facing either challenges in meeting the performance and economic matrix for the stationary applications, or limits in environment, site selection, etc. Further demonstration of existing technologies is required to obtain a better understanding of the stationary applications and provide knowledge for technology optimization. This also calls for both basic and applied research to further develop current technologies and discover new technologies that can address the needs for renewable and utility applications.

This review focuses on electrochemical storage technologies or batteries that constitute a large group of technologies that are potentially suitable to meet varied broad market needs. Although it was not intended that this paper cover every potential technology, the four categories of electrochemistries are selected and discussed in detail: redox flow batteries, Na-beta alumina membrane batteries, unique Li-ion chemistries, and lead-carbon technologies. These technologies, as any other potential technologies, appear promising to meet the requirements and economic matrices for mostly distributed and end-user applications that range from power reliability, regulation, and energy

management to renewable firming. There remain significant challenges, and the fundamental challenges are the cost that is still too high for broad market penetration and the performance that does not yet fully meet the requirement targets. The costs must be reduced, the performance must be improved, and advances in materials, chemistries, cell/stack design, and system engineering must be achieved.

It was also intended that this paper provide general guidelines for investigating other technologies, particularly emerging technologies. Lately, there have been encouraging efforts in searching for transformational technologies for grid applications. For example, there is ongoing effort to develop Na-ion batteries, given the potential resource constraints of lithium.<sup>328–331</sup> Funded by DOE, Carnegie Mellon University and its spin-off Aquion Energy are to demonstrate an aqueous Na-ion battery for electrical grid applications. The Na-ion battery made from Na<sup>+</sup> intercalation Na<sub>4</sub>Mn<sub>9</sub>O<sub>18</sub> cathode and activated carbon anode with a mass ratio 1:0.8 was capable stable cycling over 1,000 times.<sup>332</sup> Scientists at Massachusetts Institute of Technology, also being supported by DOE, are developing an all-liquid-metal battery for low-cost, large-scale storage of electrical energy.<sup>333</sup> Arizona-based Fluidic Energy is supported by DOE in developing zinc-air utility batteries that use ionic liquid electrolyte for utility applications. This may open doors for using the vast energy capacity of metal-air batteries for stationary applications.

While there has been an increased interest and attempts to improve stationary storage, investment in the area is still limited in comparison with that of Li-ion batteries for vehicle applications. Currently, there are only a few government-funded programs worldwide with limited funding for developing electricity storage technologies for stationary applications. There is a general public and political lack of awareness of the need for new technologies for these applications. Even renewable energy industries are reluctant to lend support because of concerns about adding extra cost to renewable power systems as they struggle to reduce system cost. Furthermore, wide deployment of stationary storage will not happen without changes in regulations. Government support, such as tax incentives, can also be critical to the market entrance at early stages.

Lately, however, there appears to be a sign that the current trend is reversing. The U.S. 100th Congress enacted The Energy Independence and Security Act of 2007, which authorizes \$50 million per year for the next 10 years for the basic research program, \$80 million per year for the next 10 years for the applied research program, and \$100 million per year in the next 10 years for demonstration. Following the new law, the development and demonstration of large-scale storage technologies, along with the electrical storage for vehicle applications, were included in the American Recovery and Reinvestment Act of 2009. DOE is currently funding 16 energy-storage demonstration projects under the “Smart Grid Demonstration,” with a total of \$185 million DOE share, plus \$585 million cost share. DOE’s Office of Energy Reliability and Electricity Delivery, the newly created Advanced Research Program Agency, and the Office of Science are investing in this effort from basic, applied, and integration research. In addition to the United States, a number of other countries, such as China and countries in Europe, have also planned increasing activities in stationary storage research and development. The growing interests as well as worldwide research and development activities suggest a bright outlook for

developing improved stationary energy storage technologies for the future electric grid.

## AUTHOR INFORMATION

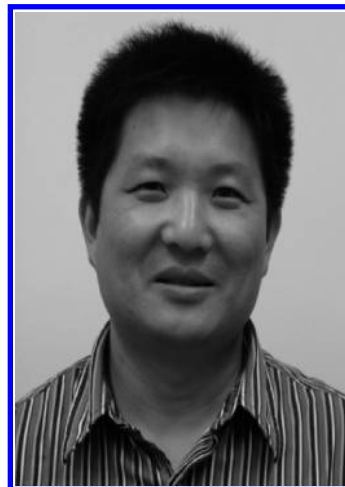
### Corresponding Author

\*E-mail: zgary.yang@pnl.gov. Telephone: 509 375 3756. Fax: 509 375 2186.

## BIOGRAPHIES



Dr. Zhenguo (Gary) Yang is a Lab Fellow at Pacific Northwest National Laboratory (PNNL), where he conducts applied research into advanced materials and energy conversion and storage. Currently, he is leading efforts to develop varied electrochemical energy storage technologies at PNNL, in particular for renewable integration and grid applications. Previously he was a chief scientist leading efforts in SOFCs and nanostructured hydrogen storage materials. Dr. Yang has authored/co-authored over 160 research papers and is an inventor/coinventor of a dozen of U.S. patents. He is a fellow of ASM International. Dr. Yang received his Ph.D. in materials science and engineering from the University of Connecticut and worked as a postdoctoral fellow at Carnegie Mellon University.

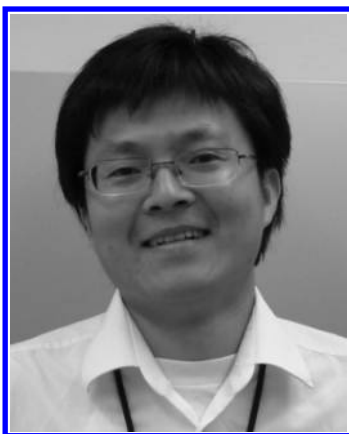


Dr. Jianlu Zhang is a Research Associate at PNNL where he conducts research on electrical energy storage techniques. Dr. Zhang joined PNNL in 2009 after his postdoctoral

appointment at the National Research Council Canada-Institute for Fuel Cell Innovation (NRC-IFCI). He authored/coauthored over 40 publications in peer-reviewed journals. Dr. Zhang received his B.S. in 1998 from Liaocheng University, a M.Sc. in 2001 from Dalian University of Technology, and a Ph.D. in 2005 from Dalian Institute of Chemical Physics, Chinese Academy of Sciences (CAS-DICP). Currently, his research interests focus on energy conversion and electrical energy storage technologies.



Dr. Michael Kintner-Meyer is a Chief Scientist at PNNL. He leads the laboratory's grid analytics for energy storage and manages the electrification of transportation research efforts. During the 2001 energy crisis in California and the Pacific Northwest, Dr. Kintner-Meyer was the technical lead for the development of a response plan required by the Presidential directive on energy conservation at Federal facilities. He holds a patent on grid-friendly control strategies of appliances. Dr. Kintner-Meyer is associate editor of the American Institute of Physics' (AIP's) "Journal of Renewable and Sustainable Energy" and a member of IEEE, ASME, and SAE, as well as the German Engineers Association, VDI. He received a Ph.D. in Mechanical Engineering from the University of Washington and an MS in Engineering from the University of Aachen, Germany.



Dr. Xiaochuan Lu is a Research Scientist at PNNL. His research interests focus on electrochemical energy storage and conversion technologies. Currently, he works on the ARPA-E program for developing advanced low-temperature planar

sodium-beta alumina batteries. Dr. Lu earned his bachelor degree in Material Science and Engineering from Hefei University of Technology in 2000 and a masters degree from Shanghai University in 2003. He completed his Ph.D. from the Department of Mechanical Engineering at Tennessee Technological University in 2008. Dr. Lu has authored/coauthored more than 20 research papers and is an inventor/coinventor of a few U.S. patents.



Dr. Daiwon Choi is a Research Scientist at PNNL. His efforts concentrate on materials synthesis and characterization in the field of Li-ion batteries for stationary and vehicle applications. He joined PNNL in 2007 after a postdoctoral appointment at Carnegie Mellon University. Dr. Choi has authored/coauthored over 30 publications in peer-reviewed journals. He received his Ph.D. in Materials Science and Engineering from Carnegie Mellon University and his B.S. and M.S. in Ceramic Engineering from Yonsei University.



Dr. John P. Lemmon is a Chief Scientist at PNNL, where he is leading the efforts to develop advanced materials and solid state electrochemical energy storage technologies. His research interests include understanding charge transfer and storage mechanisms related to fundamental phase and micro and nanostructural properties for applications in solar, sensors, and electrical energy storage materials. Previously, he worked as Senior Research Scientist and project lead at General Electric Global Research Center. Dr. Lemmon is an inventor/coinventor of over 30 patents. Dr. Lemmon received his Ph.D. in Inorganic Chemistry from Oregon State University and BS in Chemistry from the University of Northern Colorado.



Dr. Jun Liu is a Laboratory Fellow at the Pacific Northwest National Laboratory and a leader for the Transformational Materials Science Initiative. He is also a Fellow for the American Association for the Advancement of Science. In the past, he has served as Pacific Northwest National Laboratory Fellow, senior research staff for Sandia National Laboratories and Lucent Bell Laboratory, Department Manager for the Synthesis and Nanomaterials Department, Sandia National Laboratories, and Thrust Leader for Complex Functional Nanomaterials for the Center for Integrated Nanotechnologies, Sandia National Laboratories. He is recognized for his research in functional nanomaterials and their application for energy and environment. He has received an R&D 100 Award, and he was named 2007 Distinguished Inventor of Battelle. He has over 200 publications and many invited review articles in leading technical journals.

## ACKNOWLEDGMENTS

The authors would like to acknowledge financial support by DOE's Office of Electricity Delivery & Energy Reliability (OE), Advanced Research Program Agency-Energy (ARPA-E), Energy Efficiency & Renewable Energy (EERE) (under Contract Nos. 57558, 58156 and 59808, respectively) as well as by the Laboratory-Directed Research and Development Program of Pacific Northwest National Laboratory (PNNL). We are also thankful for useful discussions with Dr. Imre Gyuk of the DOE-OE Grid Storage Program and Mr. Tien Duong of the EERE Vehicle Technology Storage Program. PNNL is a multiprogram national laboratory operated by Battelle for DOE under Contract DE-AC05-76RL01830.

## ACRONYM LIST

AC	alternating current
AEM	anion exchange membrane
AGM	absorbed glass mat
BASE	Beta alumina solid electrolyte or $\beta''$ -Al <sub>2</sub> O <sub>3</sub> solid electrolyte
CAES	compressed air energy storage
CSIRO	Australian Commonwealth Scientific and Research Organization
CV	cyclic voltammetry
DC	direct current
DEC	diethyl carbonate
DMC	dimethyl carbonate
DOD	depth of discharge
DOE	U.S. Department of Energy

DVB	divinylbenzene
EC	ethylene carbonate
EDLC	electrical double layer capacitor
EMC	ethyl methyl carbonate
EES	electrical energy storage
ESA	Electricity Storage Association
ETFE	poly(ethylene-co-tetrafluoroethylene)
EV	electrical vehicle
FW	flywheel
GE	General Electric
GEL	gel electrolyte
GW	gigawatt
HEV	hybrid electrical vehicle
HRPSoC	high-rate-partial-state-of-charge
ICB	iron–chromium flow battery
ISO	Independent System Operator
LAB	lead-acid battery
LCB	lead–carbon battery
LMNO	LiMn <sub>1.5</sub> Ni <sub>0.5</sub> O <sub>4</sub>
MW	megawatt
Na–S	sodium sulfur battery
NASA	National Aeronautics and Space Administration
NASICON	sodium superionic conductor
NBB	Na-beta battery
NCB	nickel–cadmium battery
NMR	nuclear magnetic resonance
OE	DOE's Office of Electricity Delivery & Energy Reliability
O&M	operation and maintenance
ORMOSIL	organically modified silicate
PDDA	polycation poly(diallyldimethylammonium chloride)
P/E	power energy (ratio)
PE	polyethylene
PEI	polyethylenimine
PEM	proton exchange membrane
PHEV	plug-in hybrid electrical vehicle
PHS	pumped hydro storage
PNNL	Pacific Northwest National Laboratory
PP	polypropylene
PSB	polysulphide/bromine flow battery
PSS	polyanion poly(sodium styrene sulfonate)
PTFE	poly(tetrafluoroethylene)
PV	photovoltaic
PVDF	poly(vinylidene fluoride)
QPPES	poly(phthalazinone ether sulfone ketone)
QPPESK	quaternized poly(phthalazinone ether sulfone ketone)
RFB	redox flow battery
RGN	Regenesys Technologies Ltd.
SBB	sodium beta-alumina battery
SEI	solid electrolyte interface
SOC	state-of-charge
SPEEK	sulfonated poly(ether ether ketone)
SPFEK	sulfonated poly(flourenyl ether ketone)
SPTK	sulfonated poly(arylene thioether ketone)
SPTKK	sulfonated poly(arylene thioether ketone ketone)
TCNE	tetracyanoethylene
T&D	transmission and distribution
TPA	tungstophosphoric acid
TW	terawatt hour
VC	vinylene carbonate
VLA	flooded lead-acid battery

VRB	all-vanadium redox flow battery
VRLA	valve-regulated lead-acid
ZBB	zinc-bromide battery
ZEBRA	Zeolite Battery Research Africa

## REFERENCES

- (1) *World Energy Outlook 2010*; International Energy Agency: Paris, 2010.
- (2) Powell, C. A.; Morreale, B. D. *MRS Bull.* **2008**, *33*, 309.
- (3) Arunachalam, V. S.; Fleischer, E. L. *MRS Bull.* **2008**, *33*, 264.
- (4) Meier, P. J.; Wilson, P. P. H.; Kulcinski, G. L.; Denholm, P. L. *Energy Policy* **2005**, *33*, 1099.
- (5) Ginley, D.; Green, M. A.; Collins, R. *MRS Bull.* **2008**, *33*, 355.
- (6) Holdren, J. P. *Science* **2007**, *315*, 737.
- (7) Hayman, B.; Wedel-Heinen, J.; Brondsted, P. *MRS Bull.* **2008**, *33*, 343.
- (8) Lee, B. S.; Gushee, D. E. *Chem. Eng. Prog.* **2008**, *104*, S29.
- (9) Pool, R. *Power Eng.* **2007**, *21*, 10.
- (10) Yang, Z.; Liu, J.; Baskaran, S.; Imhoff, C. H.; Hollady, J. D. *JOM* **2010**, *62*, 14.
- (11) Lu, N.; Weimar, M.; Makarov, Y.; Ma, J.; Viswanathan, V. V. *The Wide-Area Energy Storage and Management System-Battery Storage Evaluation*; PNNL-18679; Pacific Northwest National Laboratory: Richland, WA, 2009.
- (12) *Smart Grid System Report*; Office of Electricity Delivery and Energy Reliability, U.S. Department of Energy, Washington, DC, 2009.
- (13) *Handbook of Energy Storage for Transmission and Distribution Applications*; Electrical Power Research Institute, Palo Alto, CA, and Department of Energy: Washington, DC, 2003.
- (14) *Environmental Assessment of Plug-In Hybrid Electric Vehicles*; Electric Power Research Institute and Natural Resources Defence Council: Palo Alto, California, 2007; Vol. 1: Nationwide Greenhouse Gas Emission.
- (15) Balducci, P. J. *Plug-in Hybrid Electric Vehicle Market Penetration Scenarios*; PNNL-17441; Pacific Northwest National Laboratory: Palo Alto, California, 2008.
- (16) Integration of renewable sources: Transmission and operating Issues and recommendations for integrating renewable sources on the California ISO-controlled grid; California Independent System Operator Corporation: Folsom, CA, 2007.
- (17) Makarov, Y. V.; Loutan, C.; Ma, J.; de Mello, P. *IEEE T. Power Syst.* **2009**, *24*, 1039.
- (18) *Bottling Electricity: Storage as a Strategic Tool for Managing Variability and Capacity Concerns in the Modern Grid*; The Electricity Advisory Committee: Washington, DC, December, 2008.
- (19) Kintner-Meyer, M. E.; Balducci, P.; Viswanathan, V.; Jin, C.; Guo, X.; Nguyen, T.; *Energy Storage for Power Systems Applications: A Regional Assessment for the Northwest Power Pools*; PNNL-2307; Pacific Northwest National Lab: Palo Alto, CA, 2010.
- (20) Electricity Storage Association; <http://www.electricitystorage.org/ESA/applications/>.
- (21) Guo, Y. G.; Hu, Y. S.; Sigle, W.; Maier, J. *Adv. Mater.* **2007**, *19*, 2087.
- (22) Lazarewicz, M., In *Electricity Storage Association Annual Meetings*; Electricity Storage Association: Washington, DC, 2003.
- (23) Electrical Storage Association. <http://www.electricitystorage.org/ESA/technologies/>.
- (24) Chen, H.; Cong, T. N.; Yang, W.; Tan, C.; Li, Y.; Ding, Y. *Prog. Natural Sci.* **2009**, *19*, 291.
- (25) *Enhancing the Value of Wind Power with Energy Storage*; Research Reports International, Inc.: Evergreen, CO, 2008.
- (26) Barton, J. P.; Infield, D. G. *IEEE Trans. Energy Convers* **2004**, *19*, 441.
- (27) Electropaedia, Energy Sources and Energy Storage, Battery and Energy Encyclopaedia and History of technology, <http://www.mpoweruk.com/performance.htm>.
- (28) Electropaedia, Energy Sources and Energy Storage, Battery and Energy Encyclopaedia and History of technology, <http://www.mpoweruk.com/history.htm#1884>.
- (29) Flow battery history, <http://poweringnow.com/flow-battery-history.shtml>.
- (30) Thaller, L. H. *Electrically Rechargeable Redox Flow Cells*, NASA TM X-71540, National Aeronautics and Space Administration: Washington, DC, 1974.
- (31) Thaller, L. H. U.S. Patent 3,996,064, 1976.
- (32) Thaller, L. H. U.S. Patent 4,159,366, 1979.
- (33) Bartolozzi, M. J. *Power Sources* **1989**, *27*, 219.
- (34) de Leon, C. P.; Frias-Ferrer, A.; Gonzalez-Garcia, J.; Szanto, D. A.; Walsh, F. C. J. *Power Sources* **2006**, *160*, 716.
- (35) *Redox Flow Cell Development and Demonstration Project*, NASA TM-97067, National Aeronautics and Space Administration: Washington, DC, 1979.
- (36) Skyllas-Kazacos, M.; Miron, R.; Robert, R. AU Patent 575,247, 1988.
- (37) Skallas-Kazacos, M.; Robins, R. G. U.S. Patent 4,786,567, 1986.
- (38) Skyllas-Kazacos, M.; Rychcik, M.; Robins, R. G.; Fane, A. G.; Green, M. A. *J. Electrochem. Soc.* **1986**, *133*, 1057.
- (39) Rychcik, M.; Skyllas-Kazacos, M. *J. Power Sources* **1988**, *22*, 59.
- (40) You, D.; Zhang, H.; Chen, J. *Electrochim. Acta* **2009**, *54*, 6827.
- (41) Skyllas-Kazacos, M. In *Encyclopedia Electrochem. Power Sources*; Dyer, C. K.; Moseley, P. T.; Ogumi, Z.; Rand, D. A. J.; Scrosati, B.; Garche, J., Eds.; Elsevier: Amsterdam, 2009; pp 444–453.
- (42) Huang, K.-L.; Li, X.-G.; Liu, S.-Q.; Tan, N.; Chen, L.-Q. *Renew. Energy* **2008**, *33*, 186.
- (43) Li, Z.; Huang, K.; Man, R. *Battery* **2006**, *36*.
- (44) Chen, J.; Wang, Q.; Wang, B. *Modern Chem. Ind.* **2006**, *26*.
- (45) Fabjan, C.; Garche, J.; Harrer, B.; Jörissen, L.; Kolbeck, C.; Philippi, F.; Tomazic, G.; Wagner, F. *Electrochim. Acta* **2001**, *47*, 825.
- (46) Rahman, F.; Skyllas-Kazacos, M. *J. Power Sources* **1998**, *72*, 105.
- (47) Oriji, G.; Katayama, Y.; Miura, T. *Electrochim. Acta* **2004**, *49*, 3091.
- (48) *Advanced Inorganic Chemistry*; Cotton, F. A.; Wilkinson, G., Eds.; John Wiley & Sons: New York, 1988.
- (49) Gattrell, M.; Park, J.; MacDougall, B.; Apte, J.; McCarthy, S.; Wu, C. W. J. *Electrochem. Soc.* **2004**, *151*, A123.
- (50) C. F. Baes, J.; Mesmer, R. E. *The Hydrolysis of Cations*; John Wiley & Sons: New York, 1976.
- (51) Vijayakumar, M.; Burton, S. D.; Huang, C.; Li, L.; Yang, Z.; Graff, G. L.; Liu, J.; Hu, J.; Skyllas-Kazacos, M. *J. Power Sources* **2010**, *195*, 7709.
- (52) Vijayakumar, M.; Li, L.; Yang, Z.; Graff, G. L.; Liu, J.; Zhang, H.; Hu, J. *J. Power Sources* **2010**, *195*, 7709.
- (53) Madic, C.; Begun, G. M.; Hahn, R. L.; Launay, J. P.; Thiessen, W. E. *Inorg. Chem.* **1984**, *23*, 469.
- (54) Kausar, N.; Howe, R.; Skyllas-Kazacos, M. *J. Appl. Electrochem.* **2001**, *31*, 1327.
- (55) Lu, X. *Electrochim. Acta* **2001**, *46*, 4281.
- (56) Pozarnsky, G. A.; McCormick, A. V. *Chem. Mater.* **1994**, *6*, 380.
- (57) Pozarnsky, G. A.; McCormick, A. V. *J. Mater. Chem.* **1994**, *4*, 1749.
- (58) Rahman, F.; Skyllas-Kazacos, M. *J. Power Sources* **2009**, *189*, 1212.
- (59) Skyllas-Kazacos, M.; Menictas, C.; Kazacos, M. *J. Electrochem. Soc.* **1996**, *143*, L86.
- (60) Kazacos, M.; Cheng, M.; Skyllas-Kazacos, M. *J. Appl. Electrochem.* **1990**, *20*, 463.
- (61) Kazacos, M. S.; Kazacos, M. U. S. Patent 6,562,514 B1, 2003.
- (62) Skyllas-Kazacos, M.; Peng, C.; Cheng, M. *Electrochem. Solid-State Lett.* **1999**, *2*, 121.
- (63) Kazacos, M.; Skyllas-Kazacos, M. WO95/12,219, 1995.
- (64) Kazacos, M.; Skyllas-Kazacos, M. WO96/35,239, 1996.
- (65) Sum, E.; Rychcik, M.; Skyllas-kazacos, M. *J. Power Sources* **1985**, *16*, 85.
- (66) Sum, E.; Skyllas-kazacos, M. *J. Power Sources* **1985**, *15*, 179.

- (67) Zhong, S.; Skyllas-Kazacos, M. *J. Power Sources* **1992**, *39*, 1.
- (68) Fang, B.; Wei, Y.; Arai, T.; Iwasa, S.; Kumagai, M. *J. Appl. Electrochem.* **2003**, *33*, 197.
- (69) Zhong, S.; Kazacos, M.; Burford, R. P.; Skyllas-Kazacos, M. *J. Power Sources* **1991**, *36*, 29.
- (70) Kazacos, M.; Skyllas-Kazacos, M. *J. Electrochem. Soc.* **1989**, *136*, 2759.
- (71) Qian, P.; Zhang, H.; Chen, J.; Wen, Y.; Luo, Q.; Liu, Z.; You, D.; Yi, B. *J. Power Sources* **2008**, *175*, 613.
- (72) Yazici, M. S.; Krassowski, D.; Prakash, J. *J. Power Sources* **2005**, *141*, 171.
- (73) Zhong, S.; Michael, K. WO9,406,164, 1994.
- (74) Brungs, A.; Haddadi-Asl, V.; Skyllas-Kazacos, M. *J. Appl. Electrochem.* **1996**, *26*, 1117.
- (75) Zhong, S.; Kazacos, M. U.S. Patent 5,665,212, 1997.
- (76) Haddadi-Asl, V.; Kazacos, M.; Skyllas-Kazacos, M. *J. Appl. Electrochem.* **1995**, *25*, 29.
- (77) Haddadi-Asl, V.; Kazacos, M.; Skyllas-Kazacos, M. *J. Appl. Polym. Sci.* **1995**, *57*, 1455.
- (78) Radford, G. J. W.; Cox, J.; Wills, R. G. A.; Walsh, F. C. *J. Power Sources* **2008**, *185*, 1499.
- (79) Hagg, C. M.; Skyllas-Kazacos, M. *J. Appl. Electrochem.* **2002**, *32*, 1063.
- (80) Inoue, M.; Tsuzuki, Y.; Iizuka, Y.; Shimada, M. *J. Electrochem. Soc.* **1987**, *134*, 756.
- (81) Kaneko, H.; Nozaki, K.; Wada, Y.; Aoki, T.; Negishi, A.; Kamimoto, M. *Electrochim. Acta* **1991**, *36*, 1191.
- (82) Xi, J.; Wu, Z.; Qiu, X.; Chen, L. *J. Power Sources* **2007**, *166*, 531.
- (83) Mohammadi, F.; Timbrell, P.; Zhong, S.; Padeste, C.; Skyllas-kazacos, M. *J. Power Sources* **1994**, *52*, 61.
- (84) Shao, Y. Y.; Zhang, S.; Kou, R.; Wang, X. Q.; Wang, C. M.; Dai, S.; Viswanathan, V.; Liu, J.; Wang, Y.; Lin, Y. H. *J. Power Sources* **2010**, *195*, 1805.
- (85) Sun, B.; Skyllas-kazacos, M. *Electrochim. Acta* **1992**, *37*, 2459.
- (86) Sun, B.; Skyllas-kazacos, M. *Electrochim. Acta* **1992**, *37*, 1253.
- (87) Sun, B. T.; Skyllas-kazacos, M. *Electrochim. Acta* **1991**, *36*, 513.
- (88) Rychcik, M.; Skyllas-kazacos, M. *J. Power Sources* **1987**, *19*, 45.
- (89) Zhong, S.; Padeste, C.; Kazacos, M.; Skyllas-kazacos, M. *J. Power Sources* **1993**, *45*, 29.
- (90) Li, X.-G.; Huang, K.-L.; Liu, S.-Q.; Chen, L.-Q. *J. Cent. South Univ. Technol.* **2007**, *14*, 51.
- (91) Wang, W. H.; Wang, X. D. *Electrochim. Acta* **2007**, *52*, 6755.
- (92) Tan, N.; Kelong, H.; Suqin, L.; Xiaogang, L.; Zhifeng, C. *Acta Chim. Sin.* **2006**, *64*.
- (93) Lee, W. H.; Lee, J. G.; Reucroft, P. *J. Appl. Sur. Sci.* **2001**, *171*, 136.
- (94) Li, X.-G.; Huang, K.-L.; Liu, S.-Q.; Tan, N.; Chen, L.-Q. *Trans. Nonferrous Met. Soc. China* **2007**, *17*, 195.
- (95) Pittman, C. U., Jr.; Jiang, W.; Yue, Z. R.; Gardner, S.; Wang, L.; Toghiani, H.; Leon y Leon, C. A. *Carbon* **1999**, *37*, 1797.
- (96) Yue, Z. R.; Jiang, W.; Wang, L.; Gardner, S. D.; Pittman, C. U., Jr. *Carbon* **1999**, *37*, 1785.
- (97) Bulska, E.; Jedral, W.; Kopysc, E.; Ortner, H. M.; Flege, S. *Spectrochim. Acta Part B: Atomic Spectroscopy* **2002**, *57*, 2017.
- (98) Chieng, S. C.; Kazacos, M.; Skyllas-Kazacos, M. *J. Power Sources* **1992**, *39*, 11.
- (99) Arora, P.; Zhang, Z. M. *Chem. Rev.* **2004**, *104*, 4419.
- (100) Mohammadi, T.; Kazacos, M. S. *J. Appl. Electrochem.* **1997**, *27*, 153.
- (101) Luo, X.; Lu, Z.; Xi, J.; Wu, Z.; Zhu, W.; Chen, L.; Qiu, X. *J. Phys. Chem. B* **2005**, *109*, 20310.
- (102) Hwang, G.-J.; Ohya, H. *J. Membr. Sci.* **1997**, *132*, 55.
- (103) Wiedemann, E.; Heintz, A.; Lichtenthaler, R. N. *J. Membr. Sci.* **1998**, *141*, 207.
- (104) Xi, J.; Wu, Z.; Teng, X.; Zhao, Y.; Chen, L.; Qiu, X. *J. Mater. Chem.* **2008**, *18*, 1232.
- (105) Sun, C.; Chen, J.; Zhang, H.; Han, X.; Luo, Q. *J. Power Sources* **2010**, *195*, 890.
- (106) Mohammadi, T.; Chieng, S. C.; Skyllas Kazacos, M. *J. Membr. Sci.* **1997**, *133*, 151.
- (107) Mohammadi, T.; Skyllas-Kazacos, M. *J. Power Sources* **1995**, *56*, 91.
- (108) Chieng, S. C., Ph.D. thesis, University of New South Wales, 1993.
- (109) Sukkar, T.; Skyllas-Kazacos, M. *J. Membr. Sci.* **2003**, *222*, 235.
- (110) Chieng, S. C.; Kazacos, M.; Skyllas-Kazacos, M. *J. Membr. Sci.* **1992**, *75*, 81.
- (111) Mohammadi, T.; Kazacos, M. S. *J. Power Sources* **1996**, *63*, 179.
- (112) Mohammadi, T.; Skyllas-Kazacos, M. *J. Membr. Sci.* **1995**, *107*, 35.
- (113) Mohammadi, T.; Skyllas-Kazacos, M. *J. Membr. Sci.* **1995**, *98*, 77.
- (114) Sukkar, T.; Skyllas-Kazacos, M. *J. Membr. Sci.* **2003**, *222*, 249.
- (115) Zeng, J.; Jiang, C.; Wang, Y.; Chen, J.; Zhu, S.; Zhao, B.; Wang, R. *Electrochem. Commun.* **2008**, *10*, 372.
- (116) Luo, Q.; Zhang, H.; Chen, J.; You, D.; Sun, C.; Zhang, Y. *J. Membr. Sci.* **2008**, *325*, 553.
- (117) Luo, Q.; Zhang, H.; Chen, J.; Qian, P.; Zhai, Y. *J. Membr. Sci.* **2008**, *311*, 98.
- (118) Teng, X.; Zhao, Y.; Xi, J.; Wu, Z.; Qiu, X.; Chen, L. *J. Power Sources* **2009**, *189*, 1240.
- (119) Schulte, D.; Drillkens, J.; Schulte, B.; Sauer, D. U. *J. Electrochem. Soc.* **2010**, *157*, A989.
- (120) Teng, X.; Zhao, Y.; Xi, J.; Wu, Z.; Qiu, X.; Chen, L. *J. Membr. Sci.* **2009**, *341*, 149.
- (121) Sang, S.; Wu, Q.; Huang, K. *J. Membr. Sci.* **2007**, *305*, 118.
- (122) Hwang, G.-J.; Ohya, H. *J. Membr. Sci.* **1996**, *120*, 55.
- (123) Chen, D.; Wang, S.; Xiao, M.; Meng, Y. *Energy Environ. Sci.* **2010**, *3*, 622.
- (124) Qiu, J.; Zhang, J.; Chen, J.; Peng, J.; Xu, L.; Zhai, M.; Li, J.; Wei, G. *J. Membr. Sci.* **2009**, *334*, 9.
- (125) Qiu, J.; Zhao, L.; Zhai, M.; Ni, J.; Zhou, H.; Peng, J.; Li, J.; Wei, G. *J. Power Sources* **2008**, *177*, 617.
- (126) Qiu, J.; Ni, J.; Zhai, M.; Peng, J.; Zhou, H.; Li, J.; Wei, G. *Radiat. Phys. Chem.* **2007**, *76*, 1703.
- (127) Qiu, J.; Zhai, M.; Chen, J.; Wang, Y.; Peng, J.; Xu, L.; Li, J.; Wei, G. *J. Membr. Sci.* **2009**, *342*, 215.
- (128) Kim, S.; Yan, J.; Schwenzer, B.; Zhang, J.; Li, L.; Liu, J.; Yang, Z.; Hickner, M. A. *Electrochem. Commun.* **2010**, *12*, 1650.
- (129) Chen, D.; Wang, S.; Xiao, M.; Meng, Y. *J. Power Sources* **2010**, *195*, 2089.
- (130) Jia, C.; Liu, J.; Yan, C. *J. Power Sources* **2010**, *195*, 4380.
- (131) Mai, Z.; Zhang, H.; Li, X.; Bi, C.; Dai, H. *J. Power Sources* **2011**, *196*, 482.
- (132) Tian, B.; Yan, C. W.; Wang, F. H. *J. Appl. Electrochem.* **2004**, *34*, 1205.
- (133) Jian, X. G.; Yan, C.; Zhang, H. M.; Zhang, S. H.; Liu, C.; Zhao, P. *Chin. Chem. Lett.* **2007**, *18*, 1269.
- (134) Xing, D.; Zhang, S.; Yin, C.; Zhang, B.; Jian, X. *J. Membr. Sci.* **2010**, *354*, 68.
- (135) Qiu, J.; Li, M.; Ni, J.; Zhai, M.; Peng, J.; Xu, L.; Zhou, H.; Li, J.; Wei, G. *J. Membr. Sci.* **2007**, *297*, 174.
- (136) Tian, B.; Yan, C. W.; Wang, F. H. *J. Membr. Sci.* **2004**, *234*, 51.
- (137) Skyllas-Kazacos, M. *J. Power Sources* **2003**, *124*, 299.
- (138) Skyllas-Kazacos, M.; Limantari, Y. *J. Appl. Electrochem.* **2004**, *34*, 681.
- (139) Skyllas-Kazacos, M. U.S. Patent 7,320,844, 2008.
- (140) Price, A.; Bartley, S.; Male, S.; Cooley, G. *Power Eng. J.* **1999**, *13*, 122.
- (141) Pawar, S.; Madhale, R.; Patil, P.; Lokhande, C. *Bullet. Mater. Sci.* **1988**, *10*, 367.
- (142) Lopez-Atalaya, M.; Codina, G.; Perez, J. R.; Vazquez, J. L.; Aldaz, A. *J. Power Sources* **1992**, *39*, 147.
- (143) Cedzynska, K. *Electrochim. Acta* **1995**, *40*, 971.
- (144) Eustace, D. J. *J. Electrochem. Soc.* **1980**, *127*, 528.
- (145) Xia, X.; Liu, H. T.; Liu, Y. *J. Electrochem. Soc.* **2002**, *149*, A426.

- (146) Wen, Y. H.; Zhang, H. M.; Qian, P.; Zhou, H. T.; Zhao, P.; Yi, B. L.; Yang, Y. S. *J. Electrochem. Soc.* **2006**, *153*, A929.
- (147) Xue, F. Q.; Wang, Y. L.; Wang, W. H.; Wang, X. D. *Electrochim. Acta* **2008**, *53*, 6636.
- (148) Wang, Y. Y.; Lin, M. R.; Wan, C. C. *J. Power Sources* **1984**, *13*, 65.
- (149) Lide, D. R. *CRC Handbook of Chemistry and Physics*, 2006–2007 ed.; CRC Press, Boca Raton, FL, 2007.
- (150) Watt-Smith, M. J.; Wills, R. G. A.; Walsh, F. C. In *Encyclopedia Electrochemical Power Sources*; Garche, J., Ed.; Elsevier: Amsterdam, 2009; p 438.
- (151) Bor, L. *J. Am. Ceram. Soc.* **1950**, *33*, 375.
- (152) Gahn, R. F.; Hagedorn, N. *Negative-Electrode Catalysts for Fe/Cr Redox Cells*; NASA technical report, report number LEW-14028; NASA: Washington, DC, 1987.
- (153) Jalan, V.; Morriseau, B.; Swette, L. *Optimization and Fabrication of Porous Carbon Electrodes for Fe/Cr Redox Flow Cells*; NASA technical report, report number: DOE/NASA/0198-1; NASA: Washington, DC, 1982.
- (154) Gahn, R. F.; Hagedorn, N.; Ling, J. S. Intersociety Energy Conversion Engineering Conference, 18th Orlando, FL, United States, 1983.
- (155) Lopez-Atalaya, M.; Codina, G.; Perez, J. R.; Vazquez, J. L.; Aldaz, A.; Climent, M. A. *J. Power Sources* **1991**, *35*, 225.
- (156) Yang, C. Y. *J. Appl. Electrochem.* **1982**, *12*, 425.
- (157) Cheng, D. S.; Hollax, E. *J. Electrochem. Soc.* **1985**, *132*, 269.
- (158) Wu, C. D.; Scherson, D. A.; Calvo, E. J.; Yeager, E. B.; Reid, M. A. *J. Electrochem. Soc.* **1986**, *133*, 2109.
- (159) Gahn, R. F.; Hagedorn, N. H.; Ling, J. S. *Single Cell Performance Studies on the Fe-Cr Redox Energy Storage Systems Using Mixed Reactant Solutions at Elevated Temperatures*; NASA technical report, report number: DOE/NASA/12726-21; NASA: Washington, DC, 1983.
- (160) Ling, J. S. *Evaluation of Developmental Membranes of the Mixed Reactant Fe-Cr Redox Systems*; NASA technical report, report number: DOE/NASA/12726-26; NASA: Washington, DC, 1984.
- (161) Bae, C. H.; Roberts, E. P. L.; Dryfe, R. A. W. *Electrochim. Acta* **2002**, *48*, 279.
- (162) Codina, G.; Perez, J. R.; Lopez-Atalaya, M.; Vasquez, J. L.; Aldaz, A. *J. Power Sources* **1994**, *48*, 293.
- (163) Pupkevich, V.; Glibin, V.; Karamanev, D. *Electrochem. Commun.* **2007**, *9*, 1924.
- (164) Codina, G.; Aldaz, A. *J. Appl. Electrochem.* **1992**, *22*, 668.
- (165) Chen, Y.-W. D.; Santhanam, K. S. V.; Bard, A. J. *J. Electrochem. Soc.* **1981**, *128*, 1460.
- (166) Wen, Y. H.; Zhang, H. M.; Qian, P.; Zhou, H. T.; Zhao, P.; Yi, B. L.; Yang, Y. S. *Electrochim. Acta* **2006**, *51*, 3769.
- (167) Szanto, D. A. Ph.D. thesis, University of Portsmouth, UK, 1999.
- (168) Cathro, K. J.; Cedzynska, K.; Constable, D. C. *J. Power Sources* **1987**, *19*, 337.
- (169) Kinoshita, K.; Leach, S. C.; Ablow, C. M. *J. Electrochem. Soc.* **1982**, *129*, 2397.
- (170) Zhao, P.; Zhang, H. M.; Zhou, H. T.; Yi, B. L. *Electrochim. Acta* **2005**, *51*, 1091.
- (171) Zhou, H. T.; Zhang, H. M.; Zhao, P.; Yi, B. L. *Electrochim. Acta* **2006**, *51*, 6304.
- (172) Zito, R. U.S. Patent 5,612,148, 1997.
- (173) Bradley, C. S. U.S. Patent 3,128,805, 1885.
- (174) Lim, H. S.; Lackner, A. M.; Knechtli, R. C. *J. Electrochem. Soc.* **1977**, *124*, 1154.
- (175) Lim, H. S.; Lackner, A. M.; Knechtli, R. C. *J. Electrochem. Soc.* **1977**, *124*, C279.
- (176) de Boer, P. Leonardo Energy Website, <http://www.leonardo-energy.org/flow-batteries>, 2007.
- (177) Johnstone, R. In *Discover*; PARS International: New York, 2008; p 6.
- (178) Linden, D.; Reddy, T. B. In *Handbook of Batteries*; The McGraw-Hill Companies, Inc.: New York, 2002.
- (179) Sudworth, J. L.; Tilley, A. R. *The Sodium Sulphur Battery*; Chapman & Hall: London, 1985.
- (180) Lu, X. C.; Xia, G. G.; Lemmon, J. P.; Yang, Z. G. *J. Power Sources* **2010**, *195*, 2431.
- (181) Kummer, J. T.; Weber, N. U.S. Patent 3,413,150, 1968.
- (182) Dustmann, C. H. *J. Power Sources* **2004**, *127*, 85.
- (183) Sudworth, J. L. *J. Power Sources* **2001**, *100*, 149.
- (184) Bragg, W. L.; Gottfried, C.; West, J. Z. *Kristallogr.* **1931**, *77*, 255.
- (185) Beevers, C. A.; Ross, M. A. S. Z. *Kristallogr.* **1937**, *97*, 59.
- (186) Bettman, M.; Peters, C. R. *J. Phys. Chem.* **1969**, *73*, 1774.
- (187) Yamaguchi, G.; Suzuki, K. *Bull. Chem. Soc. Jpn.* **1968**, *41*, 93.
- (188) Virkar, A. V.; Miller, G. R.; Gordon, R. S. *J. Am. Ceram. Soc.* **1978**, *61*, 250.
- (189) Youngblood, G. E.; Miller, G. R.; Gordon, R. S. *J. Am. Ceram. Soc.* **1978**, *61*, 86.
- (190) Baffier, N.; Badot, J. C.; Colomban, P. *Mater. Res. Bull.* **1981**, *16*, 259.
- (191) Ray, A. K.; Subbarao, E. C. *Mater. Res. Bull.* **1975**, *10*, 583.
- (192) Sheng, Y.; Sarkar, P.; Nicholson, P. S. *J. Mater. Sci.* **1988**, *23*, 958.
- (193) Oshima, T.; Kajita, M.; Okuno, A. *Int. J. Appl. Ceram. Technol.* **2004**, *1*, 269.
- (194) Morgan, P. *Mater. Res. Bull.* **1976**, *11*, 233.
- (195) Hodge, J. D. *Am. Ceram. Soc. Bull.* **1983**, *62*, 244.
- (196) Zaharescu, M.; Parlog, C.; Stancovschi, V.; Crisan, D.; Braileanu, A.; Surdeanu, T. *Solid State Ionics* **1985**, *15*, 55.
- (197) Yamaguchi, S.; Terabe, K.; Iguchi, Y.; Imai, A. *Solid State Ionics* **1987**, *25*, 171.
- (198) Jayaraman, V.; Gnanasekaran, T.; Periaswami, G. *Mater. Lett.* **1997**, *30*, 157.
- (199) Yoldas, B. E.; Partlow, D. P. *Am. Ceram. Soc. Bull.* **1980**, *59*, 640.
- (200) Takahashi, T.; Kuwabara, K. *J. Appl. Electrochem.* **1980**, *10*, 291.
- (201) Pekarsky, A.; Nicholson, P. S. *Mater. Res. Bull.* **1980**, *15*, 1517.
- (202) Green, D. J.; Hutchison, S. *Mater. Sci. Monog.* **1980**, *6*, 964.
- (203) Vanzyl, A.; Thackeray, M. M.; Duncan, G. K.; Kingon, A. I.; Heckrodt, R. O. *Mater. Res. Bull.* **1993**, *28*, 145.
- (204) Vanzyl, A. *Solid State Ionics* **1996**, *86–8*, 883.
- (205) Jones, I. W.; Miles, L. J. *Proc. Br. Ceram. Soc.* **1971**, *19*, 161.
- (206) Jatkar, A. D.; Cutler, I. B.; Gordon, R. S. In *Ceramic Microstructures*; Fulrath, R. M.; Pask, J. A., Eds.; Westview Press: Boulder, CO, 1976; p 412.
- (207) Duncan, J. H.; Bugden, W. G. *Proc. Br. Ceram. Soc.* **1981**, *31*, 221.
- (208) Virkar, A. V. *A High Temperature Electrochemical Energy Storage System Based on Sodium Beta-Alumina Solid Electrolyte (BASE)*, report to DOE; 2008.
- (209) Parthasarathy, P.; Weber, N.; Virkar, A. V. *ECS Trans.* **2007**, *6*, 67.
- (210) Virkar, A. V.; Jue, J.-F.; Fung, K.-Z. U.S. Patent 6,117,807, 2000.
- (211) Engstrom, H.; Bates, J. B.; Brundage, W. E.; Wang, J. C. *Solid State Ionics* **1981**, *2*, 265.
- (212) Bates, J. B.; Engstrom, H.; Wang, J. C.; Larson, B. C.; Dudney, N. J.; Brundage, W. E. *Solid State Ionics* **1981**, *5*, 159.
- (213) Whalen, T. J.; Tennenhouse, G. J.; Meyer, C. J. *Am. Ceram. Soc.* **1974**, *57*, 497.
- (214) Buechele, A. C.; De Jonghe, L. C. *Am. Ceram. Soc. Bull.* **1979**, *58*, 861.
- (215) Hsieh, M. Y.; De Jonghe, L. C. *J. Am. Ceram. Soc.* **1978**, *61*, 185.
- (216) Virkar, A. V.; Tennenhouse, G. J.; Gordon, R. S. *J. Am. Ceram. Soc.* **1974**, *57*, 508.
- (217) Virkar, A. V.; Gordon, R. S. *J. Am. Ceram. Soc.* **1977**, *60*, 58.
- (218) Armstrong, R. D.; Dickinson, T.; Willis, P. M. *J. Electroanal. Chem.* **1976**, *67*, 121.

- (219) Fielder, W. L.; Kautz, H. E.; Fordyce, J. S.; Singer, J. *J. Electrochem. Soc.* **1975**, *122*, 528.
- (220) Hooper, A. J. *Phys. D: Appl. Phys.* **1977**, *10*, 1487.
- (221) Yao, Y. F. Y.; Kummer, J. T. *J. Inorg. Nucl. Chem.* **1967**, *29*, 2453.
- (222) Whitting, Ms; Huggins, R. A. *J. Chem. Phys.* **1971**, *54*, 414.
- (223) Briant, J. L.; Farrington, G. C. *J. Solid State Chem.* **1980**, *33*, 385.
- (224) Engstrom, H.; Bates, J. B.; Wang, J. C. *Solid State Commun.* **1980**, *35*, 543.
- (225) Lange, F. F.; Davis, B. I.; Raleigh, D. O. *J. Am. Ceram. Soc.* **1983**, *66*, C50.
- (226) Viswanathan, L.; Ikuma, Y.; Virkar, A. V. *J. Mater. Sci.* **1983**, *18*, 109.
- (227) Binner, J. G. P.; Stevens, R. J. *Mater. Sci.* **1985**, *20*, 3119.
- (228) Green, D. J. *J. Mater. Sci.* **1985**, *20*, 2639.
- (229) Heavens, S. N. *J. Mater. Sci.* **1988**, *23*, 3515.
- (230) Green, D. J.; Metcalf, M. G. *Am. Ceram. Soc. Bull.* **1984**, *63*, 803.
- (231) Sudworth, J. L.; Tilley, A. R.; South, K. D. In *Fast Ion Transport in Solids*; van Gool, W., Ed.; North-Holland: Amsterdam, 1973; p 581.
- (232) Breiter, M. W.; Dunn, B.; Powers, R. W. *Electrochim. Acta* **1980**, *25*, 613.
- (233) Demott, D. S. *J. Electrochem. Soc.* **1980**, *127*, 2312.
- (234) Demott, D. S.; Wright, M. L.; Hames, M. D. Extended abstracts of the 159th ECS Meeting, Spring 1981, Minneapolis, 1981.
- (235) Wright, M. L. European patent 0,032,033, 1981.
- (236) Wright, M. L.; Hames, M. D. European patent 0,044,638, 1982.
- (237) Bugden, W. G.; Barrow, P.; Duncan, J. H. *Solid State Ionics* **1981**, *5*, 275.
- (238) Viswanathan, L.; Virkar, A. V. *J. Mater. Sci.* **1982**, *17*, 753.
- (239) Tischer, R. P. *The Sulphur Electrode*; Academic Press: New York, 1983.
- (240) Coetzer, J. J. *Power Sources* **1986**, *18*, 377.
- (241) Galloway, R. C. *J. Electrochem. Soc.* **1987**, *134*, 256.
- (242) Bones, R. J.; Teagle, D. A.; Brooker, S. D.; Cullen, F. L. *J. Electrochem. Soc.* **1989**, *136*, 1274.
- (243) Bones, R. J.; Coetzer, J.; Galloway, R. C.; Teagle, D. A. *J. Electrochem. Soc.* **1987**, *134*, 2379.
- (244) Moseley, P. T.; Bones, R. J.; Teagle, D. A.; Bellamy, B. A.; Hawes, R. W. M. *J. Electrochem. Soc.* **1989**, *136*, 1361.
- (245) Ratnakumar, B. V.; Attia, A. I.; Halpert, G. J. *Power Sources* **1991**, *36*, 385.
- (246) Ratnakumar, B. V.; Attia, A. I.; Halpert, G. J. *Electrochem. Soc.* **1991**, *138*, 883.
- (247) Redey, L.; Vissers, D. R.; Prakash, J. U.S. Patent 5,283,135, 1994.
- (248) Prakash, J.; Redey, L.; Vissers, D. R. *J. Electrochem. Soc.* **2000**, *147*, 502.
- (249) Redey, L.; Vissers, D. R.; Prakash, J. U.S. Patent 5,340,668, 1994.
- (250) Redey, L.; Rose, C.; Lowrey, R. Extended abstracts of the 182nd Electrochemical Society Meeting, Toronto, Canada, Fall 1992.
- (251) Lu, X. C.; Coffey, G.; Meinhardt, K.; Sprengle, V.; Yang, Z. G.; Lemmon, J. P. *ECS Trans.*, **2010**, *28*, 7.
- (252) Galloway, R. C.; Haslam, S. *J. Power Sources* **1999**, *80*, 164.
- (253) Goodenough, J. B.; Hong, H. Y. P.; Kafalas, J. A. *Mater. Res. Bull.* **1976**, *11*, 203.
- (254) Hong, H. Y. P. *Mater. Res. Bull.* **1976**, *11*, 173.
- (255) Ratnakumar, B. V.; Distefano, S.; Williams, R. M.; Nagasubramanian, G.; Bankston, C. P. *J. Appl. Electrochem.* **1990**, *20*, 357.
- (256) Distefano, S.; Ratnakumar, B. V.; Bankston, C. P. *J. Power Sources* **1990**, *29*, 301.
- (257) Sudworth, J. L.; Hames, M. D.; Storey, M. A.; Azim, M. F.; Tilley, A. R. In *Power Sources*; Collins, D. H., Ed.; Oriol Press, Newcastle upon Tyne, U.K., 1973; Vol. 4, p 1.
- (258) Silverman, H. P. T.R.W. development program for solid electrolyte batteries, E.P.R.I. Rep. EM-266, Project 127, 1976.
- (259) Singhal, S. C. a. K., K. High Temperature Solid Oxide Fuel Cells: Fundamentals, Design and Applications; Elsevier Ltd: New York, NY, 2004.
- (260) Aurbach, D.; Gamolsky, K.; Markovsky, B.; Gofer, Y.; Schmidt, M.; Heider, U. *Electrochim. Acta* **2002**, *47*, 1423.
- (261) Aurbach, D.; Talyosef, Y.; Markovsky, B.; Markevich, E.; Zinigrad, E.; Asraf, L.; Gnanaraj, J. S.; Kim, H. J. *Electrochim. Acta* **2004**, *50*, 247.
- (262) Song, J. Y.; Wang, Y. Y.; Wan, C. C. *J. Power Sources* **1999**, *77*, 183.
- (263) Mizushima, K.; Jones, P. C.; Wiseman, P. J.; Goodenough, J. B. *Mater. Res. Bull.* **1980**, *15*, 783.
- (264) Thackeray, M. M.; David, W. I. F.; Bruce, P. G.; Goodenough, J. B. *Mater. Res. Bull.* **1983**, *18*, 461.
- (265) Mohri, M.; Yanagisawa, N.; Tajima, Y.; Tanaka, H.; Mitate, T.; Nakajima, S.; Yoshida, M.; Yoshimoto, Y.; Suzuki, T.; Wada, H. *J. Power Sources* **1989**, *26*, 545.
- (266) Tarascon, J. M.; Armand, M. *Nature* **2001**, *414*, 359.
- (267) Endo, M.; Kim, C.; Nishimura, K.; Fujino, T.; Miyashita, K. *Carbon* **2000**, *38*, 183.
- (268) Huggins, R. A. *Alloys and Intermetallic Anodes*; Kluwer Academic Publisher: London, 2004.
- (269) Zhang, J. G.; Liu, J.; Wang, D. H.; Choi, D.; Fifield, L. S.; Wang, C. M.; Xia, G.; Nie, Z. M.; Yang, Z. G.; Pederson, L. R.; Graff, G. *J. Power Sources* **2010**, *195*, 1691.
- (270) Ferg, E.; Gummow, R. J.; Dekock, A.; Thackeray, M. M. *J. Electrochem. Soc.* **1994**, *141*, L147.
- (271) Ohzuku, T.; Ueda, A.; Yamamoto, N. *J. Electrochem. Soc.* **1995**, *142*, 1431.
- (272) Takai, S.; Kamata, M.; Fujine, S.; Yoneda, K.; Kanda, K.; Esaka, T. *Solid State Ionics* **1999**, *123*, 165.
- (273) Zaghbi, K.; Simoneau, M.; Armand, M.; Gauthier, M. *J. Power Sources* **1999**, *82*, 300.
- (274) Sudworth, J. L.; Tilley, A. R. *The Sodium Sulfur Battery*; Chapman and Hall: New York, 1985.
- (275) Armstrong, G.; Armstrong, A. R.; Bruce, P. G.; Reale, P.; Scrosati, B. *Adv. Mater.* **2006**, *18*, 2597.
- (276) Bavykin, D. V.; Friedrich, J. M.; Walsh, F. C. *Adv. Mater.* **2006**, *18*, 2807.
- (277) Wang, D. H.; Choi, D. W.; Yang, Z. G.; Viswanathan, V. V.; Nie, Z. M.; Wang, C. M.; Song, Y. J.; Zhang, J. G.; Liu, J. *Chem. Mater.* **2008**, *20*, 3435.
- (278) Yang, Z. G.; Choi, D.; Kerisit, S.; Rosso, K. M.; Wang, D. H.; Zhang, J.; Graff, G.; Liu, J. *J. Power Sources* **2009**, *192*, 588.
- (279) Li, J. R.; Tang, Z. L.; Zhang, Z. T. *Electrochem. Solid-State Lett.* **2005**, *8*, A570.
- (280) Wang, D. H.; Choi, D. W.; Li, J.; Yang, Z. G.; Nie, Z. M.; Kou, R.; Hu, D. H.; Wang, C. M.; Saraf, L. V.; Zhang, J. G.; Aksay, I. A.; Liu, J. *ACS Nano* **2009**, *3*, 907.
- (281) Makimura, Y.; Ohzuku, T. *J. Power Sources* **2003**, *119*, 156.
- (282) Yabuuchi, N.; Ohzuku, T. *J. Power Sources* **2003**, *119*, 171.
- (283) Lu, Z. H.; MacNeil, D. D.; Dahn, J. R. *Electrochem. Solid-State Lett.* **2001**, *4*, A191.
- (284) Whittingham, M. S. *Chem. Rev.* **2004**, *104*, 4271.
- (285) Goodenough, J. B.; Kim, Y. *Chem. Mater.* **2010**, *22*, 587.
- (286) Patil, A.; Patil, V.; Shin, D. W.; Choi, J. W.; Paik, D. S.; Yoon, S. J. *Mater. Res. Bull.* **2008**, *43*, 1913.
- (287) Yang, H.; Amiruddin, S.; Bang, H. J.; Sun, Y. K.; Prakash, J. *J. Ind. Eng. Chem.* **2006**, *12*, 12.
- (288) Pasquali, M.; Passerini, S.; Pistoia, G. In *Lithium Batteries: Science and Technology*; Nazri, G. A.; Pistoia, G., Eds.; Kluwer Academic Publishers: London, 2004; Chapter 11, pp 315–360.
- (289) Choi, D.; Kumta, P. N. *J. Power Sources* **2007**, *163*, 1064.
- (290) Padhi, A. K.; Nanjundswamy, K. S.; Goodenough, J. B. *J. Electrochem. Soc.* **1997**, *144*, 1188.
- (291) Chung, S. Y.; Bloking, J. T.; Chiang, Y. M. *Nat. Mater.* **2002**, *1*, 123.
- (292) Huang, H.; Yin, S. C.; Nazar, L. F. *Electrochem. Solid-State Lett.* **2001**, *4*, A170.

- (293) Striebel, K.; Shim, J.; Srinivasan, V.; Newman, J. J. *Electrochem. Soc.* **2005**, *152*, A664.
- (294) Yamada, A.; Chung, S. C.; Hinokuma, K. J. *Electrochem. Soc.* **2001**, *148*, A224.
- (295) Howell, D. *DOE Progress Report for Energy Storage Research and Development*; US Department of Energy: Washington, DC, 2008.
- (296) Gaines, L.; Cuenca, R. *Costs of Lithium-Ion-Batteries for Vehicles*; Argon National Laboratory: Argonne, IL, 2000.
- (297) Viswanathan, V. V.; Choi, D.; Wang, D. H.; Xu, W.; Towne, S.; Williford, R. E.; Zhang, J. G.; Liu, J.; Yang, Z. G. *J. Power Sources* **2010**, *195*, 3720.
- (298) Choi, D. W.; Wang, D. H.; Viswanathan, V. V.; Bae, I. T.; Wang, W.; Nie, Z. M.; Zhang, J. G.; Graff, G. L.; Liu, J.; Yang, Z. G.; Duong, T. *Electrochem. Commun.* **2010**, *12*, 378.
- (299) Zaghbi, K. In *DOE-BATT Merit Review Meeting*; U.S. Department of Energy: Washington, DC, 2010.
- (300) Wang, D. H.; Kou, R.; Choi, D.; Yang, Z. G.; Nie, Z. M.; Li, J.; Saraf, L. V.; Hu, D. H.; Zhang, J. G.; Graff, G. L.; Liu, J.; Pope, M. A.; Aksay, I. A. *ACS Nano* **2010**, *4*, 1587.
- (301) Akridge, J. R.; Vourlis, H. *Solid State Ionics* **1986**, *18–9*, 1082.
- (302) Jones, S. D.; Akridge, J. R. *J. Power Sources* **1995**, *54*, 63.
- (303) Kondo, S. In *Li-Ion Batteries*; Wakihara, M., Yamamoto, O., Ed.; Wiley-VCH: New York, 1998.
- (304) Salkind, A. J.; Cannone, A. G.; Trumbure, F. A. In *Handbook of Batteries*, 3rd ed.; Linden, D.; Reddy, T. B., Ed.; McGraw-Hill: New York, 2002; p 23.1.
- (305) Salkind, A. J.; Hammel, R. O.; Cannone, A. G.; Trumbure, F. A. In *Handbook of Batteries*, 3rd ed.; Linden, D.; Reddy, T. B., Ed.; McGraw-Hill: New York, 2002; p 24.1.
- (306) Winter, M.; Brodd, R. J. *Chem. Rev.* **2004**, *104*, 4245.
- (307) Lam, L. T.; Haigh, N. P.; Phyland, C. G.; Urban, A. J. *J. Power Sources* **2004**, *133*, 126.
- (308) Lam, L. T.; Haigh, N. P.; Phyland, C. G.; Huynh, T. D. *J. Power Sources* **2005**, *144*, 552.
- (309) Lam, L. T.; Louey, R. J. *J. Power Sources* **2006**, *158*, 1140.
- (310) Moseley, P. T.; Nelson, R. F.; Hollenkamp, A. F. *J. Power Sources* **2006**, *157*, 3.
- (311) Vinal, G. W. *Storage Batteries*, 4th ed.; John Wiley & Sons: New York, 1955.
- (312) Shiomi, M.; Funato, T.; Nakamura, K.; Takahashi, K.; Tsubota, M. *J. Power Sources* **1997**, *64*, 147.
- (313) Nakamura, K.; Shiomi, M.; Takahashi, K.; Tsubota, M. *J. Power Sources* **1996**, *59*, 153.
- (314) Hollenkamp, F. A.; Baldsing, W. G. A.; Lau, S.; Lim, O. V.; Newnham, R. H.; Rand, D. A. J.; Rosalie, J. M.; Vella, D. J.; Vu, L. H. *Overcoming Negative-Plate Capacity Loss in VRLA Batteries Cycled HRPSoC Duty*; Triangle Research Park: Research Triangle Park, NC, 2002.
- (315) Newnham, R. H.; Baldsing, W. G. A.; Hollenkamp, A. F.; Lim, O. V.; Phyland, C. G.; Rand, D. A. J.; Rosalie, J. M.; Vella, D. J.; Vu, L. H. *Advancement of Valve-Regulated Lead-Acid Battery Technology for Hybrid-Electric and Electric Vehicle*; Advanced Lead-Acid Battery Consortium: Durham, NC, 2002.
- (316) Buiel, E. In *Advanced Capacitor World Summit*, San Diego, CA, 2006.
- (317) Razoumov, S.; Klementov, A.; Litvinenko, S.; Beliakov, A. U.S. Patent 6,222,723, 2001.
- (318) Buiel, E.; Eshkenazi, V.; Rabinovich, L.; Sun, W.; Vichnyakov, V.; Swiecki, A.; Cole, J. U.S. Patent 2,008,113,268, 2008.
- (319) Lam, L. T.; Louey, R.; Haigh, N. P.; Lim, O. V.; Vella, D. G.; Phyland, C. G.; Vu, L. H.; Furukawa, J.; Takada, T.; Monma, D.; Kano, T. *J. Power Sources* **2007**, *174*, 16.
- (320) Cooper, A.; Furukawa, J.; Lam, L.; Kellaway, M. *J. Power Sources* **2009**, *188*, 642.
- (321) Hund, T. D. In *DOE Energy Systems Program Review*; U.S. Department of Energy: Washington, DC, 2008.
- (322) Wills, R. G. A.; Collins, J.; Stratton-Campbell, D.; Low, C. T. J.; Pletcher, D.; Walsh, F. C. *J. Appl. Electrochem.* **2010**, *40*, 955.
- (323) Collins, J.; Li, X. H.; Pletcher, D.; Tangirala, R.; Stratton-Campbell, D.; Walsh, F. C.; Zhang, C. P. *J. Power Sources* **2010**, *195*, 2975.
- (324) Collins, J.; Kear, G.; Li, X. H.; Low, C. T. J.; Pletcher, D.; Tangirala, R.; Stratton-Campbell, D.; Walsh, F. C.; Zhang, C. P. *J. Power Sources* **2010**, *195*, 1731.
- (325) Li, X. H.; Pletcher, D.; Walsh, F. C. *Electrochim. Acta* **2009**, *54*, 4688.
- (326) Pletcher, D.; Zhou, H.; Kear, G.; Low, C. T. J.; Walsh, F. C.; Wills, R. G. A. *J. Power Sources* **2008**, *180*, 621.
- (327) Pletcher, D.; Zhou, H.; Kear, G.; Low, C. T. J.; Walsh, F. C.; Wills, R. G. A. *J. Power Sources* **2008**, *180*, 630.
- (328) Barker, J.; Saidi, M. Y.; Swoyer, J. L. *Electrochem. Solid. St* **2003**, *6*, A1.
- (329) Ellis, B. L.; Makahnouk, W. R. M.; Makimura, Y.; Toghill, K.; Nazar, L. F. *Nat. Mater.* **2007**, *6*, 749.
- (330) Qu, Q. T.; Shi, Y.; Tian, S.; Chen, Y. H.; Wu, Y. P.; Holze, R. *J. Power Sources* **2009**, *194*, 1222.
- (331) Athouel, L.; Moser, F.; Dugas, R.; Crosnier, O.; Belanger, D.; Brousse, T. *J. Phys. Chem. C* **2008**, *112*, 7270.
- (332) Whitacre, J. F.; Tevar, A.; Sharma, S. *Electrochem. Commun.* **2010**, *12*, 463.
- (333) Sadoway, D.; Ceder, G.; Bradwell, D. U.S. Patent 2008/0,044,725, 2008.